2022

Development of an hiPSC-Cortical Neuron Long-Term Potentiation Model and its Application to Alzheimer's Disease Modeling and Drug Evaluation

Kaveena Autar
University of Central Florida

DEVELOPMENT OF AN HIPSC-CORTICAL NEURON LONG-TERM POTENTIATION MODEL AND ITS APPLICATION TO ALZHEIMER'S DISEASE MODELING AND DRUG EVALUATION

by

KAVEENA AUTAR
B.S. University of Florida, 2017
M.S. University of Central Florida, 2019

A dissertation submitted in partial fulfillment of the requirements
for the degree of Doctor of Philosophy
in the Department of Chemistry
in the College of Sciences
at the University of Central Florida
Orlando, Florida

Summer Term
2022

Major Professor: James J. Hickman

ABSTRACT

Alzheimer's disease (AD) is commonly characterized by a loss of cognitive function due to the deterioration of neuronal synapses from the presence of senile amyloid beta-42 (Aβ42) plaques. Evaluating cognitive deficits caused by Aβ42 using human cortical neurons poses a challenge due to sourcing difficulties, and the use of animal models to assess drug efficacy creates biological hurdles from lack of species translatability. Recent advances in induced-pluripotent stem cell technology have enabled the development of mature, human-based cortical neuron models. The development of an hiPSC-cortical neuron differentiation protocol facilitates the exploration of disease onset and functional analysis from a patient-derived cell source, and further investigation of potential therapeutic treatments, while eliminating biological efficacy concerns. Long-term potentiation (LTP) was utilized as an in vitro correlate for memory and learning to quantify cognitive deficits in sporadic AD (SAD) and familial AD (FAD) systems and assess drug treatments for the prevention of Aβ42-induced neurotoxicity. Synaptic connectivity and LTP induction through high-frequency stimulation was simulated through cortical neurons cultured on microelectrode arrays (MEAs), such that the functional activity of the neuronal population could be assessed overtime. AD therapeutic treatments were shown to block the Aβ42-induced neurotoxic loss of synaptic plasticity and maintain persistent LTP in a model for SAD. Subsequently, FAD was assessed through the differentiation of patient-derived AD iPSCs, where LTP proficiency could be evaluated to relate to clinical cognitive evaluations. This study established a serum-free, in vitro human-derived iPSC-cortical neuron protocol that could be adapted to validate disease mechanisms and drug efficacy in patient-derived neural networks as a potential platform for precision medicine.

This work is dedicated to my parents, whose unwavering support has gotten me this far in life.

ACKNOWLEDGMENTS

I would like to express my sincere appreciation to my advisor and committee chair, Dr. James J. Hickman, the other members of my committee: Drs. Xiufang “Nadine” Guo, John Ballantyne, Andre Gesquiere, and Dmitry Kolpashchikov, and all of the members of the Hickman Hybrid Systems Laboratory, new and old, who have gotten me through this journey with their constant benevolence and encouragement.

TABLE OF CONTENTS

LIST OF FIGURES

LIST OF TABLES

LIST OF ABBREVIATIONS

Amyloid-Beta 42 (Aβ42)

Alzheimer's Disease (AD)

α-amino-3-hydroxy-5-methyl-4-isoxazolepropionic acid (AMPA)

Amyloid Precursor Protein (APP)

Apolipoprotein E (ApoE)

Brain-Derived Neurotrophic Factor (BDNF)

Cyclic adenosine monophosphate (cAMP)

4′,6-diamidino-2-phenylindole (DAPI)

Familial Alzheimer's Disease (FAD)

Glial-Derived Neurotrophic Factor (GDNF)

Human Induced Pluripotent Stem Cell (hiPSC)

Induced Pluripotent Stem Cell (iPSC)

Microelectrode Array (MEA)

Microphysiological System (MPS)

Neurofibrillary Tangle (NFT)

N-methyl-D-aspartate (NMDA)

Phosphate Buffer Solution (PBS)

Presenilin-1 (PSEN1)

Presenilin-2 (PSEN2)

Sporadic Alzheimer's Disease (SAD)

Wild-Type (WT)

CHAPTER ONE: INTRODUCTION
OVERVIEW OF ALZHEIMER'S DISEASE

Alzheimer's disease (AD) affects an estimated 6 million individuals over the age of 65 and is the most common form of dementia [1]. AD is notable for its characteristic loss of cognitive function. Its symptoms commonly include detrimental effects on patient's memory, learning, and focus [2]. Its onset is considered to either be familial through genetically inherited mutations, or sporadic from the formation of senile plaques due to environmental factors. On a biological level, AD is caused by synaptic dysregulation leading to the deterioration of neural networking and neuronal cell death [3]. There are several hypotheses speculating the biochemical mechanisms leading to AD pathology, including amyloid beta-42 (Aβ42) plaque accumulation [4], hyperphosphorylated Tau neurofibrillary tangles (NFTs) [5], neuroinflammation [6, 7], oxidative stress [8, 9], cholinergic burden [10, 11], and Ca^{+2} dysfunction [12]. The most widely studied postulations for the onset of AD are the accumulation of Aβ42 oligomers to form neurotoxic plaques and NFTs of hyperphosphorylated tau.

One hypothesis on the major mechanism of the prominent synaptic dysfunction of AD is through the accumulation of Aβ42 plaques in the synaptic cleft causing excitotoxicity [13], inflammation [6, 14], and physical deterioration of neural networks [15]. The formation of Aβ42 is a direct result of the improper cleavage of Aβ40 from amyloid precursor protein (APP) [16]. The physiological function of Aβ40 is neural growth and repair, and it is mainly responsible for the appropriate differentiation of neurons from neural progenitor cells [17]. Aβ40 oligomers become neurotoxic when they are extended by 2 additional C-terminal residues, which can happen from the failure of the gamma secretase complex to cleave APP to Aβ40 at its cleavage site, leading

the Aβ42 oligomerization [16]. Once extended into its neurotoxic form, Aβ42 oligomers cluster to form plaques, which can agglomerate and cause detrimental effects on neuronal networking and several post-synaptic receptors, such as the NMDA and AMPA receptors responsible for glutamate binding in synapse transmission [18, 19]. The major role of astrocytes in the synaptic network is proper glutamate reuptake and recycling, which can also be disturbed in the presence of the plaques [20]. Additionally, the accumulation of Aβ42 plaques in the presence of microglia and/or astrocytes can trigger an immune response, leading to the release of inflammatory factors such as IL-1, IL-6, and TNF-β that can further exacerbate neurodegeneration [13, 21].

Another hypothesis of synaptic dysfunction in AD is through the accumulation of Tau neurofibrillary tangles. Tau in its benign form is responsible for microtubule stabilization and axonal transport [22]. When the Tau tubule proteins become hyperphosphorylated, the axonal stabilization is disrupted, leading to the disintegration of the axon and release of phosphorylated Tau into the synaptic cleft, where it can accumulate into neurofibrillary tangles and further aggravate synaptic deterioration [22, 23]. However, it has been cited that hyperphosphorylation of Tau is dependent on the inflammatory response due to the presence of Aβ42 within the neural network [24]. Tau neurotoxicity is predominantly an exogenous effect that is dependent on the presence of Aβ42 in the synaptic cleft [25].

AD arises either from a familial or sporadic source. Familial AD is genetically derived, characterized by an early onset from missense mutations in either the APP gene or the Presenilin-1 or Presenilin-2 genes, the latter of which are subunits of the gamma secretase enzyme responsible for the improper cleavage of APP leading to the formation of Aβ42 plaques and subsequent Tau NFTs [26]. Phenotypic symptoms of FAD start clinically as early as the patient's 20s, with the

hyperexcitation mechanism presenting itself through seizures, preceding synaptic deterioration from excitotoxicity and decline of the patient's cognitive functioning [27, 28]. The apolipoprotein E4 (ApoE4) allele has also been implicated as a cause of AD [29]. ApoE4 is one of three possible alleles for ApoE, with an E2 and E3 variant also present. ApoE4 is thought to cause AD because it is the least lipidated form of ApoE, meaning it has lower functioning in the transport of cholesterol and clearance of Aβ, affecting neuronal maturation and dendritic arborization [30-32]. Sporadic AD, also considered late-onset AD (LOAD), is speculated to be environmentally driven, taking into consideration the lesser studied mechanisms of AD, such as cholinergic burden [33], neuroinflammation [34], and oxidative stress through ROS [35, 36].

Long-term potentiation (LTP) is a means of assessing memory and learning in models of AD. It is a quantitative measurement of synaptic plasticity utilized as a correlate for cognitive function in models of neurodegeneration [37]. In vitro models of LTP have either employed the use of a dual patch-clamp technology of a probe inserted into brain tissue, measuring the EPSP slope following tetanic stimulation [38], or use chemical or electrical high-frequency stimulation on a microelectrode array to evaluate the neural population dynamics [39]. The elicited response to the stimulation of enhanced neuronal firing should persist overtime, indicating a strengthening of synaptic network integrity referred to as synaptic plasticity [40]. The enhanced activity following chemical or high-frequency electrical stimulation triggers an increase in expression of glutamate receptors on the cell membrane, allowing for more glutamate binding at the post-synaptic terminal and overall long-term enhanced activity within the neural network [41].

At the molecular level, synaptic plasticity occurs due to the heightening of the release of glutamate vesicles from the pre-synaptic neuron accompanied by the increased expression of

glutamate receptors on the post-synaptic sites, enabling the enhanced signal transmission [42]. The AMPA and NMDA receptors are glutamate receptors implicated in synaptic plasticity. AMPA receptors are endocytosed in response to LTP induction [43]. While the expression of AMPA receptors is also enhanced because of LTP induction, the NMDA receptor has been more heavily linked to neuronal LTP due to its voltage-dependent nature [44, 45]. The Mg^{+2} block within the receptor is only cleared after the membrane is depolarized to a certain voltage threshold, which can be achieved through the stimulated release of glutamate vesicles from the pre-synaptic terminal binding to AMPA receptors. Once the Mg^{+2} block is released, there is a flood of Ca^{+2} ions into the post-synaptic neuron [46].

Several therapeutics have been found to mitigate the synaptic dysfunction in AD through varying mechanisms of action. Memantine, one of the most widely used AD drugs, works against the excitotoxicity hypothesis, targeting the NMDA receptor with low-affinity binding to block the excessive stimulation of glutamate binding that ultimately leads to neuronal cell death from overexcitation [47, 48]. The presence of excessive glutamate contributes to long-term overexpression of glutamate receptors, like the AMPA and NMDA receptors. Overtime, neuronal populations experience a decrease in the release of pre-synaptic glutamate vesicles, which will not be able to fulfill the demand of the excessive expression of NMDA receptors to achieve LTP [49]. Donepezil can work at this stage of synaptic decline to enhance neuronal stimulation through an alternative neurotransmission pathway. Donepezil inhibits acetylcholinesterase, the enzyme responsible for the breakdown of acetylcholine [10]. The acetylcholine neuronal pathway is regulated by negative feedback, where it is taken up and recycled based on the necessity and availability of acetylcholine in the synaptic cleft, and since Donepezil also binds with low affinity,

it is released when necessary [50, 51]. While Memantine and Donepezil target the restoration of extracellular neuronal function at the synaptic level, other drugs, such as Saracatinib and Rolipram, work intracellularly to counteract the negative effects of Aβ42. Saracatinib inhibits the Fyn kinase, which, in its pathogenic state, phosphorylates APP, promoting the improper cleavage of APP to Aβ42 [52]. Fyn is also one of the kinases responsible for the hyperphosphorylation of tau. Additionally, the pathogenic actions of the Fyn kinase are further exacerbated in a positive feedback loop by the presence of Aβ42 plaques and Tau NFTs. Lastly, Rolipram works intracellularly to recover the spontaneous activity of the neuron intracellularly. Rolipram inhibits the phosphodiesterase-type 4 enzyme that breaks down cyclic AMP within the cell. As a result, there is an increased availability of intracellular cAMP, contributing to enhanced neuronal activity [53, 54].

Currently, there is a gap in combining human-derived neuronal models of AD with functional, in vitro surveying of the integrity of neural networks. The ability of microphysiological systems (MPS) to explore neuronal responses to the addition of compounds, including neurotransmitters and receptor inhibitors, enables for the inquiry of biological mechanisms contributing to neurological disorders. While many AD models have been developed, mouse models are limited biologically by the species gap, and many human in vitro models either lack functional evaluation of a purely glutamatergic neuronal culture or employ the use of undefined serum. The integration of human-iPSC technology in combination with MPS provides a human-based system capable of functional analysis as a platform for preclinical drug evaluation.

Induced pluripotent stem cells (iPSCs) are reprogrammed stem cells that can subsequently be differentiated into any somatic cell type [55]. This technology is advantageous because of its

low-invasive sourcing, with induction of stemness and pluripotency from either a skin biopsy of fibroblasts or peripheral blood mononuclear cells (PBMCs) [56]. These reprogrammed stem cells possess stemness properties, meaning they are self-renewing and can proliferate indefinitely [57]. Consequently, iPSCs provide a source for studying biological mechanisms and the onset of diseases where human sources are difficult to acquire, such as central nervous system (CNS) diseases. This allows for developing human-based in vitro models because of its retention of source DNA, enabling the cultivation of patient-specific disease models and therapeutic treatments [58]. Not only is it a feasible source of analyzing neuronal networking in human-derived cortical neuron cultures in vitro, but genetically-based neurological disorders can also be explored upon the development of an hiPSC-cortical neuron differentiation protocol. Once differentiated and established, iPSC-cortical neurons can be utilized in MPS to evaluate the functional properties of the neuronal population.

The establishment of an hiPSC cortical neuron model capable of assessing LTP through synaptic connectivity fill the gap not only for a species relevant, mature neuronal model of cognition, but also provides a system for in vitro, preclinical drug evaluation. This study will cover the derivation and characterization of a protocol to develop mature hiPSC-cortical neurons and illustrate their response to chemical compounds and electrical stimulation for biological efficacy. Furthermore, this model was utilized to evaluate the inhibition of LTP persistence in the presence of Aβ42 oligomers, which could be blocked through the co-administration of the neurotoxic oligomers with cited AD therapeutic compounds. Functional deficits in FAD neuronal cultures were also investigated following the differentiation of cortical neurons from AD patient-derived

hiPSCs. The validation of this model combining hiPSC and MEA technology paves a path for further exploration of mechanisms of CNS disease onset and treatment efficacy.

CHAPTER TWO: A FUNCTIONAL HIPSC-CORTICAL NEURON DIFFERENTIATION AND MATURATION MODEL AND ITS APPLICATION TO NEUROLOGICAL DISORDERS

Introduction

Functionally mature human cortical neuron in vitro models are needed for investigating numerous CNS diseases, including Alzheimer's, Parkinson's, Huntington's, epilepsy, brain injury [59] and for subsequent drug development [60-62]. The use of iPSCs provides phenotypic relevance in vitro because of the physiological accuracy of using human cells as opposed to animal models by eliminating the species gap [63]. IPSC lines can be established through the reprogramming of adult cells such as fibroblasts and blood cells. IPSCs can be propagated indefinitely, and their pluripotency easily lends itself to the differentiation of multiple cell types. This is particularly useful for modeling CNS diseases, because of the characteristic lack of proliferation in primary neurons, the difficulty harvesting and maintaining human neurons in vitro, and the ability to separately differentiate neurons, astrocytes and microglia. The establishment of iPSC-derived cortical neuronal cultures without glia would enable the further investigation of neuronal behavior where astrocytes and microglia could be used as variables to understand their influence in disease phenotypes.

To date, only few studies have reported successful differentiation of cortical neurons from either embryonic stem cells (ESCs) or induced pluripotent stem cells (iPSCs) [64-67], and only one demonstrated synapse formation in the in vitro system, but in serum-containing medium [67] or in astrocyte co-culture [68]. Synapse formation and subsequent neuronal interactions, especially induction of long-term potentiation (LTP), is the typical hallmark indicating functional circuit formation as seen previously in slice cultures and animal models [69-71]. The ability of neurons

to maintain elevated firing rates for extended time periods following a high-frequency electrical stimulation protocol is correlated with learning and memory [72]. Cortical neural circuits composed of mature cortical neurons could be more effective in modeling CNS functional impairment such as cognitive deficits in AD or dementia, both as pure cultures or with the addition of glia. One report of the induction of LTP in iPSC-derived cortical neuronal culture used co-culture from rat primary cortical astrocytes during differentiation, which is undefined and introduces nonhuman components to the process [73]. A new study has demonstrated LTP in cultures of human iPSC-derived cortical neurons and primary astrocytes but did not extensively characterize the neuronal maturity [62]. Undefined animal components during the differentiation procedure would limit the use of the cortical neurons in applications for clinical cell therapy and human cell-based preclinical pharmaceutical studies. This study aimed to develop a protocol for differentiating cortical neurons from human iPSCs in a defined xeno-free, serum-free system, and to establish an in vitro functional human cortical neural model, free from glial cells, that with the maturity level necessary to recapitulate LTP function and to model human cortical dysfunction.

In studies of iPSC-derived cortical neurons there is a knowledge gap concerning the level of maturation necessary for the accurate recapitulation of physiological function for the modeling of relevant diseases, which in many cases is determined by the level of their synaptic and functional characteristics. Additionally, in an effort to establish the use of iPSC-cortical neurons to a level of in vivo competency, confirmation of the exact neuronal subtype present in a culture model was necessary. Reports on the classification of iPSC-derived cortical neurons as excitatory or inhibitory has been cursorily examined, such as in Cao et al. in 2017 [66], but has not been well explored longitudinally, and neither has the state of this maturation on the ability of these neurons to

accurately model CNS diseases free of glial cell contributions. Similarly, modeling epilepsy can be challenging due to its primary symptom of erratic firing of neuronal networks. The randomness of these symptomatic episodes causes difficulty with in vivo studies. The employment of iPSC-cortical neurons to study this neurological disease would enable not only more accurate toxicology and efficacy modeling, but also the possibility of patient-specific treatments due to the ability to isogenetically modify iPSCs [59].

This study presents a unique protocol for differentiating iPSCs into cortical neurons, as well as a maturation process for obtaining functionally mature cortical neuron circuits, which was free of astrocytes and microglia influence, that was competent for synapse formation and LTP induction. The report described both the maturation of iPSC-derived cortical neurons and the inhibitory/excitatory subtype classification that was characterized longitudinally by immunocytochemistry, patch clamp electrophysiological as well as microelectrode array (MEA) analysis. The iPSC-derived cortical neuron on MEA model system was further applied to model aspects of epilepsy and its treatment. This human-based defined cortical neuron-on-a-chip functional system could be a valuable platform for modeling other human CNS diseases and especially for preclinical pharmacological evaluation of therapeutic drugs.

Results

Differentiation of Cortical Neurons from hiPSCs

The differentiation of cortical neurons from hiPSCs consists of four major steps (Figure 1A). To initiate the differentiation, two small-molecule inhibitors of SMAD signaling, LDN193189 and SB431542, were utilized for the induction of early neural lineages [74] (DIF1). Then DKK-1, an

antagonist of Wnt/β, which can induce telencephalic specification [75], and DMH-1, a highly selective small molecule BMP inhibitor comparable to Noggin that can promote neurogenesis of hiPSCs, were used [76] (DIF 2). It was postulated that the combination of these two molecules would facilitate the induction of the rhombomeric neuroepithelia. Next, DKK-1 was withdrawn and Cyclopamine was introduced (DIF 3). Cyclopamine, a small molecule SHH inhibitor, has been shown to specify the dorsal cortical fate in a dose-dependent manner and enhance the generation of cortical glutamate neurons [66]. The differentiation was completed by culturing these cells in the presence of trophic factors BDNF, GDNF, cAMP, ascorbic acid, and laminin that support the survival and maturation of cortical neurons [77-80] (Maturation).

Following differentiation, the iPSC-cortical neurons were characterized to confirm the identity and level of maturation of the cortical neurons and for the presence of glial cells. Figure 1B indicates the morphological progression of the iPSC-cortical neuronal cultures. On Day 7 (left), axonal and dendritic extensions from the neurons were observed, while on Days 14 (middle) and 40 (right), robust neuronal process extension was observed and networking morphology was present. On Day 40, immunocytochemistry (ICC) using the layer V cortical neuron marker ctip2 [81], along with the neuronal marker β-III tubulin, to highlight neuronal processes, confirmed cortical neuron identity (Figure 1C). To quantify the percentage of the neuronal component of the differentiated culture, cultures at Day 40 of maturation were stained with the neuronal marker β-III tubulin as well as the neuroprogenitor and glial cell marker GFAP [82]. The results indicated that the neuronal percentage in the culture was greater than 95% (Figure 1D). Longitudinal expression of these markers together with ctip2 marker was further quantified using flow cytometry, revealing that the expression of the markers ctip2 and β-III tubulin on Days 0, 14, and

28 increased over time, being >90% at the last time point, in agreement with the ICC results, while the expression of GFAP decreased over time to almost undetectable levels (Figure 1E). These analyses indicated that this differentiation protocol generated a close-to-pure cortical neuronal culture if sufficient maturation time was utilized that enables the study of neuronal only characteristics.

Characterization of Terminally Differentiated hiPSC-Cortical Neurons Via Immunocytochemistry

Following the successful differentiation to cortical neurons, immunocytochemistry was performed to further characterize the synapse formation by staining with the synaptic terminal protein synaptophysin and the postsynaptic markers including GluR1 (a subunit of the AMPA glutamatergic receptor), the NMDA receptor, and the receptor-associated molecule PICK1 (Protein interacting with C kinase 1). Day 40 cultures were utilized for this ICC analysis (Figure 2). Synaptic connectivity was observed via the co-localization of the pre-synaptic marker synaptophysin with the post-synaptic marker PICK1 (Figure 2A). Additionally, the expression of NMDA and AMPA receptors was demonstrated using MAP2 co-stained with the markers NMDAR1 and GLUR1, respectively (Figures 2B and 2C). The existence of NMDA and AMPA receptors on the neuronal cell bodies was also indicative of terminal differentiation and suggesting functional and physiological maturity at this timepoint.

Characterization of hiPSC-Cortical Neurons Via Whole-Cell Patch Clamp Electrophysiology

Whole-cell patch clamp was used to determine the electrical properties of the iPSC-cortical neurons at Days 14, 21, 28, and 40. Specifically, the cells were examined for ionic currents,

induced repetitive firing, and spontaneous firing. At Day 40, the cortical neurons expressed voltage gated Na+ and K+ channels as indicated by inward Na+ currents and outward K+ currents (Figure 3A). As the culture progressed, there was an increase in the percentage of cells showing spontaneous and repetitive firing, indicative of increasing cortical neuron excitability and functional maturation in the culture over time (Figures 3B and 3C). Additionally, other functional parameters that increased significantly over time included the action potential amplitude (Figure 3D) and the Na+ inward currents (Figure 3F), while any change of the K^+ current over time is not obvious (Figure 3G), suggesting the increase of action potential amplitude can be attributed mostly to the increase in Na+ current rather than the change in the K+ current [83, 84]. Analysis of the resting membrane potential demonstrated a progressive hyperpolarization as the culture matured (Figure 3E).

Recording of Neural Activity on MEAs

Microelectrode array (MEA) recording technology has been a powerful tool to monitor populational neural activity non-invasively and to analyze neurocircuit activity. In order to adapt these electrically active cortical neurons into an MEA system, the iPSC-cortical neurons were plated on surface patterned MEAs. Phase images in Figure 4A demonstrate an example of the patterned distribution of cortical neurons on these MEAs. Neurons were observed to successfully form patterns on electrodes, with neuronal bodies localized on the electrode surface, and axon bundles forming between the adjacent electrodes. Recording of spontaneous neural activity gave rise to representative traces as in Figure 4B. To confirm these traces were generated by neural activity, lidocaine, a Na+ channel inhibitor and well-characterized local anesthetic, was used to

block activity. Addition of lidocaine quickly reduced, and subsequently eliminated, neuronal signaling within approximately two minutes (Figure 4B and 4C).

This MEA system was then utilized to investigate the progressive changes in neural activity by measuring spontaneous activity on Days 21, 28, 35, and 40. The waveforms measured displayed lengthening of amplitude, especially in the positive direction to emphasize the biphasic properties as well as the sharpening of the waveform average over time (Figure 4D). Quantification of spontaneous activity indicated an increase of neuronal activity with increasing culture time, consistent with the patch clamp results, though non-significant (Figure 4F). Neuronal activity remained consistent past day 40 of maturation, and as a result, it enabled experimentation on mature neurons from older cultures. Subsequent MEA experiments were performed based on the presence of NMDA and AMPA receptors found in previous ICC experiments, by the addition of the chemical stimulator glutamate to increase neural activity. As in Figure 4E and G, addition of glutamate increased the frequency of neural activity within the time window of 35-40 DIV. The silencing and enhancement of neural activity by lidocaine and glutamate, respectively, confirmed the validity of the MEA recording system as well as establish the expected functionality of the terminally differentiated cortical neurons [85, 86].

Formation of Synaptic Circuits and Induction of LTP on MEAs

To evaluate neural circuit activity of the patterned cortical neurons on the MEAs, NBQX, an AMPA receptor blocker [87], was applied to the culture and the activity was analyzed. Figure 5A depicts representative waveform traces from baseline recordings (left) and then following dosage with NBQX (right). As in Figure 5B, addition of NBQX induced significant reduction of recorded

activity while there was no significant change in vehicle control. This result revealed that a portion of activity recorded is from inputs through neuronal synapses, or there were functional synapses formed in the iPSC-cortical neural culture.

Since LTP formation is an important property of cortical activity as well as a key mechanism for neural plasticity and a strong cellular basis for cognition, the capability of inducing LTP in these glial cell free cultures was investigated. In order to induce LTP, a paradigm of high frequency stimulation (HFS) was applied to all the electrodes and the spontaneous activity of these neurons were quantified before, right after and one hour post HFS [62]. As in Figure 5C, there was a significant increase in neural activity after the HFS, and this increase was maintained for at least one hour. This result indicated LTP formation in this iPSC-neural culture as previously reported in other neuronal cultures [62, 67]. As validation, similar experiments in the presence of the AMPA receptor antagonist NBQX were conducted in which glutamatergic synaptic activity was blocked and no LTP could be induced. As expected, HFS did not induce any increase in activity (Figure 5D), but rather caused the same decrease following NBQX dosage observed in Figure 5B, confirming the increase in neuronal activity following HFS was synapse-based.

Characterization of Excitatory and Inhibitory Features in Mature and Immature iPSC-Cortical Neurons

To characterize the identity of these iPSC-cortical neurons as excitatory or inhibitory (Figure 6), the vesicular glutamate transporter 1 (vGLUT1) was used as a marker for the glutamatergic neurons while GABA was used to distinguish the GABAergic neuronal phenotype. Immunocytochemical staining revealed that on Day 21 (Figure 6A), neurons were positive for both

the excitatory neuron marker vGLUT1 and the inhibitory neuron marker GABA. Subsequently, at Day 40 (Figure 6B), the neurons only stained positive for vGLUT1, indicating full maturation to an excitatory phenotype as the culture progressed. This is consistent with the increased spontaneous activity measured by patch clamp and MEA recordings in the latter days of maturation (Days 35-40). It has been previously reported that GABA is the predominantly expressed neurotransmitter in the early stages of brain development [88]. Consequently, GABA is imperative for neuroprogenitor proliferation and migration in the early stages of development [89], with GABA being cited to have excitatory properties of neurotransmission at the immature stage of development before the shift to the utilization of glutamate as the excitatory neurotransmitter [90]. This observation implied a reduced capability of inducing LTP in younger cultures. This hypothesis was then tested in culture at Day 21 compared to that at Day 35. As in Figure 6C, with additional waveforms depicted in Figure S1, LTP could be induced at Day 21 culture, but did not persist after one hour. However, one hour LTP persistence was achieved with the addition of picrotoxin to block inhibitory signals. When neurons were past Day 35 in culture as characterized as purely glutamatergic in Figure 6, and LTP was seen to persist at one hour following LTP induction without inhibiting the GABAergic signaling. This result reproduced the previous findings that modulating the percentage of inhibitory signaling in cortical neuron circuits is an important parameter for successful induction of persistent LTP [91].

The Induction and Quieting of Epileptiform Activity in Immature Cortical Neurons

The above analysis indicated a significant amount of GABAergic signaling in cultures younger than Day 40, as well as the efficiency of modulating the neurocircuit activity by regulating the

GABAergic pathway. This iPSC-cortical neuron culture at earlier days thus potentially could provide an appropriate platform for modeling epilepsy or seizures, in which one or more parts of the brain has a burst of abnormal electrical signals that interrupt normal brain activity. Additionally, the usage of mixed inhibitory and excitatory neuronal co-cultures for CNS diseases, such as epilepsy, has previously been reported in the literature [92, 93]. To explore this potential application, neural activity was modulated chemically to induce and quiet epileptiform activity in immature, Day 21 cortical neurons (Figure 7). Neural activity was enhanced by addition of 100 µM bicuculine through blocking of GABAergic signaling, and subsequently quieted following the addition of the epilepsy suppression drug valproic acid (1 mM). Representative waveforms are shown in Figure 7A depicting baseline activity, the increase in firing following the addition of bicuculine and subsequent elimination of activity following dosage with valproic acid. Figure 7B is a graphical representation of the quantified firing frequencies normalized to the baseline activity, further confirming these results. This result demonstrated the applicability of this system for modeling epilepsy.

Discussion

This study aimed to establish a functional model of mature hiPSC-cortical neurons in a serum-free environment that could be used as a platform for in vitro preclinical drug testing. By integrating MEA technology, this system demonstrated the capability for LTP induction and neural disease modeling for epilepsy. A primary application would be that this system can be tailored to evaluate iPSC induced, patient-specific phenotypes for treatments for personalized medicine applications, as we show the ability to control the level of maturation and manipulate the phenotype

in a controlled fashion. The neuronal culture was characterized using immunocytochemistry, flow cytometry, and whole-cell patch clamp as well as on MEAs in an organ-on-a-chip system to determine functional maturity as the culture progressed to terminal differentiation that was free of glial cells. Neuronal activity on MEAs demonstrated the capability for LTP induction, as well as being conducive both chemical and electrical modulation, for the modelling of neural diseases and drug testing. Astrocytes and microglia can be added selectively in the cultures in future experiments to understand their influence on neuronal behavior and disease phenotypes.

This study demonstrated the longitudinal maturation process of iPSC-cortical neurons in vitro through the characterization of excitatory/inhibitory neuronal components, electrophysiological activity of individual neurons and neuron circuits. Immunocytochemistry and flow cytometry characterization during the maturation process indicating the gradual increase of the percentage of cortical neurons (by ctip2 and β-III Tubulin) and the decrease of neuroprogenitors (by GFAP). By Day 28, more than 90% of the cells were cortical neurons. Based on patch clamp analysis, the percentage of neurons firing spontaneously and those firing repetitive action potentials under depolarization increased over time, reaching ≥ 90% by Day 40 (Figure 3). Correspondently, the firing frequencies recorded by MEA analysis demonstrated gradual increases during a similar time period in culture. Our success in the differentiation of the iPSCs into a high level of maturity and function without the need for serum, astrocytes or conditioned medium is due to our long history of utilizing serum free, defined systems to culture pure populations of cells, including hepatocytes [94], cardiac cells [95, 96], motoneurons [97], skeletal muscle [98] as well as combination of the cells in multi-organ systems for up to 28 days [99].

Long-term potentiation (LTP) has been used in research as a quantitative measurement of cognitive functions related to learning and memory [100]. It is defined as the ability of neurons to retain sustained, elevated firing rates following electrical or chemical stimulation [37, 62, 101]. In vivo, LTP has been shown in mouse models as a measurement of cognition with respect to AD [70]. Specifically, they have utilized LTP absence and deficits as the main readout following dosage with amyloid-β_{42}, showing toxicity from plaque accumulation [72, 102]. The induction of LTP on MEAs has been shown previously in rat cortical neuron models [103, 104] as well as hiPSC derived cortical neurons with astrocytes and in serum-containing medium [105, 106]. This study demonstrated the ability of iPSC-derived cortical neurons cultured on MEAs to exhibit LTP without glia in a serum-free medium. The ability of the culture to display LTP allows for modelling of CNS diseases related to learning and cognitive dysfunction, which are essential functional markers in clinical settings for neurodegenerative diseases such as Alzheimer's disease [107], epilepsy [108], and autism spectrum disorder [109].

The iPSC-cortical neuron-MEA system provides an ideal, non-invasive, and less labor intensive approach than patch clamp electrophysiology to monitor neural activity, not only verifying the aforementioned chronological maturation of the neuronal activity of the culture, but also demonstrating controlled electrical and chemical modulation of this activity. Lidocaine, a Na^+ channel blocker and local anesthetic, [85], abolishes neuronal activity, while glutamate, induced increased neuronal activity. Additionally, NBQX, an AMPA receptor antagonist, was used to investigate the neural circuit properties. The significant decrease in activity following dosage with NBQX (Figure 5B) suggests that approximately 50% of the recorded spontaneous activity are from synaptic inputs of the AMPA receptors. Furthermore, systems that were dosed with

NBQX (Figure 5D) indicated a significant decrease in activity following LTP induction for both immediate and 24 hours after HFS (Figure 5C). Therefore, it can be inferred that the persistent LTP observed in our cultures is based on the synaptic networks formed between the cortical neurons.

One important issue of in vitro cultures is controlling and defining the status of iPSC-cortical neurons as excitatory or inhibitory, which ultimately influences the ability an individual neuron to fire action potentials and its capability of generating a cascade of neuronal firing seen in LTP models [110, 111]. In alignment with the dual-transmitter phenomenon observed in multiple types of neurons during early stages of brain development [112], immunocytochemical analysis revealed that cortical neurons younger than Day 40 co-stained for both the inhibitory and excitatory markers GABA and vGLUT1, respectively, while those older than Day 40 displayed almost a pure vGLUT1 composition. As a result, it was expected that overall neuronal activity in the early cultures would be low because of the presence of GABAergic neurons in the culture; while the more functionally mature cultures would be excitatory. This hypothesis was further reinforced by weekly whole-cell patch clamp and spontaneous MEA data, indicating that neural activity did not reach its peak until Day 40.

The $GABA_A$ receptor inhibitor picrotoxin was used to manipulate the immature cortical neurons for LTP induction and maintenance due to its ability to block inhibitory signal dispersion within the synapses [113, 114]. It was discovered that, while the exclusively glutamatergic culture at Day 40 could retain LTP induction, the mixed population of immature neurons could not maintain the elevated firing rates after one hour, but could if the GABAergic inhibition was

removed by picrotoxin. This study highlights that controlling the maturation level and inhibitory component of the culture influences its synaptic capabilities important for in vitro LTP modeling.

Epilepsy is a chronic condition and occurs most commonly during childhood, and sometimes resolves of its own accord at the time of puberty. Our cortical neuron cultures younger than Day 40 had a significant amount of GABAergic signaling, and blocking this inhibitory component was shown to dramatically increase neural activity. It is hard to conclude from this study whether the high occurrence of epilepsy in young population is linked to a dysfunctional inhibitory signaling in the CNS, but the immature iPSC-cortical neuron culture could provide a valuable platform for simulating epilepsy by altering the inhibitory mechanism. Bicuculline has been previously observed in vitro to induce erratic firing deemed epileptiform activity, while valproic acid is used as a common anti-epileptic [106, 115-117]. Currently, the animal models of epilepsy are induced using compounds kainic acid [106, 118], pilocarpine [118], and bicuculline [106]. While there has been a recent shift toward modeling epilepsy in vitro using human cells to compensate for the lack of species competency in these animal models, the optimization of the neuronal culture maturation and its capability in reproducing physiological and pathological properties is still a work in progress [63, 93, 119]. To develop an epilepsy model using these iPSC-derived cortical neurons, the effects of bicuculline was evaluated on immature cortical neuron cultures (Figure 7), because its working mechanism is to inhibit the GABAergic pathway by blocking $GABA_A$ receptors to regulate the balance of excitatory and inhibitory signals [120]. Subsequently, valproic acid enhances GABA transmission by inhibiting the degradation of GABA [121]. It was observed that bicuculline was sufficient to induce an epileptic-like increase in activity

in neuronal cultures, and that the activity could subsequently be abolished following dosage with valproic acid.

The inherent co-expression of excitatory and inhibitory neurotransmission is potentially adaptable to other models that rely on this interplay such as autism spectrum disorder [122], alcoholism [123], depression, and anxiety. These models could be adapted to our system due to its ability to measure electrical activity and study both short and long-term effects of compounds.

In summary, the iPSC-cortical neuron model exhibited the inhibitory to excitatory conversion during maturation process. By integrating with the MEA technology, it demonstrated functional neurocircuit formation without the need for added glial cells, especially the capacity to recapitulate LTP induction, which is an essential mechanism for neural plasticity and cognitive capability in neurodegenerative diseases such as dementia. It also reproduced the phenotype for epilepsy. These non-invasive functional human diseased systems would provide more clinically translatable platform for drug testing. They are also potentially applicable to investigate drug interactions and off-target toxicity when adapted into a multi-organ-on-a-chip system, for either acute or chronic effects.

Materials and Methods

hiPSC-Cortical Neuron Differentiation

The differentiation of cortical neurons from hiPSCs consisted of a timeline of three stages, starting out with the use of small molecules, and ending with an array of neuron-specific factors. HiPSCs (Coriell ND41865) were first grown to 90% confluence in mTESR1 culture medium (Stemcell Technologies 85850) on a surface coated with Corning matrigel matrix (Corning Life Sciences

354230) diluted in DMEM F12 (Fisher Scientific 21041-025). To induce the differentiation, cells received a full media change and then fed every other day with Differentiation Medium I, Differentiation Medium II, and Differentiation Medium III, according to the differentiation timeline featured in Figure 1A. Differentiation Medium I consisted of N2B medium (equivalent to DMEM F12 with insulin (Millipore Sigma 407709) 20 µg/ml and 1X N2 supplement (Fisher Scientific 17502048)) supplemented with 6 µM SB431542 (Tocris 1614), 0.1 µM LDN193189 (Fisher Scientific 605310), 2 µM DMH-1 (TOCRIS 4126), and 10 ng/mL recombinant human DKK-1 protein (Fisher Scientific 5439-DK-010). Differentiation Medium II consisted of N2B medium supplemented with 6 µM SB431542, 0.1 µM LDN193189, 2 µM DMH-1, and 5 µM cyclopamine (Sigma 239803-1MG). Lastly, Differentiation Medium III (also referred to as "Maintenance Medium") consisted of Neurobasal (Fisher Scientific 21103049), supplemented with 1X Glutamax (ThermoFisher 35050-061), 1X N-2 supplement (Fisher Scientific 17502048), 1X B27 without Vitamin A (Fisher Scientific 12587-010), 20 ng/mL BDNF (Cell Sciences CRB600D), 20 ng/mL GDNF (Cell Sciences CRG400E), 200 nM Ascorbic Acid (Sigma Aldrich A4403), 1 µM cAMP (Sigma A6885), 1 µg/mL Laminin (Fisher Scientific 23017015), and 1X Antimycotic-Antibiotic (Fisher Scientific 15240062).

Culture Surface Coating for Cortical Neurons: DETA Surface Coated with Poly-L-Ornithine/Laminin Protein Adsorption Surface Coating

The surface for coverslips was first coated with self-assembled monolayer (SAM) DETA as described in [124]. Further surface modification on DETA coated surfaces was achieved by immersing the coverslips in 0.01% Poly-L-Ornithine (PLO) (Sigma Aldrich 27378-49-0) at room

temperature for 2 hours. They were then rinsed 3 times with 1X PBS (Fisher Scientific 70013-032), followed by the addition of 3.33 μg/mL laminin diluted in 1X PBS. Surfaces were left at 4°C overnight, and subsequently warmed at 37°C for 1 hour prior to the removal of laminin for cell seeding. Patterned surface on MEA was generated by the photolithography combining cell permissive SAM DETA and nonpermissive SAM PEG [125]. The patterned surface was further coated with PLO/Laminin as described above.

Cortical Neuron Plating and Maintenance

Following differentiation, cortical neurons were harvested using 0.05% Trypsin-EDTA (ThermoFisher 15400054) and neutralized by Trypsin inhibitor (Fisher Scientific 17-075-029). Cortical neuron stocks were cryopreserved in 10% DMSO (Sigma Aldrich D4540). Individual vials were thawed using a drop-by-drop method with cold 1X PBS. Cells were then centrifuged at 260g for 3 minutes, and seeded on coverslips at a plating density of 150 cells/mm^2 and on MEAs at 500 cells/mm^2. Cells were and maintained for one week in Maintenance Media. After one week, cells were further maintained in BrainPhys Neuronal Media Kit with SM1 and N2 Supplement A (Stemcell Technologies 05793) that was further supplemented with 20 ng/mL BDNF, 20 ng/mL GDNF, 200 nM Ascorbic Acid, 1 μM cAMP, 0.5 μg/mL Laminin, and 1X Antimycotic-Antibiotic. Cell maintenance consisted of a half-media change twice weekly from the time of seeding for the duration of the culture.

Immunocytochemistry

Cells were fixed in 4% paraformaldehyde for 15 minutes followed by three washes with 1X PBS. Cells were permeabilized in 0.1% Triton for 10 min and subsequently blocked 1 hour in a blocking buffer solution containing 0.5% BSA and 5% goat serum diluted in 1X PBS, then incubated with primary antibodies diluted in blocking solution at 4°C overnight. Primary antibodies used for characterization included vGLUT1 (Sigma Aldrich AB5905), GABA (Sigma Aldrich A2052), Beta-III Tubulin (Millipore AB9354), GFAP (Sigma Aldrich AB5804), Synaptophysin (abcam ab8049), PICK1 (Santa Cruz 9541), NMDAR1 (ThermoFisher MA1-2014), and GLUR1 (Millipore AB1506). Following rinsing, coverslips were then incubated with secondary antibodies diluted at 1:250 in blocking solution at room temperature for two hours. Coverslips were then washed and mounted using a Gold Antifade Reagent with DAPI (Fisher Scientific P36931) and imaged on a spinning disk confocal microscope.

Flow Cytometry

Cells were lifted using accutase (ThermoFisher 00-4555-56) and resuspended following centrifugation in FACS buffer containing 1% BSA diluted in PBS. Further methodology for this method is described in Patel et al [126]. Cytometry analysis was performed for the following antibodies: Live-Dead (using Draq7), ctip2, Beta-III Tubulin, and GFAP. Expression levels were determined by gating based on fluorophore wavelengths for cells of interest (live cells excluding dead cells and debris).

Whole-Cell Patch Clamp Electrophysiology

Measurement of spontaneous firing, repetitive firing, and ionic currents were achieved through whole-cell patch clamp. Each experiment was repeated 3 times per timepoint, and 3 cells were patched per experiment for a total of 9 cells per data point. Cells were recorded in a recording chamber filled with Brainphys medium (buffered with 10 mM Hepes with ~300 mOsm/ kg, maintained at room temperature (22-25^{o}C). Patch clamp methodology was performed as described in Caneus et al [62].

Microelectrode Array Recordings and LTP Induction

Cells were cultured on custom TiN electrode chips containing 10 electrodes, each 80 μm diameter, spaced at between 1000 and 1500 μm. The chips were coated with DETA [127] followed by a Poly-L-Ornithine (PLO) and laminin protein adsorption coating. Cells were seeded at a density of 500 cells/mm^2 and maintained for 28 days before neuronal activity could be recorded using a Multi-Channel Systems (MCS) rig. Spontaneous activity was recorded for 5 minutes prior to the induction of long-term potentiation (LTP) via electrical stimulation using a high-frequency stimulation (HFS) protocol: 10 repetitions of 4X biphasic 500mV, 5ms pulses [69]. All recordings were taken for a duration of 5 minutes unless otherwise specified.

MEA Recording Analysis

Analysis of waveform shape and firing rate were done by filtering raw data with a 100 Hz high-pass filter and superimposing all spikes surpassing -5 standard deviations from the mean of the

noise [128]. Raw electrode data recorded from customized MEA chips was filtered using a Butterworth 2nd order 100Hz high-pass filter. Subsequently, spikes occurring at the same microsecond on more than two electrodes were deemed as artifacts and removed. Artifacts were identified and removed by filtering out events that occurred at the same timestamp across multiple electrodes. It has been observed that transient noise effects tend to co-occur simultaneously across multiple electrodes, whereas coupled biological events (such as co-firing neurons) co-occur at timestamps that are very close, but which are not identical to each other. Removing events across multiple electrodes with the same timestamp has not been observed to impede the detection of biological activity, as identified by identifying the activity that is removed when neural signaling is abolished by administration of a compound such as lidocaine. Following filtering, electrodes with a firing frequency lower than 0.1Hz were removed from analysis. The statistical analysis was performed on data collected over at least 3 independent experiments, with specific statistical methodology indicated in the manuscript. These include one-way ANOVA followed by Fisher's LSD and Student's T test, depending on the experimental design for each dataset.

Compound Preparations

All compounds except lidocaine were prepared in 0.1% DMSO diluted in BrainPhys Neuronal Medium at a working concentration of 10X final desired concentration. Lidocaine was dissolved in sterile water. Compounds used for chemical modulation of neuronal activity included glutamate (Aldrich 855642), lidocaine HCl (Sigma L5647), NBQX (Tocris 0373), picrotoxin (Tocris 1128), bicuculine (Sigma 14340), and valproic acid (Sigma P4543-25G).

Figures

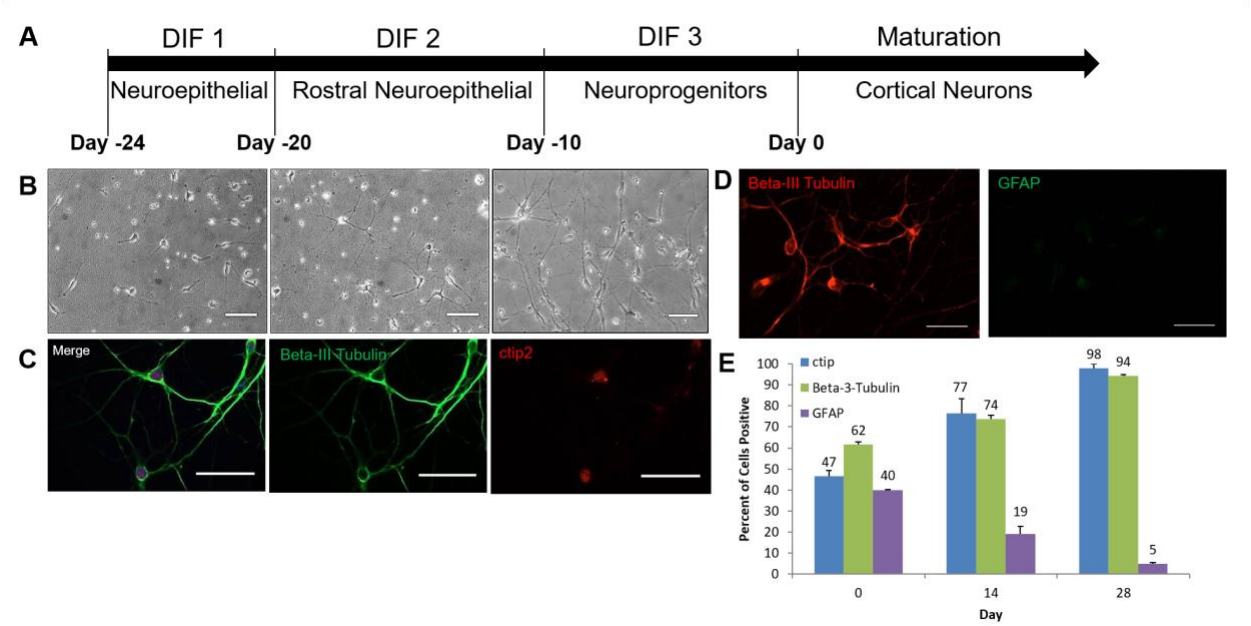

Figure 1: **Characterization of hiPSC-cortical neuron maturation via phase microscopy, immunocytochemistry, and flow cytometry**. A) Timeline detailing the differentiation process from hiPSCs to cortical neurons. B) Phase images depicting cell morphology on Day 7 (left), Day 14 (middle), and Day 40 (right). C-D) Immunocytochemistry of cortical neurons stained for β-III Tubulin and ctip2 (D40) in (C) and for β-III Tubulin and GFAP(D28) in (D). E) Graph of flow cytometry data on Days 0, 14, and 28 illustrating neuron maturation by the expression of layer V cortical neuron marker ctip2, neuronal marker β-III Tubulin, and glial cell marker GFAP, Error bar: SEM. N = 3 independent experiments. Scale bar = 50 μm.

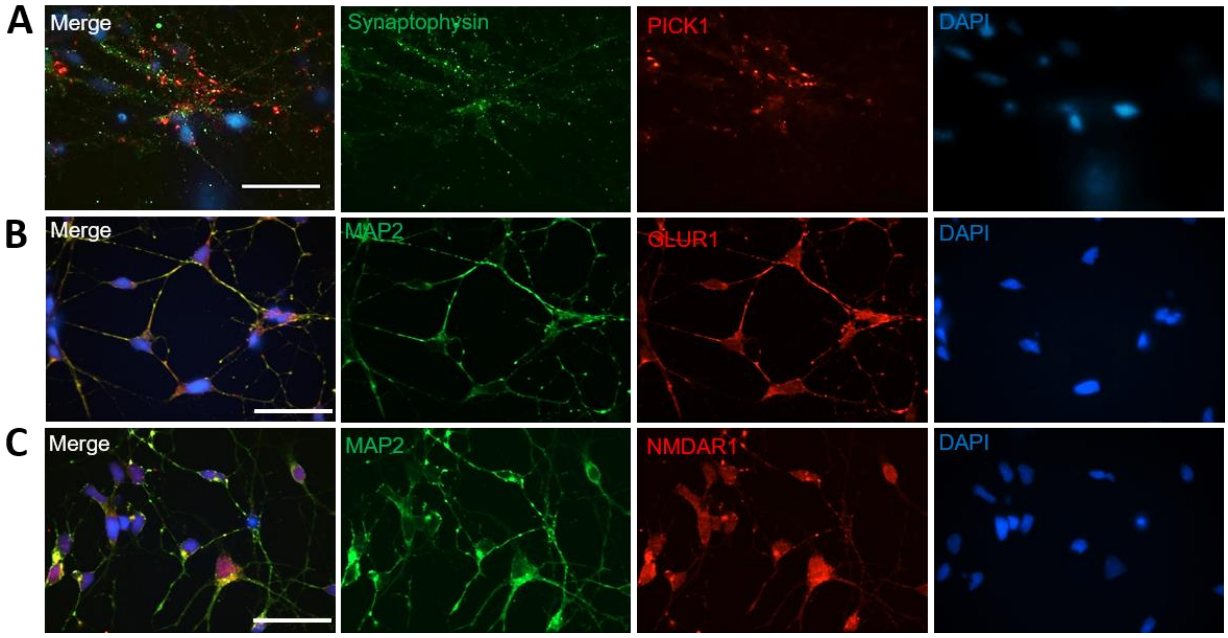

Figure 2: **Characterization of mature hiPSC-cortical neurons (D40) via immunocytochemistry.** A-C) Immunocytochemistry of Day 40 cortical neurons stained for pre-synaptic marker Synaptophysin post-synaptic marker PICK1 (A), for neuronal microtubule marker MAP2 and AMPA receptor marker GLUR1 (B), and for neuronal microtubule marker MAP2 and NMDA receptor marker NMDAR1. Scale bar = 50 μm.

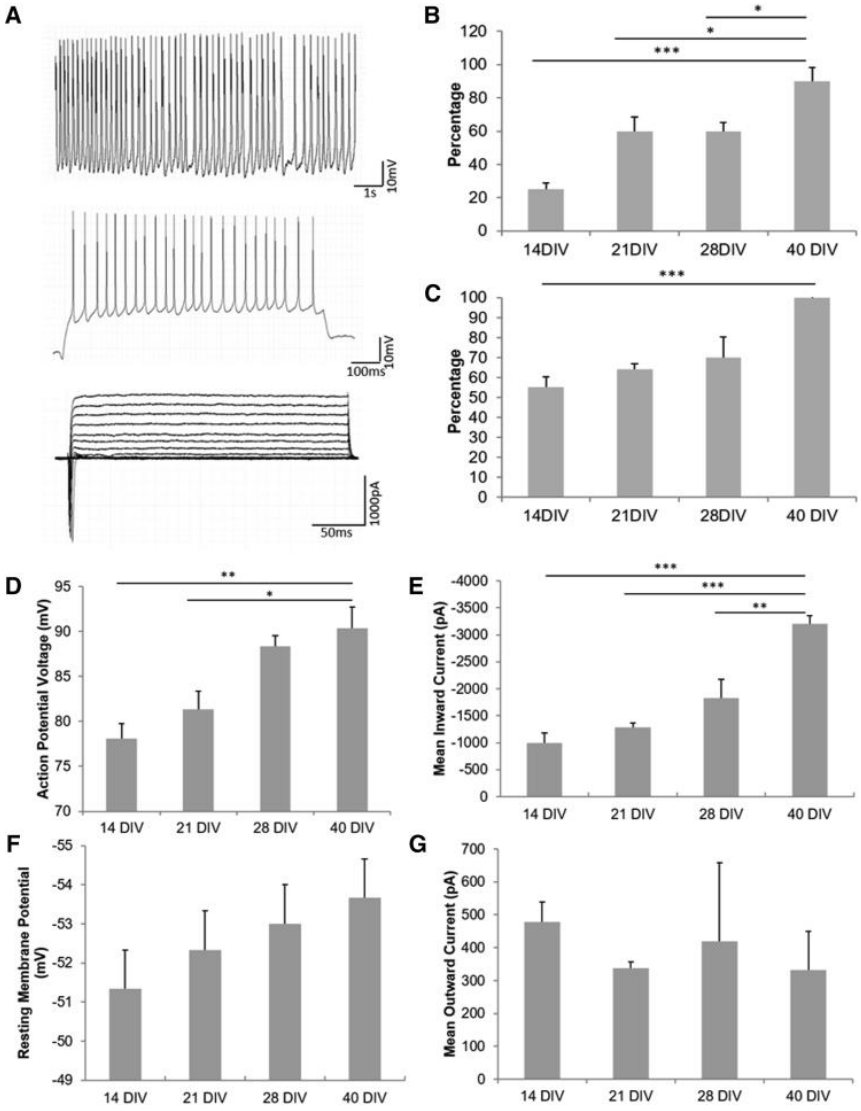

Figure 3: **Electrophysiological characterization of hiPSC-cortical neurons via whole-cell patch clamp.** A) Representative traces of spontaneous firing (top), depolarization-induced repetitive firing (middle), and Na+ and K+ currents (bottom) recordings from Day 40 neurons. B-C) Percentage of cells experiencing spontaneous firing (B) and repetitive firing (C), indicating maximal activity at Day 40. D-E) Quantification of action potential voltage (D), mean inward Na+ current (E), indicating maximum level at Day 40.F-G) Quantification of resting membrane potential (F) and mean K+ outward current (G). Statistical analysis was performed using one-way ANOVA followed by Tukey's test, * $p<0.05$, ** $p<0.01$, *** $p<0.001$. Error bar: SEM. N = 9 cells total from 3 independent experiments.

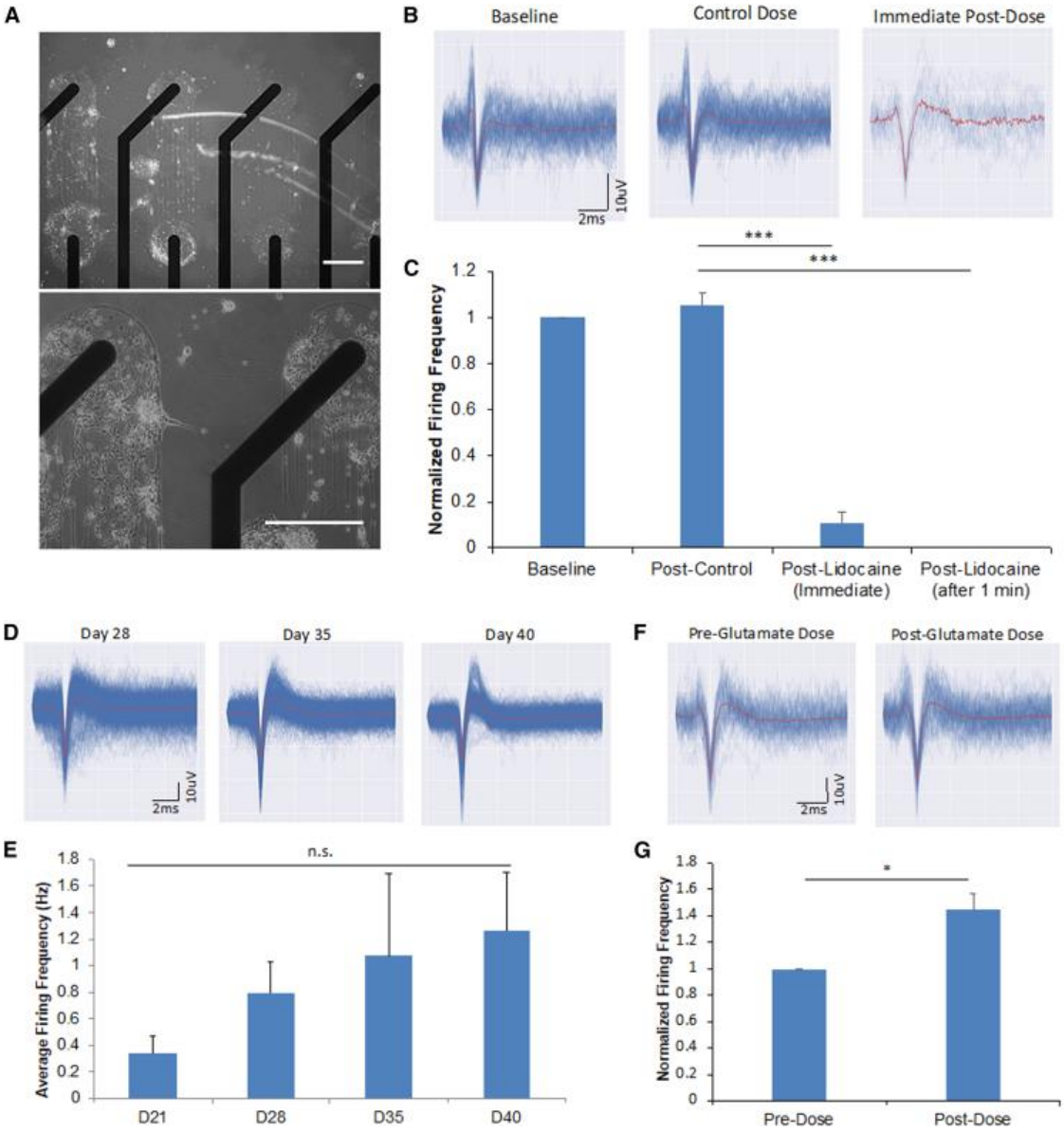

Figure 4: **Microelectrode array (MEA) neuronal patterning and signal validation. A) Phase images showing neuronal patterning on electrodes at day 40.** B) Representative waveforms of spontaneous activity on a single electrode on day 75 at baseline, immediately following vehicle control, and with 1mM lidocaine. C) Graphical representation of neuronal firing frequency during the lidocaine dosing experiment outlined in B. D) Representative waveforms of spontaneous activity on a single electrode on days 28, 35, and 40 indicating increasing maturation. E) Quantification of MEA recordings indicating neuronal firing frequency during cortical neuron maturation over 40 days. F) Representative waveforms of spontaneous activity on a single electrode on day 75 during pre- (left) and post-dosage (right) with 100μM glutamate. G) Graph representation of neuronal firing frequencies during the glutamate dosing experiment outlined in F. Statistical analysis was performed using one-way ANOVA followed by Tukey's test or Student's t-test, * $p<0.05$, ** $p<0.01$, *** $p<0.001$. Error bar: SEM. Scale Bar = 50 μm.

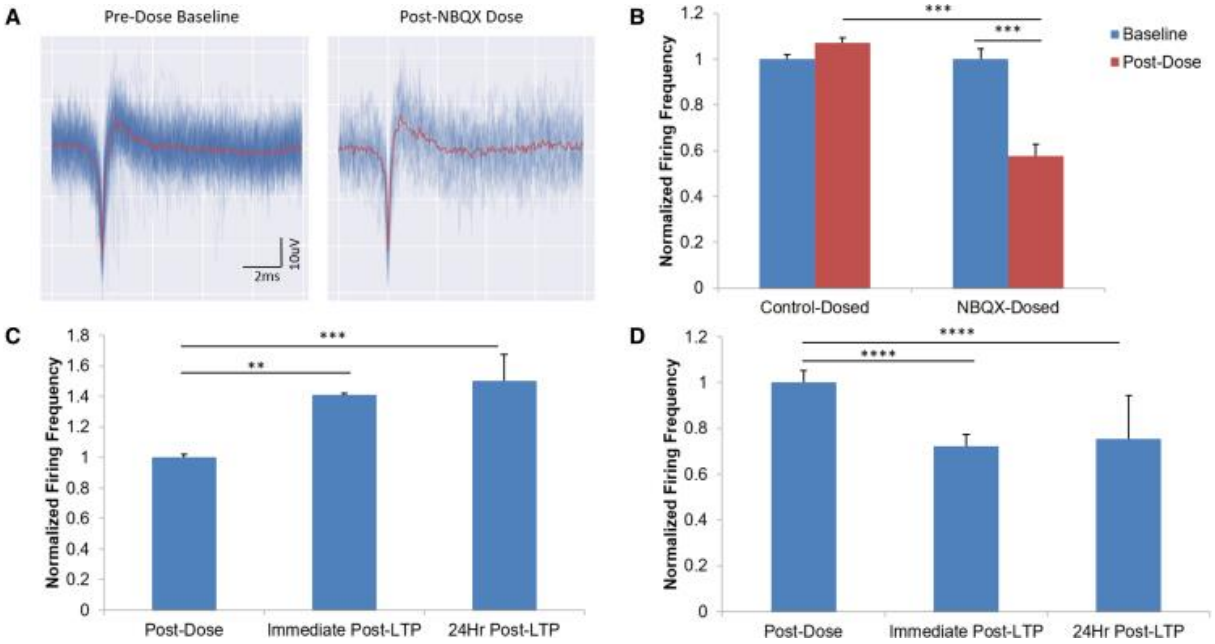

Figure 5: **Microelectrode array recordings confirming synaptic connectivity via dosage with NBQX and LTP induction.** A) Representative waveforms of spontaneous activity on a single electrode on Day 75 during pre- (left) and post-dosage (right) with 25 µM NBQX. B) Graph representation of neuronal firing rates normalized to baseline activity before and after control 0.1% DMSO or 25 µM NBQX dose. C) Graph of normalized firing rates of control dose of 0.1% DMSO, and following LTP stimulation immediately and 1 hour after dosage, normalized to post-dose, pre-LTP baseline. D) Graph of normalized firing rates of 25 µM NBQX-dosed, and following LTP stimulation immediately and 1 hour after dosage, normalized to post-dose, pre-LTP baseline. Statistical analysis was performed using using a Kruskal-Wallis test followed by Dunn's multiple comparisons test, * $p<0.05$, ** $p<0.01$, *** $p<0.001$, ****$p<0.0001$. Error bar: SEM. N = 10 electrodes from 3 individual experiments.

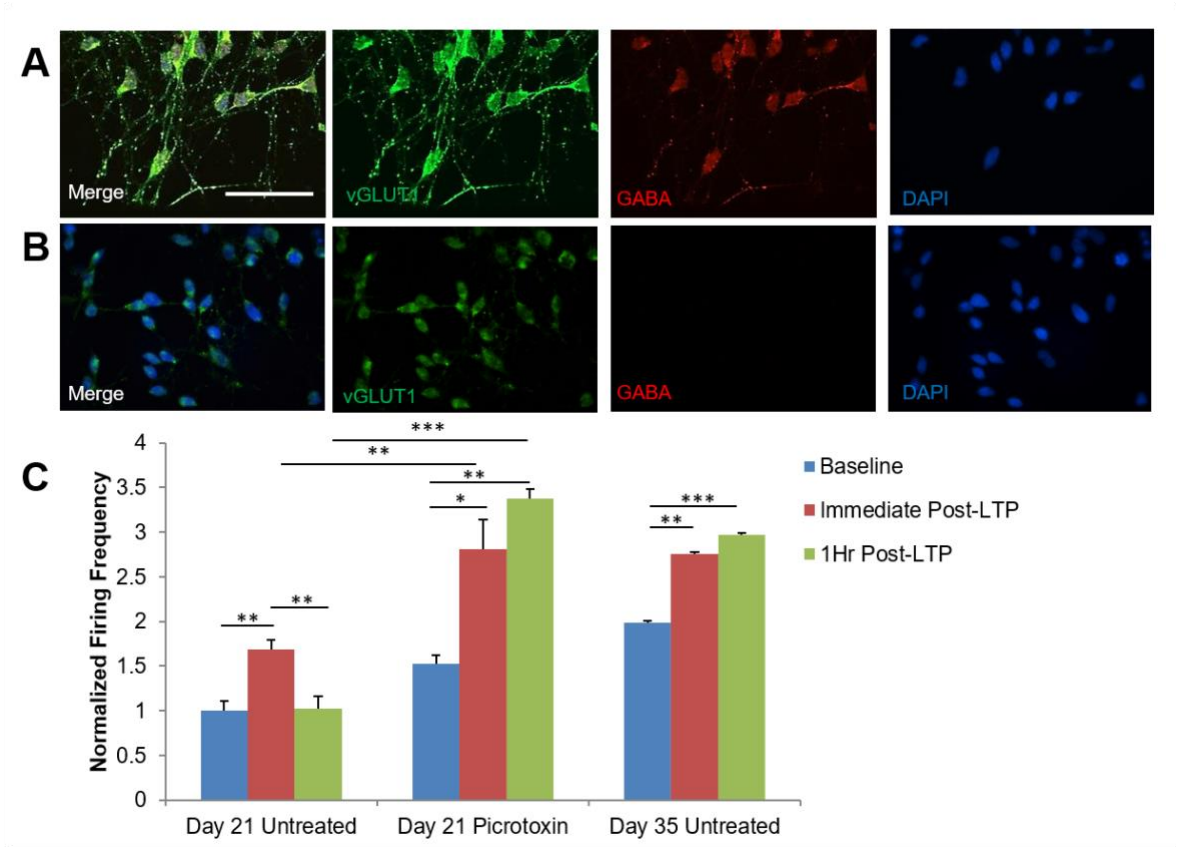

Figure 6: **Confirmation of excitatory and inhibitory character in mature and immature iPSC-cortical neurons.** A-B) Immunocytochemistry cortical neurons stained for vGLUT1 (green) and GABA (red) indicating the neurons are expressing both excitatory and inhibitory markers at Day 21 (A), but are typically glutamatergic at D 40. C) Quantitative MEA analysis of LTP induction for Day 21 and D35 neurons. LTP induction in D21 neurons did not persist in after 1 hour when dosed with vehicle control but did so when dosed with 100 µM picrotoxin prior to LTP induction, while was similar to those observed in innate Day 35 neurons without any picrotoxin addition. All the data were normalized to the Day 21 undosed baseline. Statistical analysis was performed using one-way ANOVA followed by Tukey's test, * $p<0.05$, ** $p<0.01$, *** $p<0.001$. Error bar: SEM. Scale bar = 50 µm, N = 10 electrodes from 3 individual experiments.

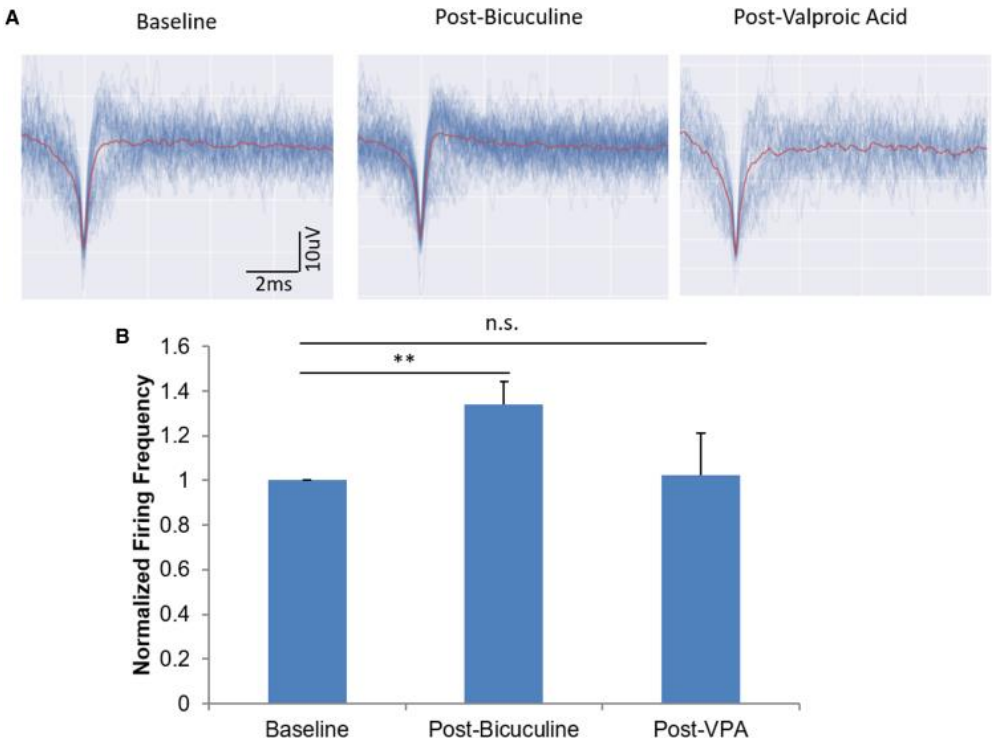

Figure 7: **The induction and quieting of epileptiform activity via dosage with bicuculine and valproic acid in immature (21 DIV) cortical neurons.** A) Waveform representations of baseline activity (left), 100 µM bicuculline dosed (middle), and 1 mM valproic acid (right)-dosed systems. B) Graphical representation of immature the firing rates normalized to baseline. Statistical analysis was performed using one-way ANOVA followed by Tukey's test, * $p<0.05$, ** $p<0.01$, *** $p<0.001$. Error bar: SEM. N = 10 electrodes from 3 individual experiments.

CHAPTER THREE: A HUMAN-BASED AD MODEL UTILIZING HIPSC-DERIVED CORTICAL NEURONS ON MEAS FOR HIGH THROUGHPUT DRUG SCREENING

Introduction

Today, a majority of prospective new drug candidates that showed great promises in preclinical studies failed in clinical trial [129-133]. This disparity can be attributed in part to the types of experimental models used during preclinical studies for assessing drug safety and efficacy [134, 135]. These shortcomings, especially as they are related to the limitation of biological models, underscore the urgent need to develop better approaches and models that will improve the drug discovery and development process. To date, animal models are the most commonly used models for scientific research and drug screening at the preclinical stage [129]. While animal models are vital and play key roles in scientific research, they are, however, limited due to interspecies differences, which can lead to many inconsistencies in basic research, preclinical assessment, and clinical trials [136-139]. For instance, many diseases, such as AD, which is associated with APP/Aβ, Tau and APOE dysregulation, are affected by several genetic factors. As such, it is very difficult to establish human-specific disease models using other organisms [140, 141]. Therefore, the need to have more suitable and compatible models that can better replicate human disease physiology and phenotypes and predict drug effects (e.g., toxicity, efficacy) is of the utmost importance.

Advances in the development and utilization of human cells derived from induced pluripotent stem cells (iPSCs) now offer a unique opportunity to create more appropriate biological systems to model human diseases for in vitro study [142-145]. Further, those models, when

incorporated with other technologies, such as microelectrode arrays (MEAs), have the potential to be even more significant by offering advantages to developing better preclinical and functional models for drug screening [146] [147]. Additionally, progressions made in biomaterials have now made it possible to design and create physiologically-relevant microphysiological systems (MPS) [148, 149] that provide a more relevant and representative human-based platform for accelerated and large-scale drug testing of potential drug candidates and a path for early therapeutic interventions [145].

Using cortical neurons derived from human induced pluripotent stem cells incorporated with microelectrode array (MEA) technology, we developed a more compatible micro-physiology system (cortical-HoAC) to study certain aspects of AD in vitro [150, 151]. Previously, using the systems to assess neuronal cell functions, we demonstrated that the application of $A\beta_{42}$ and Tau oligomers to hiPSC-derived neuronal cultures resulted in pronounced deficits in stimulus-induced LTP maintenance [150]. Those results, which were also confirmed by patch clamp electrophysiology, are significant partly because they illustrated the capability of the system to reproduce aspects of AD neuropathology. Moreover, they highlighted the system prospect as a potential tool for long-term drug testing.

To evaluate the system's capacity to assess the therapeutic effects of AD-related drugs and its potential as a prospective tool in drug development, cortical human-on-a-chip (HoaC) systems were established and treated with $A\beta_{42}$ oligomers and different classes of AD-based drugs, which included Donepezil, Memantine, Rolipram and Saracatinib. Following $A\beta_{42}$ and drug dosing, the functional activity and LTP maintenance of the cortical neurons were examined. The results

revealed a pronounced decrease in cell activity within 1hr of $A\beta_{42}$ dosing, which was blocked by co-administration of $A\beta_{42}$ oligomers and AD drugs simultaneously. These results underline the significance and potential of the system as an applicable tool in the drug development process, which can be employed to quickly analyze promising therapeutic compounds for translation to clinical trials. Moreover, this system provides a foundation for the development of higher order, more complex models, which can be used to not only study the drug effects, but also the mechanism of action of the drugs as well.

Results

Analysis of iPSC-derived cortical neurons for the expression of AD drug targets

Several AD-related drugs from different drug classes, including Donepezil, Saracatinib, Memantine and Rolipram were used in this study. Currently, Donepezil, Memantine, and Rolipram are all FDA-approved drugs for the treatment of AD. Donepezil targets and binds to acetylcholinesterase enzyme (AChE), subsequently preventing it from catalyzing the hydrolysis of the neurotransmitter acetylcholine (ACh). Memantine binds to the NMDA receptor and blocks the channel from opening and sequentially cell excitotoxicity by glutamate. Rolipram inhibits the excessive degradation of cyclic AMP (cAMP) in the presence of Aβ42 by inhibiting the enzyme phosphodiesterase type 4 (PDE4) that catalyzes its breakdown. Lastly, Saracatinib binds to Fyn and block its action (i.e., to phosphorylate and activate other proteins). To determine whether the drugs targets (e.g., Fyn, NMDAR, AChE, nAChRand PDE4) are expressed in the cortical neurons, the cells were fixed and stained with specific antibodies for each marker followed by microscopy analysis. Figure 8 illustrates neuronal morphology (Figure 8B) and alignment on patterned MEA

chips (Figures 8A-8C). Additionally, the cells were stained positive for all the markers, including PDE4 (Figure 8D), Fyn (Figure 8E), AChE (Figure 8F), nAChR (Figure 8G) and NMDAR (Figure 8H).

Analysis of AD-based drugs' effects on Aβ oligomers-induced electrophysiological dysfunction in hiPSC-derived cortical neurons

To assess the capacity of the system for evaluating drug effects and its competence as a prospective tool for drug sceening and development, iPSC-derived neuronal cells were plated on both coverslips and the HoAC systems and maintained for 28-35 days in culture prior to testing. On the day of testing the cells were dosed with either $A\beta_{scr}$ oligomers (5μM), $A\beta_{42}$ oligomers (5μM) alone or $A\beta_{42}$ oligomers co-administered with AD-related drugs followed by incubation. At 1h (HoAC) and 24h (patch) post-dosed, neuronal function was recorded and analyzed. Patched cortical neurons displayed a marked decrease in cellular activity, including a decrease in sodium currents (Figure 9A), lower or lack of induced (Figure 9B) and membrane potential (Figure 9C) in the samples treated with $A\beta_{42}$ oligomers relative to samples treated with $A\beta_{scr}$ or co-treated with $A\beta_{42}$ oligomers together with AD-based drugs at 24h post-treatment. To examine cell activity with the cortical-HoAC systems, first, the baseline (i.e., spontaneous) activity (Figure 9D) was taken prior to dosing followed by stimulation using a high frequency stimulation (HFS) to induce LTP (Figure 9E). Immediately after stimulation and recording, the cells were dosed and incubated for 1h. LTP induction and maintenace were determined by measuring and comparing cell activity taken immediately after and at 1h post-stimulation (Figure 9F) relative to baseline activity in both samples dosed with Aβ oligomers only or in combination with AD-related drugs. As shown in

Figure 9, the cells exhibited a pronounced increase in cell firing from baseline activity following stimulation. The induced activity was grealty abolished in $A\beta_{42}$-oligomers-treated samples but continue to be maintained in $A\beta_{scr}$- and $A\beta_{42}$+AD drug treated samples (Figure 9E).

Deficits in cell firing caused by Aβ42 oligomers in iPSC-derived cortical neurons is blocked by Donepezil

A reduction in acetylcholine neurotransmitters in the brain, due in part to its breakdown and degradation by the actetylchonlinesterase enzyme, has been implicated in the development and/or progression of Alzheimer's disease pathogenesis [152, 153]. Donepezil is an acetylcholinesterase inhibitor drug and has received FDA approval for the treatment of AD [153]. To evaluate the cortical-HoAC system proficiency to assess drug effects and its potential as a prospective tool for drug screening, the effect of Donepezil was analyzed in this system for its therapy of AD-relevent phenotypes, which is generated by $A\beta_{42}$ oligomers as desribed above. Donepezil was used together with $A\beta_{42}$ oligomers to dose neuronal cultures. The effects of $A\beta_{42}$ and Donepezil on hiPSC-derived cortical neuron activity were measured both extracellularly using our cortical-HoAC systems and intracellularly by patch electrophysiology at 1h and 24h post-treatment respectively. As the results shown in Figure 10, the administration of $A\beta_{42}$ oligomers to the cultures resulted in a stark decrease in cell firing potential. Notably, a significant decrease in both sodium and potassium currents was observed in cells exposed to $A\beta_{42}$ oligomers compared to $A\beta_{scr}$ oligomer-treated cells (Figure 10A). Additionally, the data revealed a pronounced reduction and sometimes a complete lack of activity of both action potential and spontaneous firing in the cells dosed with $A\beta_{42}$ oligomers relative to samples dosed with $A\beta_{scr}$ oligomers or co-treated with $A\beta_{42}$ and

Donepezil (1µM) simultaneously (Figure 10B-10D). Electrical stimulation of hiPSC-derived cortical neurons in the cortical-HoAC systems resulted in a significant increase in cell activity (i.e., firing frequency). Comparable to the samples dosed with $A\beta_{scr}$, the addition of Donepezil together with $A\beta_{42}$ oligomers to the cultures blocked the $A\beta_{42}$-induced neurotoxic effects and preserved the stimulus-induced cell activity (Figure 10E).

hiPSC-derived Cortical neurons retained normal electrical function following co-treatment with Saracatinib and beta amyloid (Aβ42) oligomers

To further investigate the neuroprotective effects of Saracatinib against $A\beta_{42}$ oligomers neurotoxicity and confirm the cortical-HoAC results, the cells were plated on coverslips and treated with Aβ oligomers with or without the Saracatinib treatment in parallel experiments. The neuronal functional activity was measured intracellularly by whole cell patch electrophysiology. Comparable to the results obtained with the HoAC systems, the addition of $A\beta_{42}$ oligomers to the cortical cultures resulted in prominent cell dysfunction within 24h post-dosing, including reduced currents (Figure 11A), induced potential amplitude (Figure 11B) and spontaneous firing (Figure 11C-D) compared to $A\beta_{scr}$-treated samples. In sum, the data suggests some protective effects by Saracatinib against $A\beta_{42}$ toxicity in cortical cultures. To investigate whether Saracatinib offers some protective effects against $A\beta_{42}$-induced neurotoxicity, cortical-HoAC systems were established and co-treated with Saracatinib together with $A\beta_{42}$ oligomers. The cells were dosed with either $A\beta_{scr}$ or $A\beta_{42}$ oligomers with or without Saracatinib (10nM) immediately after stimulation, followed by incubation at 37°C and 5% CO_2. Subsequently, at 1h post-dosing and incubation, the systems were tested for cell activity. As indicated in Figure 11E, the cells exhibited

a significant increase in firing frequency from baseline activity following stimulation (PostStim). The induced activity was significantly diminished in the samples dosed with $A\beta_{42}$ oligomers relative to $A\beta_{scr}$-treated samples at 1h post-dosed. However, simultaneous administration of Saracatinib together with $A\beta_{42}$ oligomers inhibits the $A\beta_{42}$-induced deficits in cell firing and preserved the induced cell activity in the $A\beta_{42}$-drug treated samples compared to $A\beta_{42}$ only treated samples (Figure 11E). Further, these findings highlight the potential of the cortical-HoAC system to assess drug effects on neuronal cultures and its potental as a prospective tool for use in the drug development process.

Effects of Memantine on AB42-induced neurological defects in iPSC-derived neuronal cells activity

To further evaluate the effects of Memantine on $A\beta_{42}$-induced cell defects, the cell were treated for 24hrs and analyzed by whole-cell patch electrophysiology. Based on the results demonstrated in Figure 12, the application of $A\beta_{42}$ oligomers to the cultures greatly abolished most of the neuronal activity, including cell currents (Figure 12A), induced potential amplitude (Figure 12B) and spontaneous firing (Figure 12C-D), in comparison to samples treated with Aβscr or co-treated with Aβ42+Memantine.To assess the protective effects of Memantine in AD and against the neurotoxic effects of $A\beta_{42}$ oligomers, neuronal cell cultures (both cortical-HoaC systems and coverslips) were established and maintained for 28-35 days in culture prior to testing. On the day of treatment and testing, the systems were dosed either with AB_{scr}, $A\beta_{42}$ oligomers alone or $A\beta_{42}$ plus Memantine following stimulation. Subsequently, after 1h post-dose and incubation at 37°C and in 5% CO_2, the samples were tested and analyzed for cellular activity. The results

demonstrated a marked increase in cell firing frequency from baseline recording following stimulation in all the samples (Figure 12A). Whereas the samples treated with $A\beta_{scr}$ oligomers continued to maintain this activity at 1h after dosing, the samples treated with $A\beta_{42}$ oligomers demonstrated a prominent decrease in cell activity from post-stimulation recording. However, although not statistically significant, Memantine demonstrated an ability to inhibit the $A\beta_{42}$-induced deficits in cell activity (Figure 12A). In all, these findings show the effects of Memantine to block some Aβ42-induced neurotoxicity and indicate the ability and potential of the system to measure drug effects.

Co-treatment of hiPSC-derived cortical neurons with Rolipram suppresses the neurotoxic effects of Aβ42 oligomers on electrical function

Rolipram hampers the degradation of intracellular cAMP by inhibiting phosphodiesterase type 4 (PDE4) [154]. An increase in intracellular cAMP levels has been cited to increase the action potential frequency of excitatory cholinergic neurons. Whole-cell patch clamp results revealed the potential of Rolipram to prevent neurotoxic effects of $A\beta_{42}$. Though not significant, the co-administration of Rolipram along with $A\beta_{42}$ oligomers for 24hrs blocked sodium current deficits observed in $A\beta_{42}$ only condition (Figure 13A). Rolipram did, however, significantly block deficits in spontaneous firing frequency and amplitude (Figure 13B-D) [155]. To evaluate the neuroprotective abilities of Rolipram against $A\beta_{42}$, cortical-HoAC systems were first maintained for 28-35 days. For treatment and evaluation, the systems were stimulated via HFS following baseline recording, then dosed and incubated at 37°C and in 5% CO2 prior to assessment of LTP persistence at 1hr. Rolipram was observed to have neuroprotective effects, as co-administration of

Rolipram with $A\beta_{42}$ oligomers caused a highly significant increase in the neuronal event rate at 1h following LTP, consistent with the persistent LTP observed in the $A\beta_{scr}$ treated condition. In contrast, the systems dosed with only $A\beta_{42}$ oligomers had a significant decrease in activity at 1hr post-stimulation (Figure 13E). Overall, Rolipram was observed to inhibit the neurotoxic effects of Aβ42 oligomers in a matter consistent with the mechanism of action of the drug.

Discussion

The drug discovery and development process has been an area of great interest to scientists both in academia and pharmaceutical companies [156-158]. Yet, despite the significantly large investments being dedicated towards drug discovery and development [159-162], the process remains stagnant and inefficient, with less than 15% of all promising new therapeutic compounds receiving marketing approval [131, 135]. This paucity is even more striking for neurological disorders [163, 164]. For instance, it had been more than 18 years since the last drug was approved for AD treatment, before the recent approval of Aducanumab by the FDA [165-168]. Nevertheless, during that same period, there have been many candidate drugs that showed great promises in preclinical studies but failed in clinical studies [163, 169, 170]. While there may be many factors that contribute to the high attrition rate of investigative drugs, preclinical models, especially animal models, are believed to be the predominant reason, where efficacy (52%) or safety (24%) accounts for the majority of drug failures in clinical trials [171]**.** Historically, the drug discovery process has relied largely on animal models for toxicology (i.e., safety and efficacy) research in order to obtain preclinical evaluation of promising new therapeutic compounds [134, 172, 173]. However, genetic–differences between animals and humans is regarded as one of the main factors

contributing to the very high attrition rate in human studies [129, 134, 139]. The lack of compatible models to study human diseases has greatly impeded the drug development process. The limitation of animal models combined with recent advances in the development and differentiation of iPSC into mature cells now provide a new source [146, 151] and endless possibilities to create more relevant models. Today, based on the relative ease with which different types of human cells (especially neuronal cells, which are normally inaccessible for scientific research prior to death) can be generated from iPSC cells, many researchers are re-evaluating their research approaches and putting more emphasis towards developing more compatible, iPSC-derived-cells-based in vitro models to study human diseases and for drug development [174]. Previously, we generated a human-based (cortical-HoAC) system using cortical neurons derived from iPSC to study aspects of AD pathophysiology [150]. Here, using a subset of different classes of FDA-approved, AD-related drugs, the system's capacity and potential for investigation as a potential platform for drug screening. As indicated in the results above, a significant increase in cell firing frequency from baseline activity was detected in the system following stimulation using a HFS protocol. This HFS-induced increase was maintained at least for 1 hour and was defined as LTP [175]. The stimulus-induced change in cell activity was subsequently abolished by $A\beta_{42}$ oligomers dosing. Both Donepezil and Memantine have been approved by the FDA as separate or a combined (Namzaric) drug for AD treatment, [176]. Both drugs, as well as Rolipram and Saracatinib, were used simultaneously with $A\beta_{42}$ oligomers to dose the cortical systems. The $A\beta_{42}$ oligomers neurotoxic effects was inhibited in the presence of AD-related drugs. Furthermore, the results demonstrated the system proficiency to capture drug effects using different AD-related drugs simultaneously with $A\beta_{42}$ oligomers.

While more studies are needed to expand on the findings presented here and to further validate the effectiveness and applicability of the system as a platform for drug screening, the findings, nonetheless, provide evidence to support the utility of the system as a more relevant human-based in vitro system to model human disease at the preclinical stage. Furthermore, this system is potentially significant for various reasons: 1) it provides (and can be utilized as) a human-based in vitro model to study disease pathophysiology (i.e., mechanisms and pathways) in vitro, 2) it provides a simple, reproduceable and economically effective tool for screening drug toxicity and efficacy, 3) it provides a foundation for designing and creating more complex systems which can be used to study the mechanism of drug reaction, mode of transport and to screen libraries of already approved drugs for drug repurposing, 4) it is scalable, it can be used for low- or high-throughput drug testing, and 5) it can be used in the application of personalized medicine.

Materials and Methods

Neuronal Cells

Human cortical neurons were used in this study to assess the effects of multiple AD-related drugs on Aβ oligomers induced neuronal cell dysfunction. The cells were derived from human induced pluoripotent stem cells from healthy individuals and were either purchased from Cellular Dynamics International (CDI, iCell GlutaNeurons, Cat. #: C1033, Madison,WI) or defferentiated directly in our lab as described previously [150, 177] and Autar, *et al.* [151].

Cell Culture

The cells were seeded on surfaces (MEA chips and coverslips) coated with DETA (*N*-1(3-[trimethoxysilyl]propyl)-diethylenetriamine) followed by top coat with either poly-L-ornithine and laminin (PLO/LM, 20 µg/ml and 10 µg/ml respectively) or fibronectin and laminin (FB/LM, 10 µg/ml each for 2 hours at RT]. A monoculture of cortical neurons were plated at a density of 150 cells/mm^2 on coverslips for immunostaining (ICC) analysis and patch-clamp electrophysiology as decribed previously [127, 150]. For the MEA cultures, a co-culture of cortical neurons and astrocytes were seeded directly onto patterned chips to promote cell aggregation and/or formation of separated cell-clusters on the individual electrodes, as well as the formation of synaptic connections between two adjacent electrodes. The neuronal cells were plated at a density of 500 cells/mm^2 and the astrocytes at 250 cells/mm^2. The cells were were first plated in the manufacture's (CDI) recommended medium for the first 24h before they were switched to a serum-free medium. The cells were maintained in culture in the serum-free medium for 28-35 days prior to dosing and testing [150].

Aβ Oligomer Preparation

The Aβ oligomers were prepared using peptides from rPeptide ($A\beta_{1-42}$ catalog number A-1002-2; $A\beta_{-scrambled}$ A-1004-2) as described previously [178]. First, the peptides were resuspended in 500µL of HFIP (catalog number AC445820100; Fisher Scientific) and left to dry overnight under a ventilated hood. The next day the samples were spun in a SpeedVac until dry and stored

desiccated at -20°C until use. Prior to using, the solution was sonicated for 5 minutes and centrifuged at 1400 x g for 5 minutes.

AD Drugs

Several classes of drugs use in the treatment of Alzheimer's disease were used in this study, including Rolipram, Saractinib, and FDA-approved Memantine and Donepezil. Memantine is an noncompetitive NMDA receptor antagonist that binds to the receptor and blocks the binding of glutamate and thus cell excitotoxicity caused by glutamate [179]. Donepezil is an FDA-approved drug for AD, it is an acetylcholinesterase inhibitor which prevents the breakdown of acetylcholine in the synapse by the acetylcholinesterase enzyme [180, 181]. Saracatinib inhibits the action of Fyn, a member of the tyrosine kinase family that phosphorylates other proteins including tau and NMDAR, resulting in tau hyperphosporylation and synaptoxicity, or cell excitotoxicity from NMDAR activation [182-185]. Rolipram is a selective phosphodiesterase-4 (PDE4) inhibitor that helps to restore cAMP levels, which is reduce) in AD as a result of adenylate cyclase (synthesizes cAMP) inactivation by Aβ42 peptides [186].

Drug Treatment of Cortical Neurons

On the day of treatment, or at ~24hrs prior to patch recording, a half medium change was performed, followed by the administration of either $A\beta_{scr}$ or $A\beta_{42}$ oligomers with or without AD drugs for patch electrophysiology. Only the half medium change was performed in the systems with the MEAs at 24 hours prior to treatment. For treatment groups, the cells were either dosed with a final concentration of 5μM $A\beta_{scr}$, 5μM of $A\beta_{1-42}$ alone, or 5μM of $A\beta_{1-42}$ plus drug (either 10nM of Saractinib, 1μM of Donepezil, or 5μM of Memantine, 1μM of Rolipram). To examine

the neurotoxic effects of $A\beta_{42}$ oligomers on cell electrophysiological function, the cells or cultures were tested at either 1 hour (MEAs) or 24 hours (patch-clamp) following treatment.

Immunocytochemistry and Confocal Microscopy

To analyze the cells for gene expression of the drug targets, the cells were fixed in 4% paraformaldehyde (PFA), followed by cell permeabilization and incubation in primary and secondary antibodies solutions (diluted in BSA/NGS/T20 buffer) for each specific marker. Following antibodies staining, the cells were counterstained with DAPI (4',6-diamidino-2-phenylindole) and mounted on glass slides for analysis. The cells were imaged using a confocal microscopy (Zeiss, Axioskop 2, Germany). The following primary antibodies (at 1/1000 dilution) were used: Rabbit Anti-Microtubule-Associated Protein 2 (Millipore, Cat. #: AB5622), Mouse Anti-MAP2 (Abcam, Cat. #:ab11257), Mouse Anti-Fyn (ThermoFisher, Cat. #: MA1-15865), Mouse Anti-NMDAR2B (ThermoFisher, Cat. #: MA1-2014), Mouse Anti-Acetylcholinesterase (Abcam, Cat. #: ab2803), Mouse Anti-muscarinic Acetylcholine Receptor (Abcam, Cat. #: ab90805), Rabbit Anti-nicotinic Acetylcholine Receptor (Abcam, Cat. #: ab221868), Rabbit Anti-Phosphodiesterase Type 4 (Abcam, Cat. #: ab14628). The secondary antibodies used: Alexa-Fluor 488 goat anti-rabbit (ThermoFisher, Cat. # A11008), AlexFluor 488 Goat anti-mouse (ThermoFisher Cat. #: A11001), AlexFluor 568 Goat anti-Rabbit (ThermoFisher Cat. #: A11036), and AlexFluor 568 Goat anti-mouse (ThermoFisher Cat. #: A11004).

Patch Clamp Electrophysiological Recording of Cortical Neurons

Neuronal electrophysiological activity was evaluated at 28-35div. To measure cellular activity intracellularly, whole cell patch-clamp recordings were taken using a Zeiss, upright microscope (Axioscope, FS2, Carl Zeiss, Germany) equiped with a multiclamp 700B amplifier and an intracellular solution consisting of 140 mM K-gluconate, 4 mM NaCl, 0.5mM $CaCl_2$, 1mM $MgCl_2$, 1mM EGTA, 5mM HEPES Acid, 5mM HEPES base and 5 mM Na_2ATP as described previously [150]. Depolarization-evoked inward and outward currents were examined in voltage-clamp mode while induced action potentials (APs) were recorded in current-clamp mode. Sucessive analysis of the data were carried out using pClamp 10 software (Axon Instrument, Foster City, CA, USA) followed by quantification using Microsoft Excel and GraphPad Prism.

Induction of Long-Term Potentiation on MEAs

To induce LTP on cortical neurons cultured on MEAs, a high frequency stimulation (HFS) protocol was used as described previously [150]. Test stimuli were delivered to all the electrodes in the form of 80 pulses at 100Hz. The evoked response or induced cell activity was then analyzed using Anaconda with Python (i.e., Monday.com) software. The waveforms (e.g., action potential spikes and frequency) were thresholded at -5 standard deviations from the noise and high-pass filtered at 100Hz. Any electrodes with firing frequency post-stimulation less than or equal to baseline levels were excluded from the data analysis.

Analysis of Cortical Neuron Activity on MEAs

The cellular activity of the cells was measured extracellularly on MEAs as described previously [127, 150, 187]. The cells were plated directely onto the MEA chips in housing and maintained in culture for 28-35 days before acute treatment with Aβ oligomers and AD drugs. Prior to treatment, spontaneous activity (baseline) of the neurons was recorded (for 5 minutes) followed immediately by electrical stimulation (LTP induction) and another 5 minutes recording post-stimulation. Immediately following LTP induction and recording, the cultures were treated with Aβ oligomers and/or Aβ oligomers AD drugs and incubated for 1 hour at 37°C and 5% CO_2. Next, the neuronal firing potential (e.g., firing frequency) was once again recorded for 5 minutes before analysis. The data was analyzed using Anaconda with Python software**.**

Statistical Analysis

Comparison of the mean of at least three or more replicates and more than 15 electrodes between groups was performed. For computational analyses, Microsoft Excel software and GraphPad Prism were used. Student t-tests were used for statistical comparison analysis between two experimental groups, whereas one-way analysis of variance (ANOVA) with Tukey's post hoc test was used for multiple experimental groups. The SEM was used with statistical significance taken at $p \leq .05$.

Figures

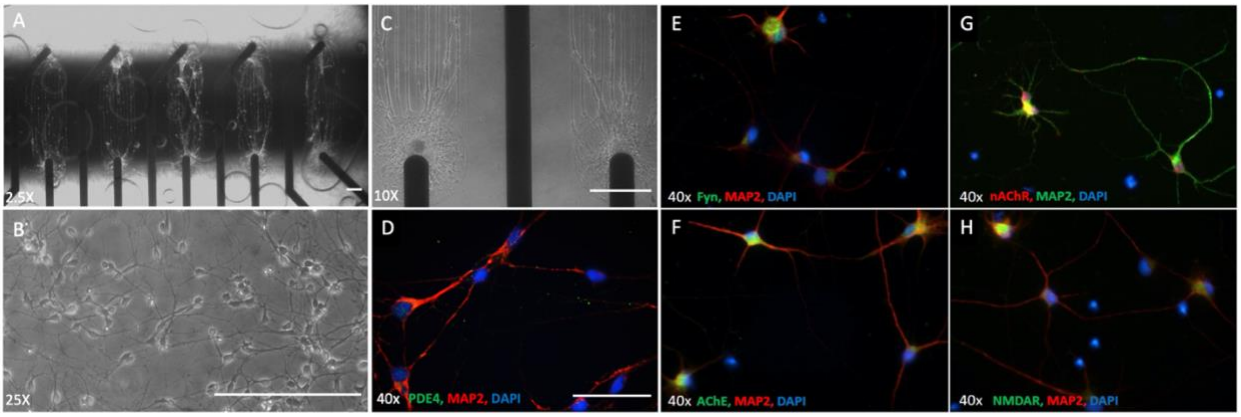

Figure 8: **Expression of gene targets of AD drugs in hiPSC-derived cortical neurons**. Phase image of hiPSC-derived cortical neurons aligning in pattern on coated MEAs at the magnification of 2.5X(A), and 10X magnification (C). Phase image of hiPSC-cortical neuron morphology on coverslips at 25X magnification (B). (D-H) Immunocytochemistry of hiPSC-derived cortical neurons with antibodies specific to target gene/proteins for AD drugs revealed cells expression for all markers. Scale bar = 100μm.

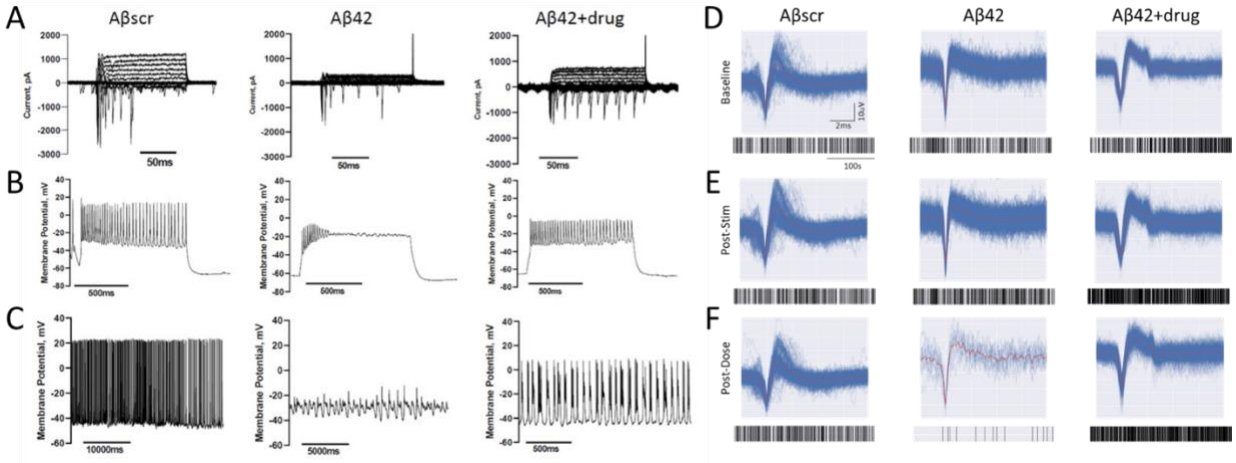

Figure 9: **Protective effects of AD-related drugs against Amyloid beta42 oligomers induced neurotoxicity in cortical cells.** (A-C) Patch clamp electrophysiology recordings showed a marked reduction in sodium currents (A) in hiPSC-derived cortical neurons following 5µM Aβ42 oligomer application at 24hrs post-treatment. Additionally, a significant decrease in both induced action potential firing under depolarization (B) and spontaneous firing peak amplitudes (C) was detected in cells treated with Aβ42 relative to cells dosed with amyloid beta scrambled (Aβscr), but the decrease was recovered by co-treatment with drug. (D-F) A similar reduction in cell activity was observed in the cortical-HoAC systems. Following establishment of baseline activity levels (D), an immediate increase in cell activity (i.e., firing frequency) was observed in hiPSC-derived cortical neurons following LTP induction (E). While the induced activity was maintained at 1hr post dosing in samples treated with the amyloid beta scrambled (Aβscr, 5µM), a sharp decrease was observed in the samples dosed with Aβ42 oligomers alone within 1hr of treatment (F). However, co-treatment of the Aβ42 oligomers and AD drugs rescued the decrease.

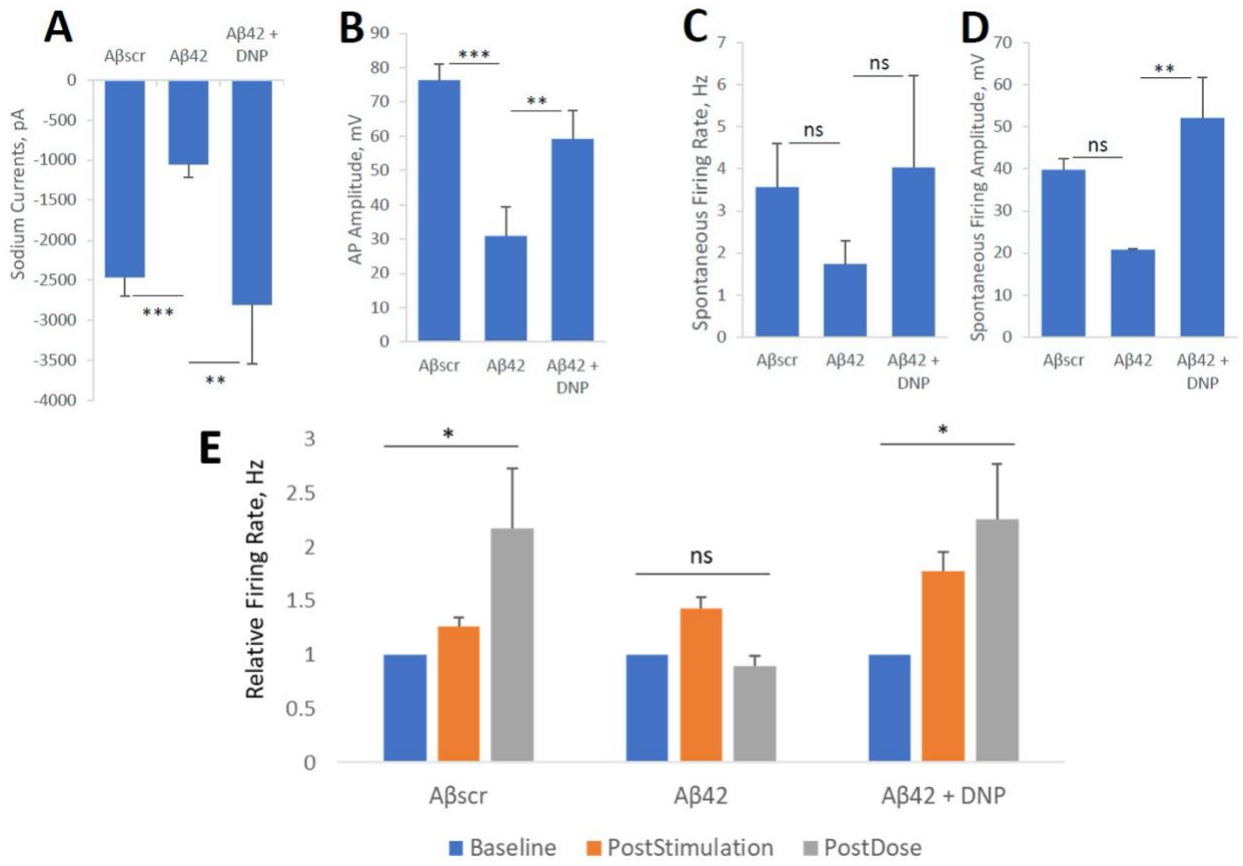

Figure 10: **Amyloid beta42 oligomers induced neurotoxicity of hiPSC-derived cortical neurons is inhibited by Donepezil.** (A-D) Patch clamp electrophysiology recordings from the hiPSC-derived cortical neurons showed the blocking of the Aβ42-induced defects by co-treatment with Donepezil (1µM) for 24 hours, as demonstrated for the readouts of sodium currents (A), action potential (AP) amplitude (B), and spontaneous firing rate (C) and amplitude (D). (E) Analysis of cell function on cortical-MEA systems revealed a stimulus-induced increase in cell activity (i.e., firing frequency) was maintained in control samples dosed with amyloid beta scrambled (Aβscr, 5µM), but was completely abolished within 1h of Aβ42 oligomers dosing. However, this Aβ42-induced abolishment was blocked by co-treatment with Donepezil (DNP, 1µM)(E). Statistical analysis was computed using either Student t-test or One-Way ANOVA with Tukey's test and Alpha (0.05) is significance. (N≥16), *p≤0.05, **p≤0.01, ***p ≤0.001.

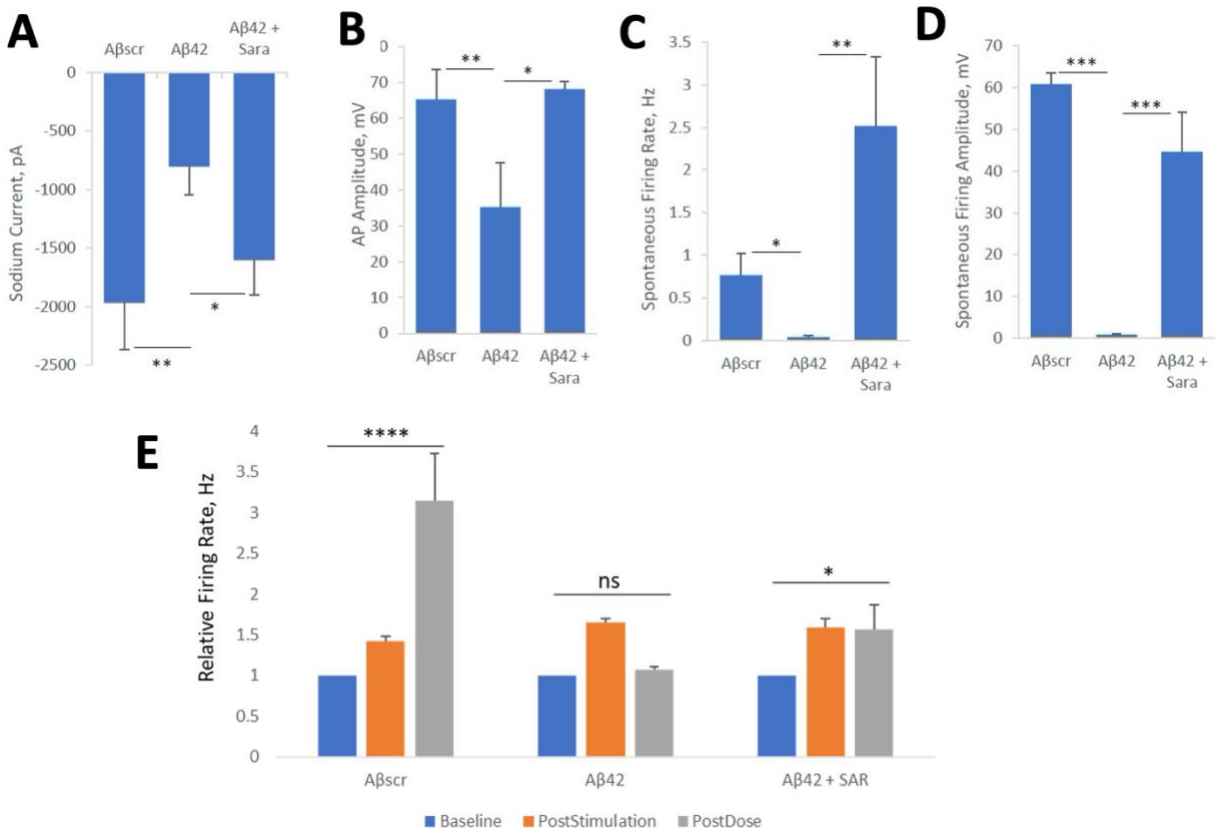

Figure 11: **Figure 4. Saracatinib blocks amyloid beta42 oligomers toxic effects on hiPSC-derived cortical neurons.** (A-D) Patch clamp electrophysiology recordings from the hiPSC-derived cortical neurons showed the blocking of the Aβ42-induced defects by co-treatment with Saracatinib (10nM) for 24 hours, as demonstrated for the readouts of Sodium currents (A), action potential (AP) amplitude (B), and spontaneous firing rate (C) and amplitude (D). (E) Analysis of cell function on cortical-MEA systems. A stimulus-induced increase in cell activity (i.e., firing frequency) was maintained in control samples dosed with amyloid beta scrambled (Aβscr, 5μM), but was completely abolished within 1h of Aβ42 oligomers dosing. However, this Aβ42-induced abolishment was blocked by co-treatment with Saracatinib (10nM). Statistical analysis was computed using either Student t-test or One-Way ANOVA with Tukey's test where applicable. Alpha (0.05) is significance. (N≥25), *p≤0.05, **p≤0.01, ***p ≤0.001.

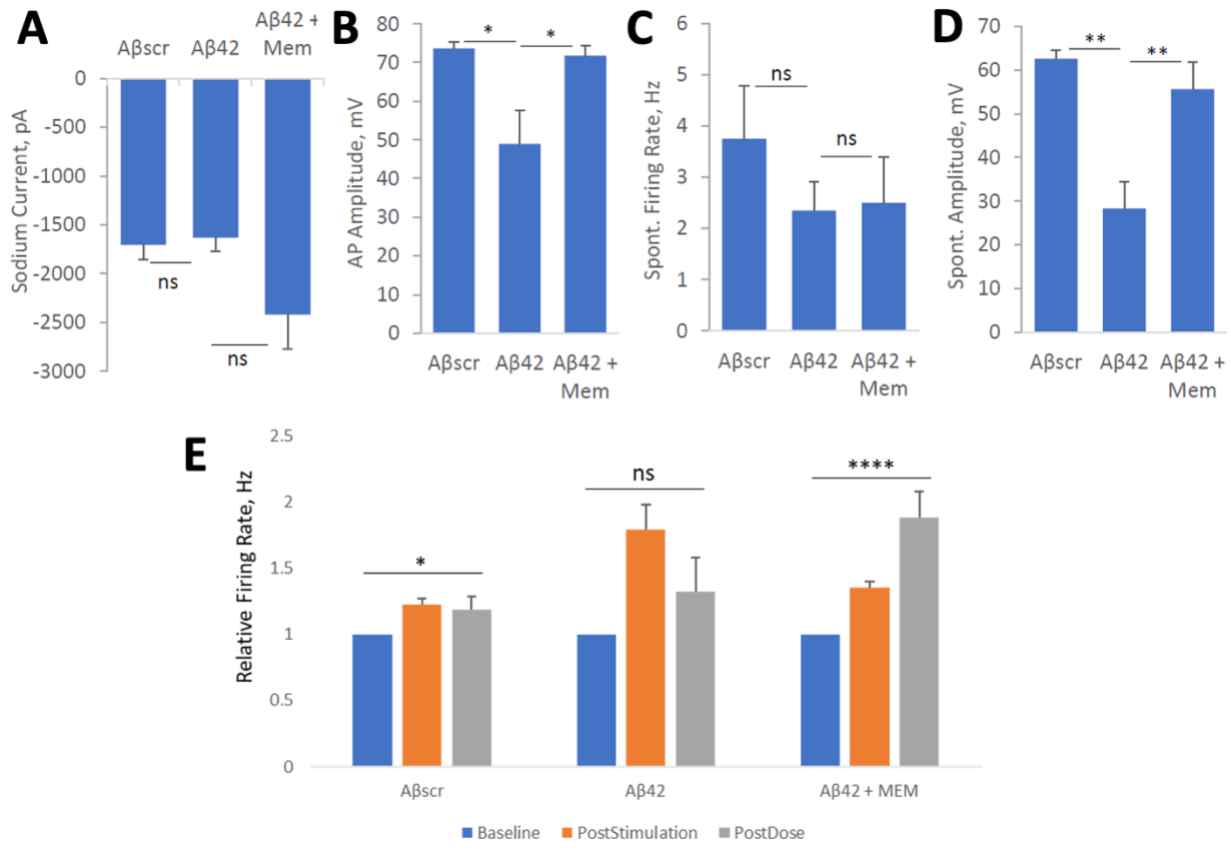

Figure 12: **Memantine suppresses amyloid beta42 oligomers neurotoxic effects on hiPSC-derived cortical neurons.** (A-D) Patch clamp electrophysiology recordings from the hiPSC-derived cortical neurons showed the blocking of the Aβ42-induced defects by co-treatment with Memantine (5μM) for 24 hours, as demonstrated for the readouts of Sodium currents (A), action potential (AP) amplitude (B), and spontaneous firing rate (C) and amplitude (D). (E) Analysis of cell function on cortical-MEA systems. A stimulus-induced increase in cell activity (i.e., firing frequency) was maintained in control samples dosed with amyloid beta scrambled (Aβscr, 5μM), but was completely abolished within 1h of Aβ42 oligomers dosing. However, this Aβ42-induced abolishment was blocked by co-treatment with Memantine (5μM). Statistical analysis was computed using student t-test or One-Way ANOVA with Tukey's test and Alpha (0.05) is significance. (N≥25), *p≤0.05, **p≤0.01, ***p ≤0.001, ****p ≤0.0001.

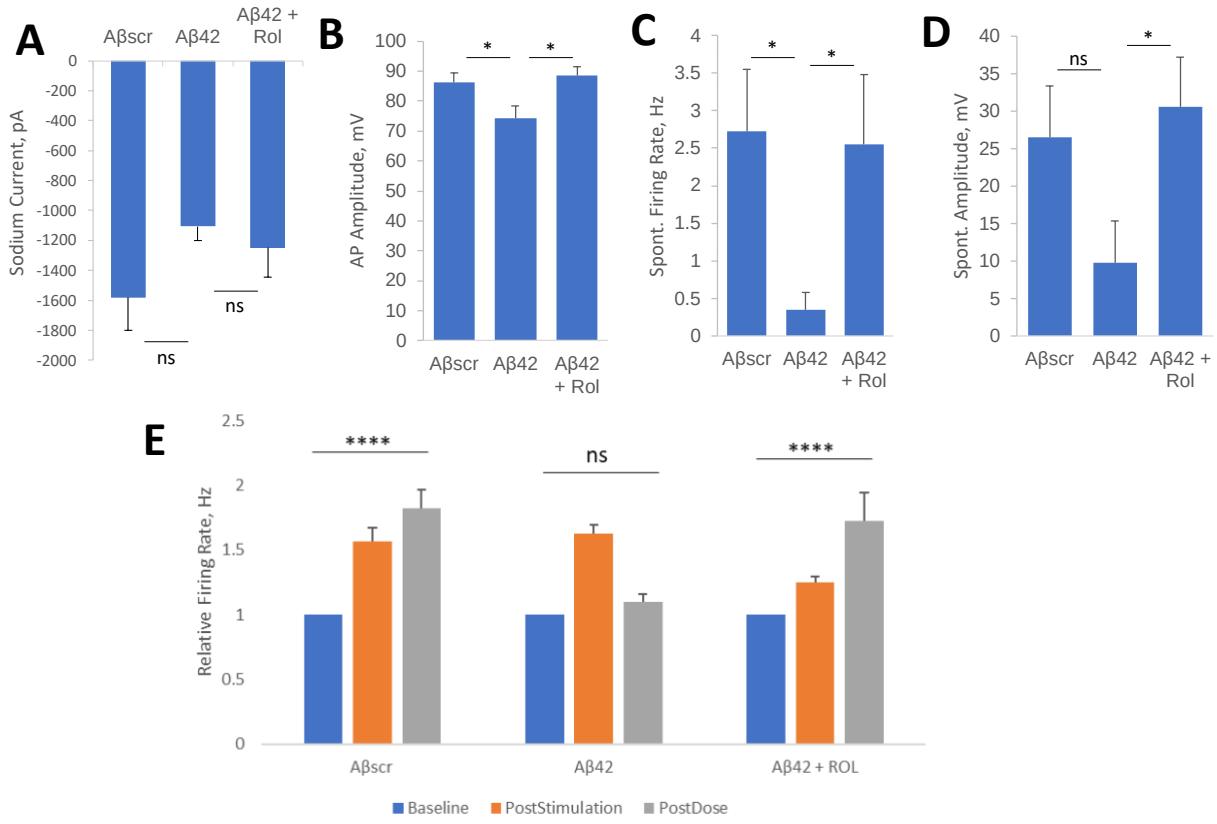

Figure 13: **Rolipram suppresses amyloid beta42 oligomers neurotoxic effects on hiPSC-derived cortical neurons.** (A-D) Patch clamp electrophysiology recordings from the hiPSC-derived cortical neurons showed the blocking of the Aβ42-induced defects by co-treatment with Rolipram (1µM) for 24 hours, as demonstrated for the readouts of Sodium currents (A), action potential (AP) amplitude (B), and spontaneous firing rate (C) and amplitude (D). (E) Analysis of cell function on cortical-MEA systems. A stimulus-induced increase in cell activity (i.e., firing frequency) was maintained in control samples dosed with amyloid beta scrambled (Aβscr, 5µM), but was completely abolished within 1h of Aβ42 oligomers dosing. However, this Aβ42-induced abolishment was blocked by co-treatment with Rolipram (1µM). Statistical analysis was computed using student t-test or One-Way ANOVA with Tukey's test and Alpha (0.05) is significance. (N≥18), *p≤0.05, **p≤0.01, ***p ≤0.001, **** p ≤0.0001.

CHAPTER FOUR: VALIDATION OF SYNAPTIC CONNECTIVITY-DEPENDENT LONG-TERM POTENTIATION IN A HUMAN IPSC-CORTICAL NEURON MODEL FOR ASSESSING NEURODEGENERATION

Introduction

Neurodegenerative diseases, such as frontotemporal dementia (FTD), Alzheimer's disease (AD), Parkinson's disease (PD), and epilepsy are characterized by a loss of neuronal function [188-191]. More specifically, deficits in motor and cognitive functions are the main symptoms that present themselves during disease onset. In AD, the accumulation of Aβ42 oligomers form plaques that cause synaptic deterioration and a characteristic loss of memory and learning [4]. Current models of neurodegeneration and AD have either been in vivo models examining animal learning and memory, including mice [192], rats [193], and non-human primates [194], or in vitro models that employ the use of cortical neurons from rat brain slices [195] and rat dissection sources [196], or human iPSC derived sources [39, 175]. Human iPSC cortical neurons have been commonly utilized for studying diseases in the CNS. The utilization of a human cell source rather than an animal cell source provides more optimized biological efficacy. When combined with in vitro human organ-on-a-chip (HoaC) technology, they are expedient for the evaluation of neuronal function in a biologically relevant system. There are limited in vitro models that focus on the synaptic deterioration by evaluating synaptic plasticity in a biologically accurate manner.

Long-term potentiation (LTP) has been used both in vivo and in vitro as a means of assessing synaptic strength, and its maintenance has been largely used as an in vitro, quantitative readout of cognitive functions such as memory and learning. LTP has been widely studied as a dual-patch clamp readout, with few studies looking at LTP as a readout of synaptic connectivity

of neuronal populations on MEAs. Some studies have evaluated connectivity on MEAs of neuronal populations seeded on a bed of electrodes in a randomized assortment [39, 175]. However, when the neurons are arranged in a disorganized fashion, changes in neuronal activity resulting from synaptic communication cannot be well tracked and defined within the system. That being said, it has been previously shown that surface chemistry patterning allows for organized cell culture [125]. By combining surface patterning with HoaC technology on MEAs, a tool can be created for more optimized assessment of synaptic plasticity.

This study sought to validate a system for studying synapse-dependent neurodegeneration by developing a model of LTP induction via synaptic connectivity. We evaluated the communication between patterned neuronal populations, where the synapses were organized between two distinct populations on individual electrodes. Although other papers have cited LTP induction on MEAs with the employment of a serum-free, hiPSC-cortical neuron and astrocyte co-culture, none have been able to induce the LTP through synaptic connectivity in a paired-patterned fashion. By emphasizing synaptic strength as the only means for attaining LTP, this system is more advantageous in evaluating neurodegeneration, and can be further adapted for evaluating drug effects in a human-based system as a platform for preclinical compound assessment.

Results

Culture Timeline and Testing Procedure

Astrocytes were pre-cultured for expansion 3 days prior to iPSC-cortical neuron thawing and plating. Following seeding of the co-culture, MEAs were maintained for at least 40 days prior to experimentation (Figure 14A). For MEA testing, spontaneous neuronal activity was first recorded

to establish a baseline and determine channels of interest. Next, the electrodes paired to the channels of interest were electrically stimulated using HFS to evaluate the ability of the neurons to experienced elevated firing levels (induced LTP). The channels of interest were then stimulated for further assessment. A dosage of 1mM lidocaine was added following all testing in each experiment to confirm biological signals (Figure 14B).

Characterization of Co-Culture and Confirmation of Neuronal Signals on cMEAs

Neuronal paired-electrode patterning could be visualized via phase microscopy. Representative phase images demonstrate the patterning abilities and morphology of the co-culture at 45 DIV (Figure 15A). Immunocytochemical staining of the MEA co-culture illustrates the neuronal and astrocyte components using MAP2 and GFAP, respectively (Figure 15B). Neuronal signals were confirmed as biological with the addition of lidocaine to the MEAs following recording of spontaneous activity. Waveform representations and raster plots exemplify the abolishment of neuronal signals after 1-minute of lidocaine addition (Figure 15C). A quantitative representation of this abolishment shows that the change is very significant, with the signals being almost non-existent in the presence of lidocaine (Figure 15D).

Induction of LTP via Synaptic Connectivity

Synapse formation in cortical neuron culture was first visualized for confirmation via immunocytochemical staining. Synaptic puncta illustrated the presence of post-synaptic densities (PSD95) as well as synaptophysin pre-synaptic synaptic vesicles (Figure 16A). Next, electrodes of interest were determined as either the top row or bottom row electrodes, synaptically connected

through neuronal patterning. Electrical stimulation via a high frequency stimulation (HFS) protocol was first performed on the adjoining electrodes to synaptically stimulate the electrodes of interest. Waveform traces and corresponding raster plots reveal that neuronal activity increased in the electrodes of interest increased following stimulation of the paired electrode, while it did not in the non-stimulated control (Figure 16B). Quantification of the neuronal firing rate revealed the induction of heightened activity on the electrode of interest following the stimulation of the paired channel was significantly higher than the baseline (Figure 16C). However, when the channel of interest was stimulated proceeding stimulation of the paired channel, there was no notable increase compared to the previous stimulation. No significant change was observed in non-stimulated controls, emphasizing that any changes in neuronal activity were a response to electrical stimulation. It was also found that the induced increase following HFS in the channels that were stimulated via their synaptic connections was not significantly different than the increase in the electrodes that were directly stimulated (Figure 16D).

Confirmation of Synaptic LTP Through AMPA Receptor Inhibition

The presence of AMPA receptors on the surface of iPSC-cortical neurons was visualized via immunocytochemical staining for the AMPA receptor subunit GLUR1, co-stained with synaptophysin for further synapse confirmation (Figure 17A). Following recording of baseline neuronal activity levels, AMPA receptors were blocked through the addition of NBQX or 0.1% DMSO vehicle control. Next, stimulation was performed as mentioned in Figure 3, with the paired channels stimulated first, followed immediately by the stimulation of the channels of interest. LTP was then evaluated by recording the spontaneous neuronal activity again 1 hour following the HFS

stimulation protocol. The results revealed a significant decrease in the induction and maintenance of LTP in the presence of NBQX (Figure 17B). Waveform traces and raster plots further demonstrate this difference (Figure 17C).

Confirmation of Synaptic LTP through NMDA Receptor Inhibition

The presence of NMDA receptors in our cortical neuron culture was first assessed via immunocytochemical staining using an NMDAR antibody. MEAs were co-stained with vGLUT1 to confirm the excitatory character of our neurons through the release of vesicular glutamate as a neurotransmitter (Figure 18A). The addition of D-AP5 to inhibit NMDA receptors significantly blocked the induction and maintenance of LTP through synaptic connectivity compared to vehicle control (Figure 18B). Waveform traces and raster plots further illustrate the differences observed in neuronal activity on MEAs (Figure 18C).

Discussion

This study sought to evaluate LTP from a high-frequency electrical stimulation, synaptically-induced change in paired neuronal populations. Current models of LTP analyze the results of direct stimulation, but the utilization of synaptically-induced LTP enables for a more robust system for investigating neurodegeneration as a result of synaptic decline. Models of synaptic plasticity in Alzheimer's disease commonly employ a tetanic high-frequency stimulation protocol, and subsequently measure the slops of the excitatory post-synaptic potential (EPSP). Recently, the use of MEAs has encouraged the exploration of neuronal population dynamics and network integrity [128, 197, 198].

A cortical neuron and astrocyte co-culture was used for the evaluation of LTP induced through synaptic connectivity of distinct neuronal populations on MEAs. The cortical neuron and astrocyte co-culture was seeded according to the culture timeline depicted in Figure 14A, where astrocytes were first expanded prior to co-seeding of cortical neurons and astrocytes. The co-culture was allowed to pattern and form strong synaptic networks between the neuronal populations for 40-50 days following cell seeding prior to evaluation of neuronal activity. This timeline has been previously validated as a mature cortical neuron time window [151]. The utilization of paired neuronal patterning on MEA chips allowed for distinct neuronal populations to form with guided synaptic networking for controlled stimulation and neural communication. The LTP protocol detailed in Figure 14B sought to investigate the differences in electrical stimulation from the synaptically connected neuronal population compared to the direct stimulation of the neuronal population localized on a given electrode. This technique has been used previously to evaluate synaptic connectivity between differing neuronal populations to evaluate the communication via the release of different neurotransmitters [199].

Photolithographic patterning allowed for the successful formation of paired neuronal populations visualized through phase microscopy (Figure 15A). Cortical neuron and astrocyte co-cultures have been widely used in vitro for the investigation of synaptic plasticity and LTP [175, 200-202]. The utilization of astrocytes within the neuronal culture aids in the synaptic strength and axonal robustness within the culture as well as culture duration [203]. Staining of MEA chips allowed for visualization of the neuron and astrocyte co-culture using MAP2 and GFAP, respectively (Figure 15B), illustrating the integration of the astrocytes within the neuronal population, which is imperative for glutamate recycling within the synaptic cleft. Lidocaine, a

widely cited local anesthetic, was used for confirmation of biological neuronal signals by blocking Na^+ channels and were shown to abolish neuronal signals within 1 minute following administration (Figure 15C and 15D) [151].

Following the characterization of the astrocyte and neuronal culture and confirmation of biological signals, high frequency electrical stimulation (HFS) was employed following the protocol described in Figure 14B. Synaptic connectivity between neurons was visualized through immunocytochemical staining of synaptic puncta using PSD95 and Synaptophysin (Figure 16A). Following this, the LTP induction was performed according to the protocol in Figure 15B. Similar levels of neuronal activity were present in stimulated and non-stimulated neuronal populations (Figure 16B). A significant increase was observed in neurons stimulated through synaptic networking when the connected electrode was stimulated, however, the neurons could not be further stimulated through the subsequent direct stimulation (Figure 16C). Additionally, the increase in neuronal activity when stimulation occurred through synaptic stimulation of the opposite electrode was not significantly different than the increase observed from the direct stimulation of the neurons, indicating that the LTP induction is statistically equivalent when stimulated through the neuronal synaptic networks (Figure 16D). While previous works have investigated the LTP phenomenon on MEAs, they have not looked specifically at the induction of LTP through synaptic connectivity, but rather through trained test-pulses on the neuronal population localized on the same electrode [39].

For further validation, AMPA and NMDA receptors were blocked to affirm that the LTP induction from adjacent, connected neuronal population was occurring through the synaptic networks. It has been cited that LTP is NMDA-dependent, due to the fact that NMDA receptors

are voltage-dependent [45]. AMPA receptors were visualized using GLUR1, with Synaptophysin used as a comparative stain to fully visualize the synaptic networks (Figure 17A). AMPA receptors were blocked using a potent AMPA receptor antagonist, NBQX [204]. Baseline activity was taken prior to dosing with NBQX, where a notable, though non-significant, decrease in neuronal activity was observed. In comparison to the 0.01% DMSO control, where LTP was induced synaptically, there was a significant difference in the LTP induction in the NBQX dosed systems. This difference was also observed 1 hour following induction, where the control systems maintained their elevated firing, and the cultures dosed with NBQX did not experience any long-term effects following stimulation (Figures 17B and 16C). This indicates that the notable increases in neuronal activity are from synaptic stimulation. Similar results were attained when neuronal NMDA receptors were blocked with D-AP5, which has been correlated to blocking LTP capabilities [205]. NMDA receptors were first visualized using an NMDAR antibody co-stained with vGLUT1 for complete depiction of the synaptic connections (Figure 18A). Because NMDA receptors are only activated following depolarization of the membrane to a threshold voltage, there was less of an observed decrease in neuronal activity following the administration of the compound. However, when compared to the vehicle control, the lack of induced and persistent LTP immediately following and 1 hour after stimulation was significantly different (Figure 18B and 18C). Therefore, the blocking of the post-synaptic receptors activated by glutamate released from pre-synaptic vesicles also blocked the synaptic induction of LTP [206].

The validation of a functional, in vitro LTP model that emphasizes the synaptic integrity allows for further advancements in neurodegenerative diseases, such as AD, that is hallmarked by synaptic decline. Furthermore, because the populations have an isolated locality, other cell types

can be integrated into this system to look at networking of many types of neurons present within the brain. Combining this system with iPSC technology provides a platform for patient-specific disease models of neurodegeneration, and the utilization of a fully human-based, in vitro system easily lends itself to surveying drug efficacy in precision medicine.

Materials and Methods

MEA Patterning and Surface Prep

MEAs were first coated with poly-ethylene glycol (PEG) as per [207]. Next, the PEG-coating was ablated using a laser using a mask that formed the paired pattern, where the neuronal populations were localized on the electrode tips, and axonal tracks were present to connect and pair the populations. Following laser ablation, the surfaces were backfilled with a DETA coating to encourage neuronal binding to the patterns. The surfaces were then coated with a solution of 10μg/mL Fibronectin (Sigma-Aldrich #F1141) and Laminin (Invitrogen #23017-015), diluted in 1X PBS. The laminin solution was cured at RT for 3 hours preceding the seeding of the cortical neuron and astrocyte co-culture.

Cell Culture

Primary astrocytes were pre-cultured for 3 days in a T-75 flask using a vendor media formulation (ScienCell Human AM #1801) before being co-cultured with cortical neurons. At culture D0, astrocytes were lifted using accutase (Sigma Aldrich #A6964) at 37°C following a 1X PBS rinse. Astrocytes were then centrifuged at 300g for 4 minutes. iPSC-cortical neurons (iCell

Glutaneurons) were purchased from CDI (Cellular Dynamics #R1116) and thawed following vendor specifications in CDI media, consisting of BrainPhys Neuronal Media (Stemcell Technologies #05790) supplemented with Nervous System Supplement (Cellular Dynamics #M1031), Neural Supplement B (Cellular Dynamics #M1029), 1X N2 Supplement (ThermoFisher 17502048), 1μg/mL Laminin (Invitrogen #23017-015), and 1X Pen/Step (15-ThermoFisher 140-122). Cells were seeded at a 2:1 neuron-to-astrocyte ratio, with neurons seeded at 500cells/mm^2 and astrocytes seeded at 250cells/mm^2 on cMEAs. One day following seeding, a full media change was performed on the cultures to switch them to NMJ medium. A half-media change was performed every other day for the duration of the culture. Full-media washouts were performed after testing to remove added compounds.

Immunocytochemistry

Coverslips were fixed and permeabilized as previously published [151]. Following permeabilization, coverslips were blocked in blocking solution containing 1% BSA and 5% goat serum in 1X PBS. Primary antibodies were diluted in blocking solution and incubated at 4°C overnight. Antibodies used for visualization included Rabbit-anti-GFAP (Sigma ab5804, 1:1000), Mouse-anti-MAP2 (Invitrogen MA5-12823, 1:500), Mouse-anti-Synaptophysin, Rabbit-anti-PSD95, Guinea Pig-anti-vGLUT1 (Invitrogen ab5905, 1:200), Rabbit-anti-GLUR1 (Invitrogen ab1504, 1:250), and Mouse-anti-NMDAR (Invitrogen MA1-2014, 1:250). Secondary antibodies used included: Goat anti-Rabbit Secondary Antibody Alexa Fluor 568 (ThermoFisher A-11011), Goat anti-Mouse Secondary Antibody Alexa Fluor 568 (ThermoFisher A-11004), Goat anti-Rabbit Secondary Antibody Alexa Fluor 488 (ThermoFisher A11008), Goat anti-Mouse

Secondary Antibody Alexa Fluor 488 (ThermoFisher A-11001). Coverslips were additionally counterstained with DAPI (Fisher D1306) for nuclear visualization (1:500) and mounted using Invitrogen DAPI mounting media (Fischer P36931).

Compound Preparation

All compounds were prepared as a stock such that the concentration was 100X final dosing concentration and could be dosed as 8μL in a total system volume of 800μL. Lidocaine HCl (Sigma 6108-05-0) was reconstituted in cell culture media at a concentration of 100mM, final concentration 1mM. NBQX (TOCRIS 0373) was reconstituted in 0.1% DMSO diluted in cell culture media and dosed at a final concentration of 25μM. D-AP5 (TOCRIS 0106) was reconstituted in cell culture media and dosed at a final concentration of 25μM.

LTP Induction and Analysis

MEA recordings were taken using a multi-channel systems rig (MCS). Electrical stimulation was performed using a high-frequency stimulation (HFS) LTP induction protocol that has been previously used in our other works. All recordings of neuronal activity were taken for a duration of 5 minutes. Raw data was processed with a 100Hz high-pass 2^{nd} order Butterworth filter. In addition, a -5 standard deviation threshold was used for event detection. Events crossing the threshold were further filtered using a principal component analysis (PCA) filter.

Figures

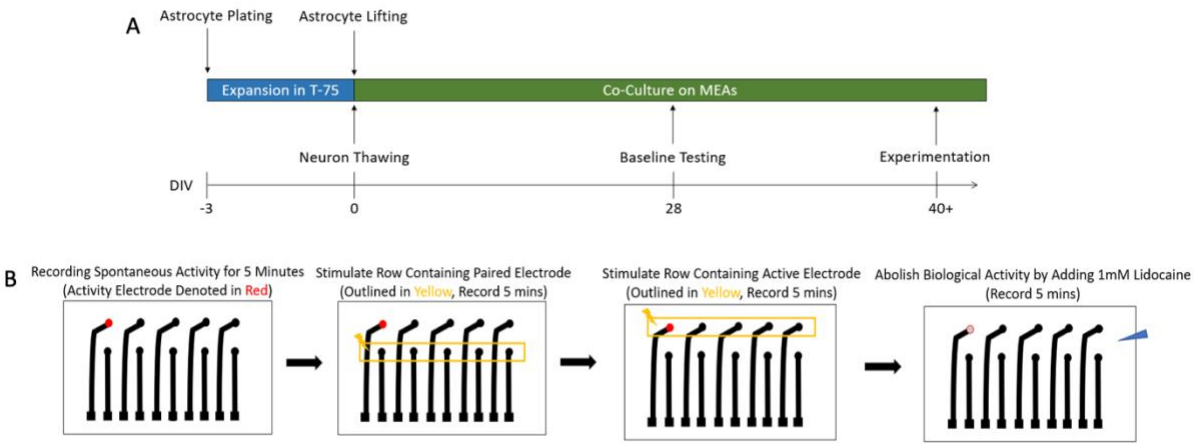

Figure 14: **Culture timeline and testing procedure. (A)** Culture timeline illustration of co-culture plating, where astrocytes were pre-plated and expanded in T-75 flask 3 days prior to lifting and co-seeding with cortical neurons. Experimentation was performed 45-55 days following cell seeding. **(B)** Illustration depicting testing procedure, where baseline activity was recorded. HFS was performed on electrodes opposite of visibly active electrodes. Then the opposite row was stimulated. Last, lidocaine was administered for confirmation of biological activity. All recordings were taken for a duration of 5 minutes.

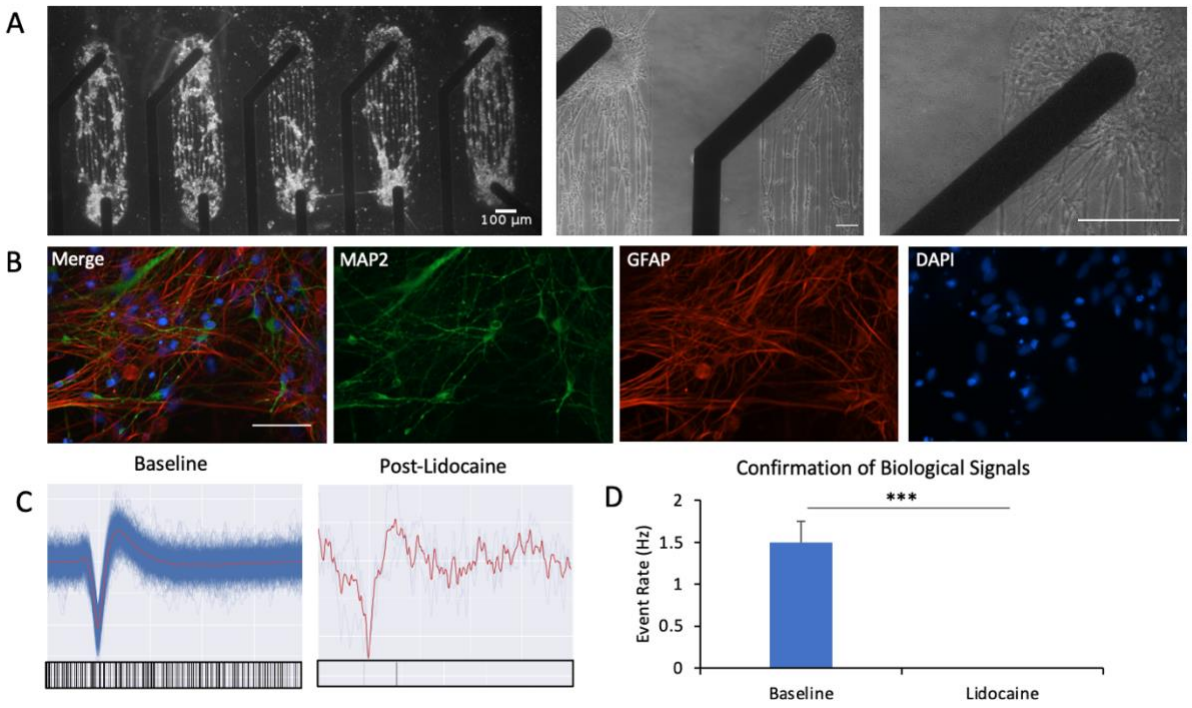

Figure 15: **Co-culture characterization and confirmation of neuronal activity. (A)** Phase images depicting patterning of neuronal population on cMEA chips using 2.5X (left), 10X (middle), and 25X (right) objective lenses (Scale Bar = 100µm). **(B)** Immunocytochemistry staining of hiPSC-cortical neuron and astrocyte co-culture depicting neurons (MAP2, green), astrocytes (GFAP, red) and nuclear counterstain (DAPI, blue) utilizing 40X objective confocal microscopy (Scale Bar = 50µm). **(C)** Representative waveform illustrations and accompanying raster plots of neuronal frequency in a 5-minute baseline recording (left) and 1 minute following addition of 1mM lidocaine (right). **(D)** Graphical representation of neuronal firing frequencies at baseline and 1-minute following addition of lidocaine from 3 independent experiments. Statistical analysis was performed using a Student's t-test, *$p < 0.05$, **$p < 0.01$, ***$p < 0.001$.

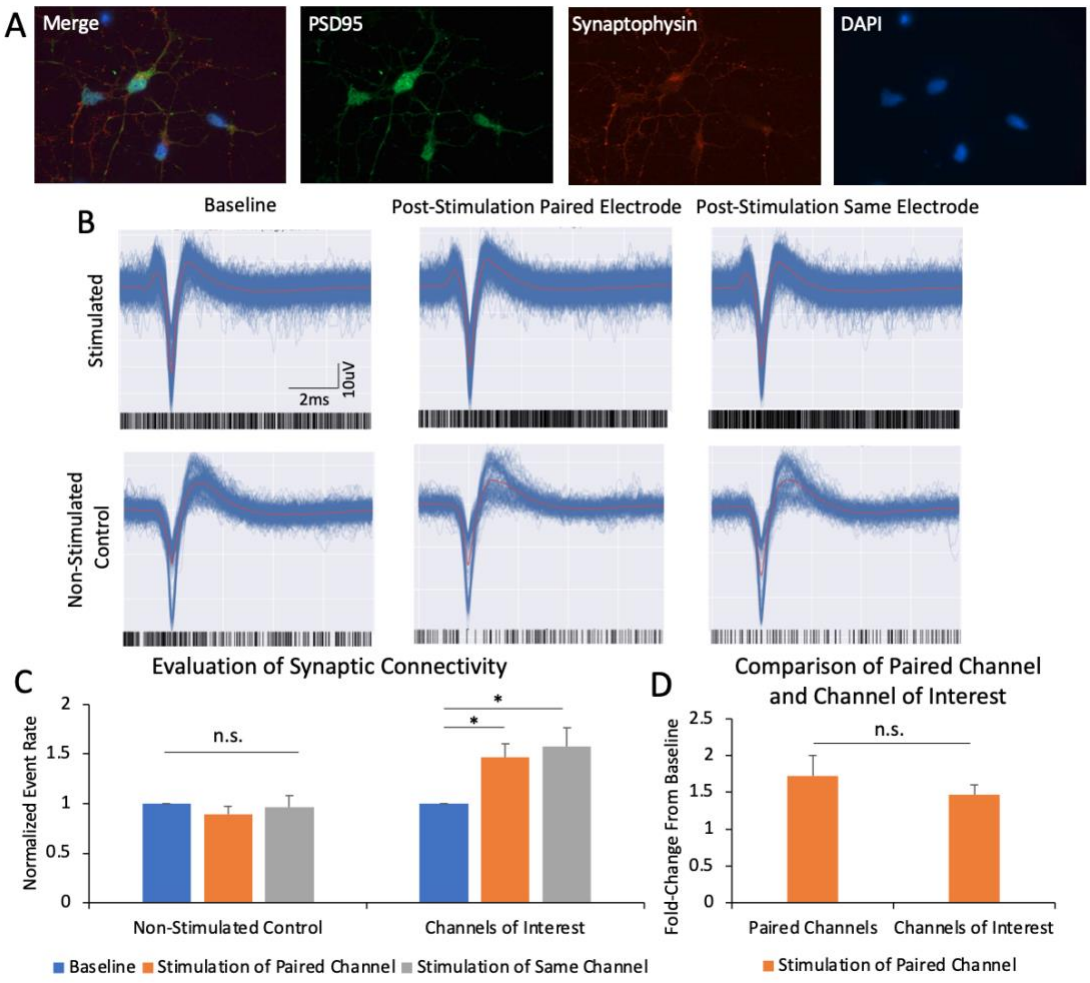

Figure 16: **Evaluation of synaptic connectivity via LTP induction. (A)** Immunocytochemical staining for visualization of synaptic connectivity using PSD95 (green), Synaptophysin (red) and nuclear counterstained with DAPI (blue) using confocal imaging 40X objective (Scale Bar = 50μm). **(B)** Representative waveform traces and accompanying raster plots for neuronal baseline activity, stimulation of opposing electrodes, and stimulation of active electrodes for stimulated systems and non-stimulated controls, confirming that neuronal activity does not change without stimulation. **(C)** Graphical representation of stimulated and non-stimulated systems, where a significant change in activity was not observed in non-stimulated systems, but a significant increase in neuronal activity was observed in active channels when the opposing channel was stimulated. **(D)** Graphical comparison of increased neuronal activity following direct HFS of the active electrode and indirect HFS (stimulation of the opposite electrode) of the active electrode, concluding that the increases in activity are not statistically different. Statistical analysis was determined via One-Way ANOVA and post-hoc analysis via Tukey's HSD and Student's t-test, *$p < 0.05$, **$p < 0.01$, ***$p < 0.001$.

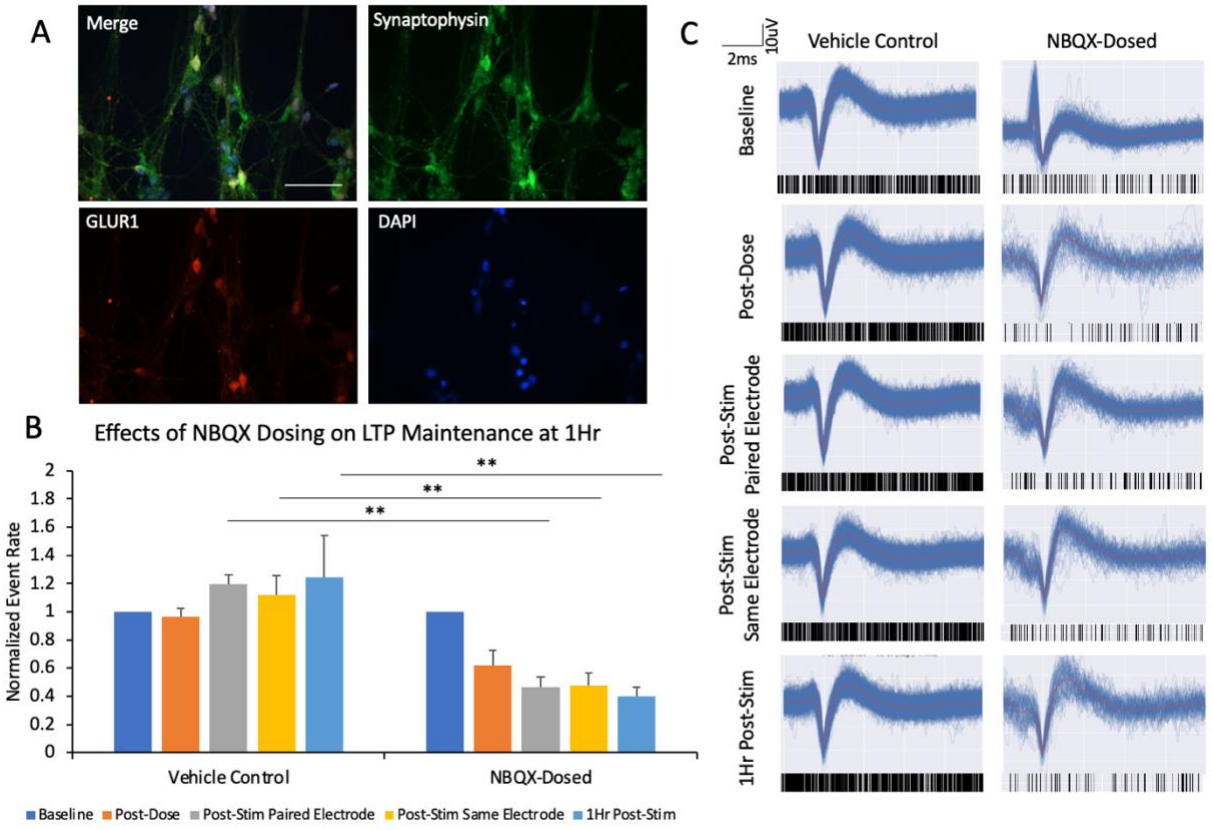

Figure 17: **Figure 4: Validation of LTP induction and maintenance through addition of NBQX. (A)** Immunocytochemical staining for confirmation of AMPA receptor presence using Synaptophysin (green), AMPA receptor subunit GLUR1 (red) and nuclear counterstained with DAPI (blue) using confocal imaging 40X objective (Scale Bar = 50µm). **(B)** Graphical representation of LTP induction and maintenance via HFS in the presence of AMPA receptor antagonist NBQX and vehicle control 0.01% DMSO, where LTP could be induced and maintained for 1 hour in vehicle control systems but could not in the presence of NBQX. **(C)** Representative waveform traces and accompanying raster plots for neuronal baseline activity, following the addition of NBQX, and following HFS and LTP maintenance at 1-hour post-stimulation. Statistical analysis was determined via One-Way ANOVA and post-hoc analysis via Tukey's HSD and Student's t-test, *$p < 0.05$, **$p < 0.01$, ***$p < 0.001$.

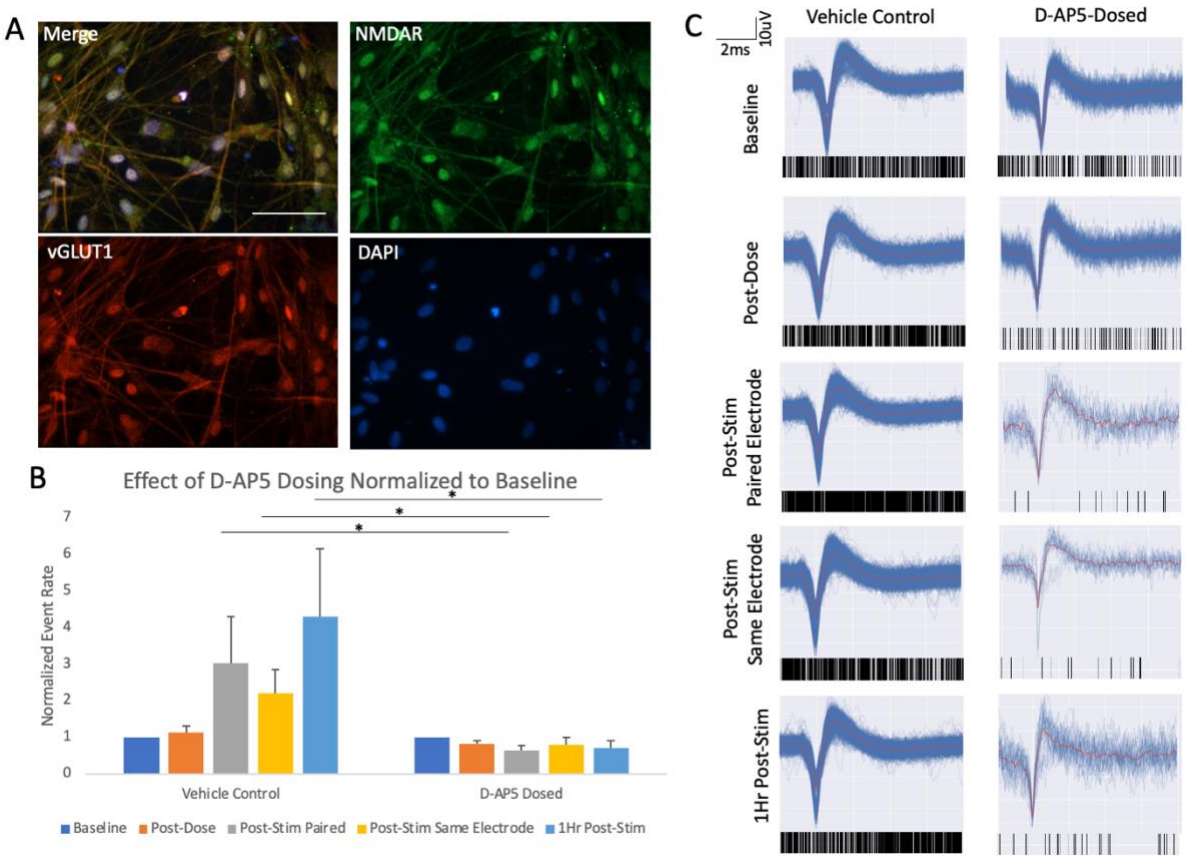

Figure 18: **Validation of LTP induction and maintenance through addition of D-AP5. (A)** Immunocytochemical staining for confirmation of NMDA receptor presence using NMDAR (green), vesicular glutamate antibody vGLUT1 for visualization of the presence of the neurotransmitter glutamate (red) and nuclear counterstained with DAPI (blue) using confocal imaging 40X objective (Scale Bar = 50μm). **(B)** Graphical representation of LTP induction and maintenance via HFS in the presence of NMDA receptor antagonist D-AP5 and vehicle control, where LTP could be induced and maintained for 1 hour in vehicle control systems but could not in the presence of D-AP5. **(C)** Representative waveform traces and accompanying raster plots for neuronal baseline activity, following the addition of D-AP5, and following HFS and LTP maintenance at 1-hour post-stimulation. Statistical analysis was determined via One-Way ANOVA and post-hoc analysis via Tukey's HSD and Student's t-test, *$p < 0.05$, **$p < 0.01$, ***$p < 0.001$.

CHAPTER FIVE: EVALUATION OF LONG-TERM POTENTIATION IN AN IPSC-CORTICAL NEURON MODEL OF FAMILIAL ALZHEIMER'S DISEASE

Introduction

Alzheimer's disease (AD) is a neurodegenerative disease defined pathologically as the deterioration of synaptic networks attributing to the cognitive functions of memory and learning [208]. The main hypothesis for the mechanism of neurodegeneration in AD is through the accumulation of neurotoxic Aβ42 plaques and/or tau neurofibrillary tangles, the latter of which may be dependent on the pathology of the former [209]. The formation of Aβ42 plaques is further hypothesized to non-specifically bind to post-synaptic receptors when released from the pre-synaptic neuron to trigger excitotoxity [210] and inflammation [211] among other detrimental effects. There is much speculation regarding the source of the Aβ42 plaques, the most explored of which is from familial AD (FAD) mutations.

AD is theorized to be caused by the accumulation of Aβ42 oligomers following the neurotoxic elongation caused by improper cleavage of amyloid precursor protein (APP) into the non-pathologic Aβ40 oligomer [4]. The cleavage of APP to Aβ40 is the responsibility of the gamma secretase complex, which is comprised of four main components: presenilins 1 and 2 (PSEN1 and PSEN2), nicastrin, anterior pharynx defective 1 (APH-1), and presenilin enhancer 2 (PEN-2) [212]. The presenilin genes encode for the PSEN1 and PSEN2 subunits, which are the main catalytic components of the complex. Missense mutations in these genes can lead to dysfunction of the catalytic proficiency of the gamma secretase complex [213, 214]. Notably, mutations in the PSEN1 vs. the PSEN2 gene can cause dramatically different downstream effects, due to being shuttled to differing subcellular locations [215].

The PSEN1 gene is the main catalytic subunit of the gamma secretase complex [216]. When it harbors an FAD mutation, it tends to have increased neurogenesis, leading to the spontaneous differentiation of iPSCs [217, 218]. PSEN1 subsequently gets shuttled to the plasma membrane, generating the predominant extracellular pool of Aβ42 oligomers, which then accumulate into plaques within the synaptic cleft and cause the detrimental deterioration of neural networks [219]. Mutations in the PSEN1 gene are most heavily linked to the excitotoxicity hypothesis, which claims that Aβ42 plaques interfere with proper glutamate reuptake, leading to hyperexcitability preceding excitotoxicity-mediated synaptic deterioration and neuronal cell death [83, 220, 221].

In contrast, the PSEN2 subunit becomes localized within the cell's endosomes and lysosomes to generate intracellular Aβ peptides [215, 222]. It has been speculated that a PSEN2 subunit derived from an FAD mutated gene may increase the activity of the gamma secretase subunit, leading to a heightened generation of Aβ42 oligomers [223]. The presence of excessive pathological Aβ42 intracellularly potentially leads to premature neuronal maturation encompassing the rapid depletion of the neural progenitor population and cellular apoptosis [224-226].

Apolipoprotein E4 (ApoE4) is a gene variant that has been linked to a genetic predisposition for the development of AD. It is mainly expressed in the blood-brain barrier (BBB) and liver [227]. The physiological function of ApoE is the metabolism of fat by processing lipids to form lipoproteins responsible for cholesterol transport [228]. While there are several variants, (E2, E3, and E4,) E3 being the most widely expressed, the E4 variant has been associated with an increased genetic risk for developing AD due to its hypolipidation [227]. The mechanism of action

of AD onset from ApoE4 suggests that E4 causes Aβ accumulation through improper clearance [32, 229, 230] and dysfunction in lipid metabolism within the brain [231, 232]. This lipid dysfunction is thought to be primarily contributed by astrocytes in the BBB, which promote increased APP and subsequently the generated pool of Aβ [233]. It has also been cited that the possession of the ApoE4 gene leads to accelerated neuronal maturation and rapid depletion of the neural progenitor pool throughout development, clinically linked to premature aging, due to a characteristic lack of cholesterol binding affecting the neuronal maturation cycle [234, 235].

Several in vivo knock-out and knock-in mouse models have evaluated the neuronal function and neural population dynamics with and without FAD mutations for the designated genes [236-238]. While there have also been several in vitro studies examining neuronal function and analyzing the effects on neuronal function, few have looked at human-derived neurons from FAD iPSCs, and even less have been able to evaluate synaptic plasticity in a quantifiable, in vitro assay for cognition and memory: LTP. This study aimed to characterize the differentiation of human iPSC-cortical neurons from multiple, pre-established FAD iPSC lines. Following the differentiation, neuronal activity and LTP capabilities will be evaluated to establish a mechanism of AD onset and neurodegeneration. Developing functional, in vitro systems for the assessment of neurodegeneration in FAD provides a tool for surveying the potency of drug treatments and preclinical AD therapeutics.

Results

Characterization of Accelerated Maturation and Apoptosis in Mutant Lines

One notable result following the differentiation of AD cortical neurons was the distinct behavior of each line throughout maturation (Figure 19). It was discovered that the PSEN1 line experienced heightened proliferation and enhanced Nestin character compared to our WT control. In contrast, the PSEN2 and ApoE4 lines, both cited as possessing accelerated maturation phenotypes, had less Nestin expression and significantly increased cellular apoptosis detected by Cell Titer Glo Luminescence Assay by 14 DIV. Consequently, subsequent cell seedings were performed at higher plating densities to counteract neuronal apoptosis and encourage culture preservation to 28 DIV.

Characterization of Cortical Neurons

Following differentiation, cortical neuron character was determined via immunocytochemical staining with ctip2. This layer V cortical neuron transcription factor has been previously shown in literature as a marker for confirming the successful differentiation of cortical neurons [66, 151]. All differentiated lines expressed ctip2 at 28 DIV (Figure 20). For enhanced visualization of neuronal morphology, neurons were co-stained with MAP2, which is distinct to mature cortical neurons [239]. Excitatory character confirmation and synaptic puncta visualization was achieved through staining with vGLUT1, which was co-stained for the expression of AMPA receptor subunit GLUR1, a common post-synaptic marker (Figure 21).

Characterization of Cortical Neurons Via Whole-Cell Patch Clamp Electrophysiology

Whole-cell patch clamp recordings revealed an accelerated maturation phenotype in AD mutant PSEN1 and PSEN2 cortical neurons, which was not significantly obvious in ApoE4 cortical neurons compared to our WT control (Figure 22). Gap-free recordings of spontaneous neuronal activity illustrated hyperexcitation in PSEN1 cortical neurons at 14 and 21 DIV, and a significant decline in neuronal activity at 28 DIV, all of which were statistically significant from WT control cortical neurons. Firing rates of PSEN2 cortical neurons were only significantly higher than WT cortical neurons at D21, while ApoE4 cortical neurons were not significantly different than WT control neurons. Similarly, induced repetitive firing of PSEN1 cortical neurons were significantly higher than WT control on D14 and D21, and significantly lower on D28 (Figure 23), indicating hyperexcitability at the earlier timepoints and neuronal decline through excitotoxicity at D28, when the WT neurons were functionally mature. PSEN1 cortical neurons did not exhibit significantly higher firing rates on D14 and D21, but did have a significantly lower firing rate on D28. Unlike the spontaneous firing of ApoE4 cortical neurons, the induced repetitive firing was significantly higher than WT control cortical neurons at D28. This trend was correspondingly reflected in the sodium current measurements at each timepoint (Figure 24). While none of the evaluated lines showed a significant difference when compared to the WT control on D21, the PSEN1 and PSEN2 cortical neurons currents were both significantly higher than WT on D14 and significantly lower than WT on D28. These readings illustrate that the PSEN1 line possesses the most dramatic difference from our WT control line, with the PSEN2 line following a similar trend, and the ApoE4 line being the least different when characterized for phenotypic changes on an individual neuron level.

Evaluation of Long-Term Potentiation in WT and AD Cortical Neurons

The evaluation of long-term potentiation on MEAs enables for the assessment of the synaptic integrity of neuronal networks overtime. LTP maintenance for each line was consistent with neuronal firing trends from whole-cell patch clamp recordings. At D21, it was observed that LTP was achieved at 1-hour in the PSEN1, PSEN2, and ApoE4 lines, but was not displayed in WT control cortical neuron cultures (Figure 25). Previous data has concluded that WT control neurons reach functional maturation at D28, which was reflected in D28 LTP recordings (Figure 26). LTP was observed at 1-hour recordings in the WT control cortical neurons, but was not achieved in the PSEN1, PSEN2, and ApoE4 lines, confirming the synaptic decline within this timepoint akin to AD onset.

Discussion

Although AD has been widely studied, many models of FAD have either employed rat-based in vivo or in vitro models with knock-in AD mutations or have lacked the functional basis for analyzing LTP at the synaptic level [236-238, 240]. By integrating a human-derived, mature iPSC-cortical neuron model with a system capable of assessing neuronal connectivity, we have been able to evaluate LTP in FAD-derived cortical neurons as a function of synaptic integrity and monitor the neuronal behavior and network degradation overtime. This study has demonstrated that our iPSC-cortical neuron differentiation protocol can be adapted to develop patient-specific disease models for assessing cognitive dysfunction in vitro.

Following iPSC expansion and neuronal differentiation, immediate differences were noted between the AD lines and our WT control. The differences in the exhibition of neuroprogenitor

and mature neuronal character in the cultures following characterization has been cited in literature as specific to each mutation. The PSEN1 mutation has been noted to possess heightened neurogenesis, meaning iPSCs carrying this mutation tend to self-differentiate into neurons and glial cells [241]. While glial cells were present in our PSEN1 cultures, we still observed a substantial amount of ctip2 positive cortical neurons that co-expressed MAP2. In contrast, the PSEN2 and ApoE4 AD lines have both been cited as having an accelerated maturation profile, where the neuroprogenitor pool was depleted compared to WT control neurons, and neurons experienced expedient maturation and culture decline. As a result, these lines were plated at a higher plating density to compensate for density loss and encourage culture preservation.

The PSEN1 mutation has been widely hypothesized to follow the excitotoxicity theory for AD onset, which states that hyperexcitation due to improper glutamate reuptake from the presence of Aβ42 in the synaptic cleft precedes synaptic deterioration from excitotoxicity [83, 220, 242]. Our findings support this hypothesis, as whole cell patch clamp results illustrate a premature hyperexcitation of the PSEN1 cortical neurons in the spontaneous and induced repetitive firing readouts at 14 and 21 DIV, which then decline rapidly within the time window of the maturation of the WT control cortical neurons. While other literature sources have cited hyperexcitation of the PSEN1 mutation [28, 214, 217] evident through whole-cell patch clamp recordings [83], they did not evaluate LTP or other neuronal population dynamics.

Neurons were cultures on MEAs to evaluate differences in LTP proficiency overtime. MEA recordings of 1hr LTP persistence demonstrate that, while the PSEN1 neuronal population did show induced LTP following HFS, it could only maintain LTP at 14 DIV, with 21 and 28 DIV showing a graded decrease in activity 1 hour following stimulation (Figures 25-26). Other

literature sources charactering PSEN1 iPSC-cortical neurons have illustrated hyperexcitation at earlier timepoints compared to isogenic WT controls through whole cell patch clamp recordings, showing a significant increase in sodium currents as well as induced and spontaneous neuronal firing [83, 243]. This is consistent with clinical claims that patients possessing a PSEN1 mutations exhibit hyperexcitation symptoms in the form of epileptic seizures in their early adult years (20s-30s), which precedes the deterioration of neural networks and cognitive decline [27, 28].

The PSEN2 mutations differs from PSEN1 in that it is theorized to generate an intracellular pool of Aβ42 as opposed to amassing extracellular oligomers [215, 244, 245]. As a result, it is hypothesized that the effect of the PSEN2 mutation on AD onset would be less severe because it would not have a direct effect on the extracellular synaptic deterioration, but more likely implicated in Ca^{+2} homeostasis [246]. While our results show that the PSEN2 mutation performed similarly to the PSEN1 mutations in patch clamp electrophysiology recordings, the results were less significant in comparison to our WT control. This result was also depicted in the 1-hour LTP maintenance recordings, where we were able to achieve LTP at 21 DIV, but we did not observe persistent LTP at 28 DIV, where the WT control cortical neuron population exhibits LTP capabilities.

Although our ApoE4 line showed accelerated maturation and premature apoptosis, we were able to preserve the culture to assess functional activity and LTP up to 28 DIV by increasing the seeding density. ApoE is responsible for cholesterol transport by the formation of lipoproteins, but ApoE4 is hypolipidated, meaning it possesses lower cholesterol transport capabilities [247]. This has been shown to contribute to improper neuronal maturation and excessive cellular apoptosis [234], which is reflected in our culture conditions, as illustrated through a lower

expression of the neuroprogenitor marker Nestin and cell viability assays. The onset of AD through the ApoE4 gene is postulated to be due to the agglomeration of Aβ to form plaques through improper clearance mechanisms [230, 248, 249]. However, this was not shown to have marked effects on neuronal electrophysiological properties, as the ApoE4 cortical neurons did not perform significantly differently than the WT control cortical neurons, except with a slightly heightened induced firing frequency at 21 DIV that was found to be significant. Like the PSEN1 and PSEN2 lines, the ApoE4 cortical neuron population was able to maintain persistent LTP at 1-hour at 21 DIV. However, MEA recordings confirmed synaptic decline at the timepoint of WT control maturation and LTP assessment, as we were unable to achieve LTP at 28 DIV.

Overall, our previously established protocol for the differentiation of iPSC-cortical neurons for the evaluation of LTP on MEAs has been shown to be adaptable to patient-derived lines for assessing cognitive decline in CNS diseases, such as AD, as illustrated in this study. Our findings support literature hypothesis on common FAD mutations of the PSEN1 and PSEN2 subunits affecting the cleavage of Aβ, where we observed significant premature hyperexcitation that was translatable from patch clamp recordings to LTP persistence. The functional assessment was extended to the ApoE4 genetic predisposition for AD, where we could not achieve LTP within the normal maturation window of our WT control cortical neurons. By integrating the use of patient-derived AD iPSC-cortical neurons with our in vitro system for the functional evaluation of synaptic integrity, we have provided a platform that can be further expounded upon for the assessment of drug efficacy in the prevention and treatment of AD in precision medicine.

Materials and Methods

Cell Lines and iPSC Expansion

WT control iPSCs (ND41865) were purchased from the Coriell Institute. Patient-derived iPSCs for the PSEN1 (CS40iFAD) and PSEN2 (CS08iFAD) AD mutations were purchased from Cedars Sinai. The ApoE4/4 line was purchased from Bioneer (BIONi010-C-4) and was expanded according to manufacturer specifications prior to adopting the standard protocol listed in these methods. Surfaces used for iPSC expansion were 1μg Corning Matrigel (Fisher CB-40230) diluted in DMEM F-12 without phenol red (Fisher 21-041-025). Matrigel was deposited onto the surface and allowed to equilibrate for 1 hour at RT and aspirated prior to cell seeding. iPSCs were maintained in mTESR1 Basal Media (Stemcell 85850) that was supplemented with 5μM Y-27632 (Stemcell 72304) for the first 24 hours following iPSC thawing and passaging with Relesr (Stemcell 05872). A full medium exchange was performed each day throughout culture maintenance. Following the initial thawing, iPSCs were passaged at 70% confluency for expansion and differentiated after at least five passages at 90% cell confluency.

iPSC-Cortical Neuron Differentiation

Cortical neuron differentiation was initiated at 90% iPSC confluency. A full medium exchange was performed every other day throughout differentiation. Differentiation medium I was used for the first 4 days to induce neuroepithelial character, which was composed of a base of N2B media (Table 1), with the addition of Differentiation medium I factors outlined in Table 2. Following neuroepithelial induction, the neurons were directed into the rostral neuroepithelial lineage through

differentiation medium II (Table 3). Lastly, a neurobasal-based cortical neuron media was used for 10 days before neuronal harvesting to establish cortical neuron character (Table 4).

Cortical Neuron Plating and Maintenance

Cortical neurons were harvested following differentiation using 1X trypsin (Fisher 15-400-054) incubated for 5 minutes at 37°C followed by trypsin inhibitor (Fisher 17075029). Once the cell suspension was collected, cells were centrifuged at 260g for 3 minutes. Cell stocks were frozen in a 10% DMSO (Sigma D4540-100ml) solution of cortical neuron maintenance media (Table 4). Following harvesting or thawing using the drop-by-drop methods with cold 1X PBS, cortical neurons were maintained for 7 days in maintenance media (Table 4) with half-medium exchanges twice weekly. After day 7, the half-medium exchanges were performed using BrainPhys media (Table 5) for the duration of the culture. Viability assessments were performed using Cell Titer Glo Luminescence Cell Viability Assay (Fisher G7571). Staurosporine (Sigma 19-123MG) was used at a concentration of 1mM incubated at 37°C for 24h in the cell culture as a negative control for cell viability.

Immunocytochemistry

Cells intended for immunocytochemical analysis were seeded onto 18mm glass coverslips coated with DETA [250]. Cells were fixed for 15 mins at RT using a 4% paraformaldehyde solution (16%, ThermoFisher 28908) diluted in 1X PBS. Coverslips were rinsed thrice following fixing, and permeabilized for intracellular stains for 15 mins at RT using 0.1% Triton X-100 (Sigma 9036-19-5). Non-specific binding sites were then blocked in a blocking solution of 5% BSA (Cayman

Chemicals A23016) and 5% goat serum (Sigma S26-100 ml) diluted in 1X PBS for 1hr at RT. Primary antibodies were diluted in blocking solution and incubated overnight at 4°C. Following overnight incubation, coverslips were again rinsed thrice with 1X PBS and incubated with secondary antibodies for 2-4hrs at RT in the dark. Coverslips were adequately rinsed prior to coverslip mounting using Prolong Gold Antifade Mountant with DAPI (Fisher P36931). Primary antibodies used included Nestin (Novus MAB1259), MAP2 (Fisher MA5-12823), vGLUT1 (Sigma AB5905), GLUR1 (Fisher PA5-111797), and ctip2 (Abcam ab18465). Secondary antibodies utilized were Goat anti-Rabbit Secondary Antibody Alexa Fluor 568 (ThermoFisher A-11011), Goat anti-Mouse Secondary Antibody Alexa Fluor 568 (ThermoFisher A-11004), Goat anti-Rabbit Secondary Antibody Alexa Fluor 488 (ThermoFisher A11008), Goat anti-Mouse Secondary Antibody Alexa Fluor 488 (ThermoFisher A-11001), Goat anti-Rat Secondary Antibody Alexa Fluor 488 (ThermoFisher A-11006), and Goat anti-Guinea Pig Secondary Antibody Alexa Fluor 488 (ThermoFisher A-11073). Imaging was performed using confocal microscopy (Zeiss, Axioskop 2, Germany).

Whole-Cell Patch Clamp Electrophysiology

Whole-cell patch clamp recordings were taken using a Zeiss, upright microscope (Axioscope, FS2, Carl Zeiss, Germany) equipped with a multiclamp 700B amplifier [177]. The intracellular patch solution consisted of 140 mM K-gluconate, 4 mM NaCl, 0.5 mM $CaCl_2$, 1 mM $MgCl_2$, 1 mM EGTA, 5 mM HEPES Acid, 5 mM HEPES base, and 5 mM Na_2ATP [151]. Spontaneous neuronal firing, induced repetitive firing, and sodium and potassium currents were evoked as described in Caneus *et al.* [62]. Data was processed using Clampfit, Microsoft Excel, and GraphPad Prism.

Statistical analysis was determined using Student's t-test or One-Way ANOVA and Tukey's post-hoc analysis.

MEA

MEAs were fabricated and surface patterned as described in Autar *et al.* [151]. Following surface patterning, MEAs were coated using a 0.01% poly-L-ornithine solution (Sigma 27378-49-0) for 1hr at RT. Surfaces were subsequently rinsed thrice with 1X PBS before being incubated overnight at 4°C with a 3.33μg/mL laminin (Fisher 23017015) solution. Surfaces were warmed to 37°C in the incubator, and the laminin solution was aspirated immediately prior to cell seeding. WT control cortical neurons were seeded on MEAs at a plating density of 400cells/mm^2, PSEN1 cortical neurons at 200cells/mm^2, PSEN2 and ApoE4 cortical neurons were both seeded at 1000cells/mm^2 to compensate for cell loss due to line viability.

LTP Induction

MEA recordings were taken using a multi-channel systems (MCS) rig. LTP was induced via a 100Hz high-frequency stimulation protocol of 10 repetitions of 4X biphasic 500mV, 5ms pulses [62, 69, 151]. A pre-stimulation baseline was recorded for 5 minutes preceding HFS. All recordings following LTP were also taken for 5 minutes, and normalized frequency comparisons were used for determining LTP.

MEA Analysis

Raw MEA data was filtered through a second order Butterworth 100Hz high-pass filter. Only events crossing a threshold of +/- 5 standard deviations from the noise were taken as signal [251]. Any spikes co-occurring on more than 2 channels at the same millisecond time stamp were eliminated as artifacts [62, 151]. A signal template was designed using eliminated signals following lidocaine addition to develop a principal component analysis filter to further eliminate system noise. Data was processed using Microsoft Excel and GraphPad Prism. Statistical analysis was determined using Student's t-test or One-Way ANOVA and Tukey's post-hoc analysis.

Figures

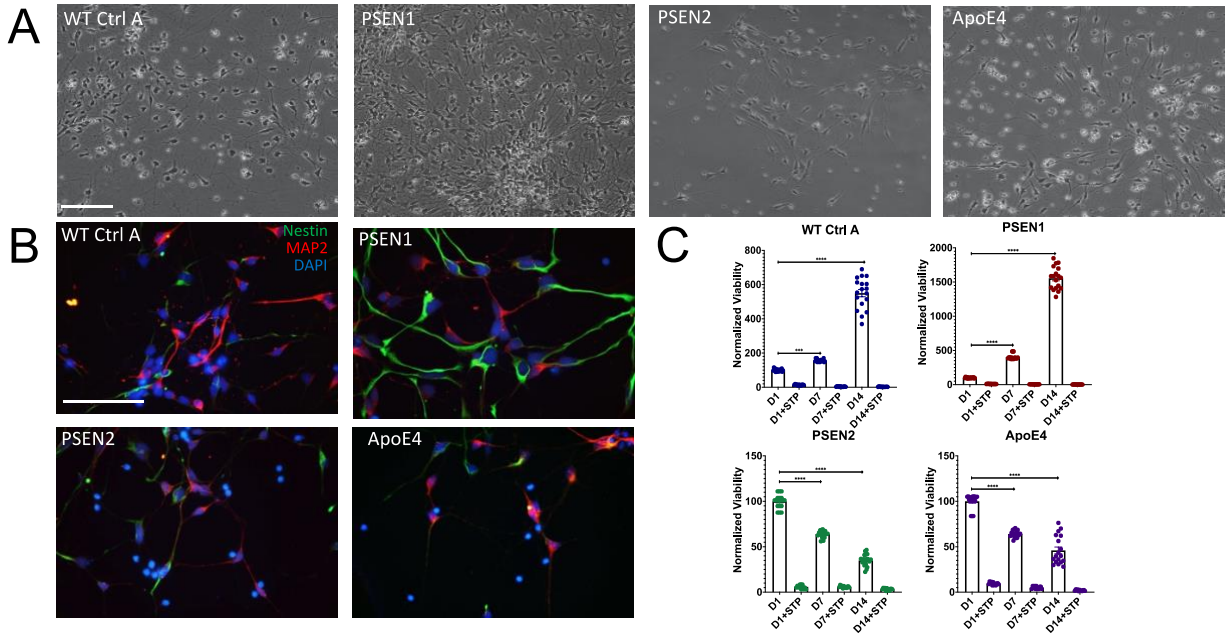

Figure 19: **Characterization of Accelerated Maturation and Apoptosis in Mutant Lines.** All cortical neuron lines showed typical phase morphology at 14 DIV **(A).** The mutant lines at 14 DIV had differing expression of neuroprogenitor protein Nestin and neuronal cytoskeletal protein MAP2, suggesting differing maturation timelines **(B),** and decreased cell viability overtime indicating increased apoptosis **(C).** Scale bar = 100μm.

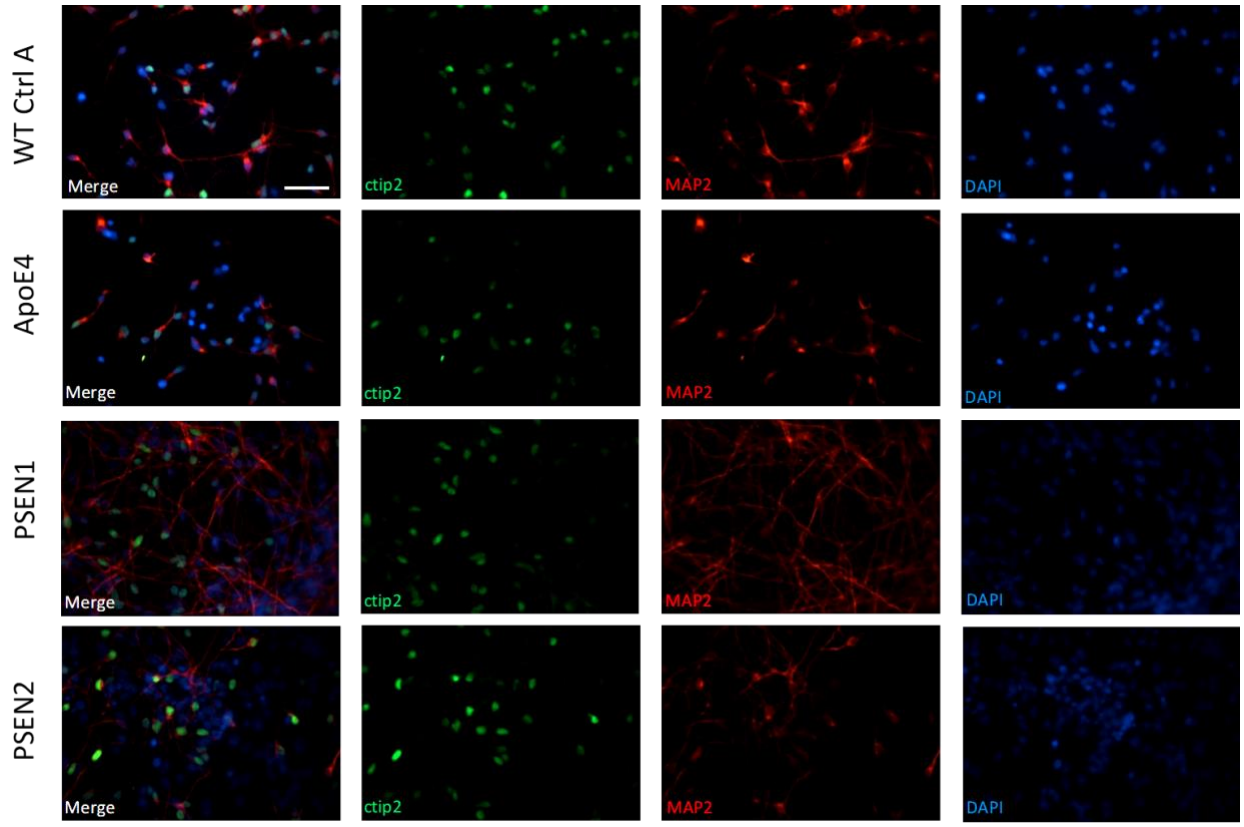

Figure 20: **Characterization of Cortical Neuron Character Via Immunocytochemistry.** Immunocyotochemical analysis revealed that all lines showed successful expression of layer V cortical neuron transcription factor ctip2 (green) at 28 DIV. Neurons also expressed mature neuronal marker microtubule associated protein 2 (MAP2, red). Coverslips were counterstained with DAPI for nuclear visualization. Scale bar = 100μm.

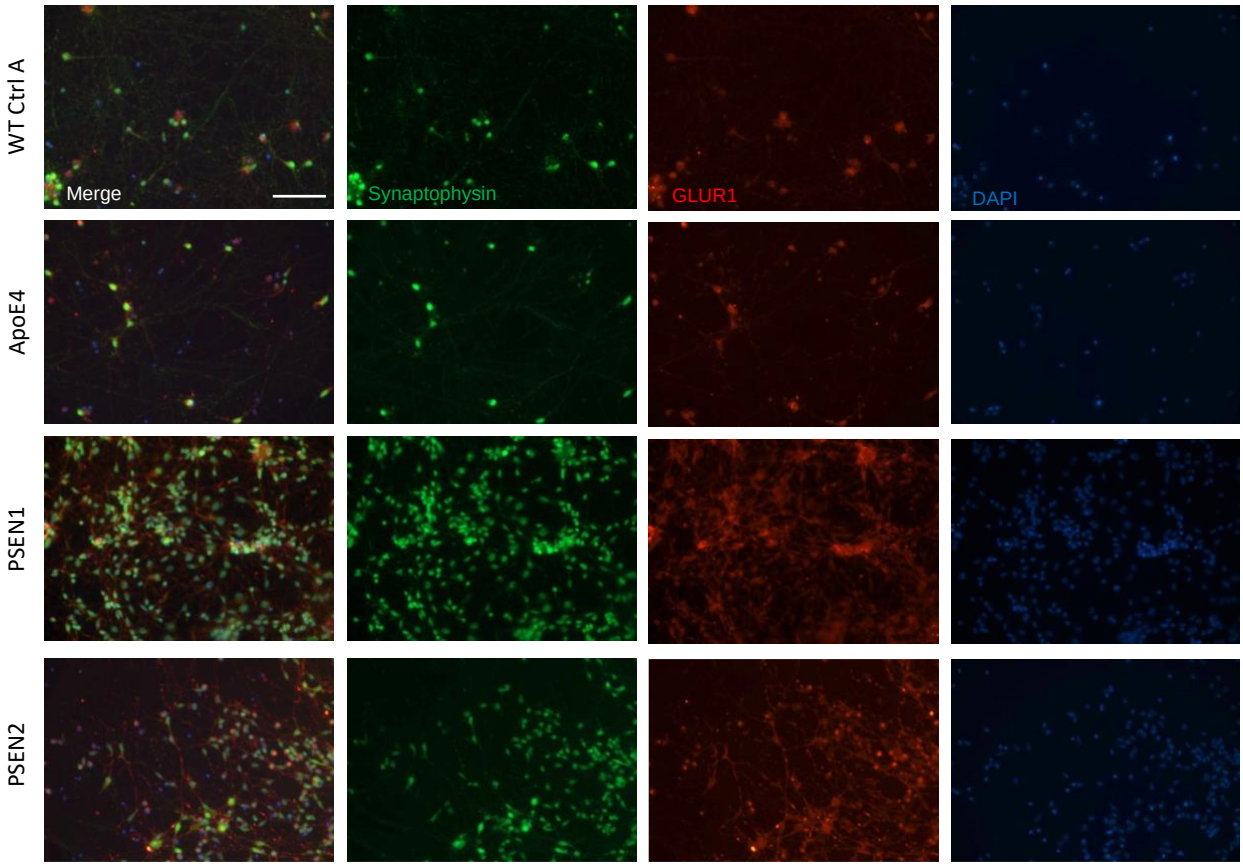

Figure 21: **Characterization of Neuronal Synapses via Immunocytochemistry.** Immunocytochemical staining depicting synaptic connectivity in WT and AD lines at 28 DIV. Pre-synaptic and excitatory neuronal marker vesicular glutamate 1 (vGLUT1, green) illustrates synaptic puncta. Post-synaptic marker GLUR1 (red) highlights a subunit of the AMPA glutamate receptor. Scale bar = 100μm.

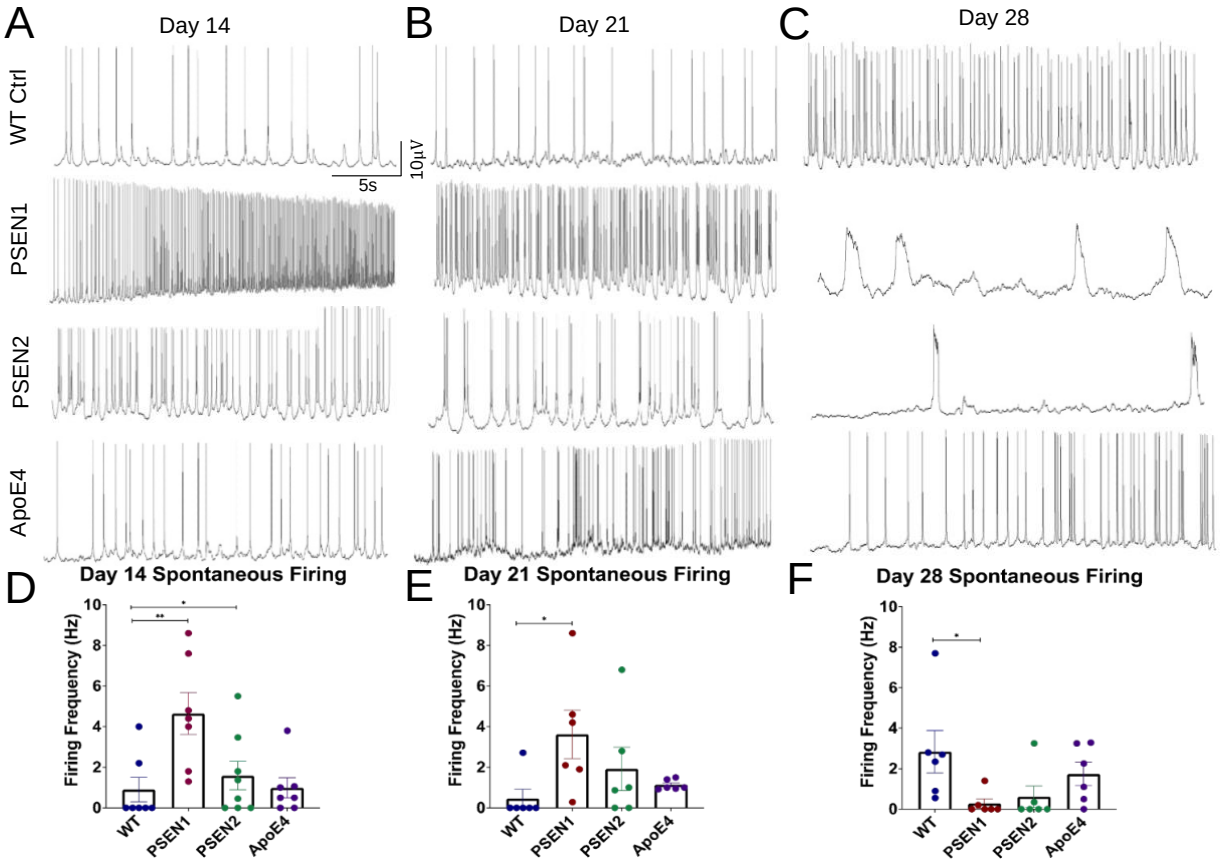

Figure 22: **Whole-Cell Patch Clamp Recordings of Spontaneous Neuronal Firing Overtime.** Representative traces of gap-free spontaneous neuronal activity of WT and AD neurons on **(A)** 14 DIV, **(B)** 21 DIV, and **(C)** 28 DIV. Graphs detailing neuronal firing in patch clamp experiments on **(D)** 14 DIV, **(E)** 21 DIV, and **(F)** 28 DIV portraying hyperactivation in PSEN1 and PSEN2 cortical neurons at 14 DIV that is also present in the former at 21 DIV and is statistically significant compared to WT control cortical neurons, that ultimately drops significantly at 28 DIV. Statistical significance was determined via Student's t-test, * $p<0.05$, ** $p<0.01$, *** $p<0.001$.

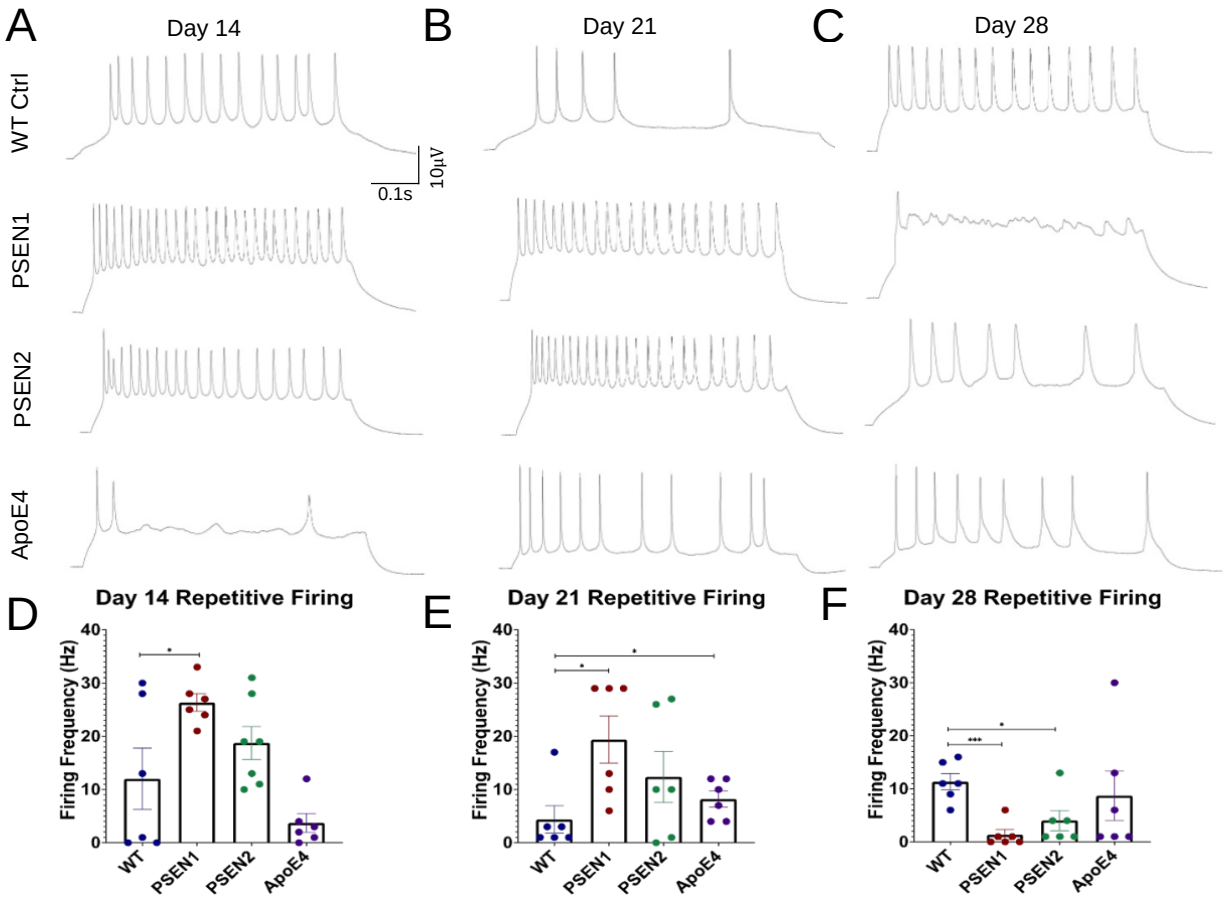

Figure 23: **Whole-Cell Patch Clamp Recordings of Induced Repetitive Neuronal Firing Overtime.** Representative traces of induced, repetitive neuronal activity of WT and AD neurons on **(A)** 14 DIV, **(B)** 21 DIV, and **(C)** 28 DIV. Graphs detailing neuronal firing in patch clamp experiments on **(D)** 14 DIV, **(E)** 21 DIV, and **(F)** 28 DIV depicting the hyperactivation present in PSEN1 cortical neurons at 14 and 21 DIV that is significantly reduced in PSEN1 and PSEN2 cultures compared to WT controls at 28 DIV. The ApoE4 cortical neurons also experienced hyperactivation at 21 DIV, but were otherwise not significantly different than the WT control. Statistical significance was determined via Student's t-test, * $p<0.05$, ** $p<0.01$, *** $p<0.001$.

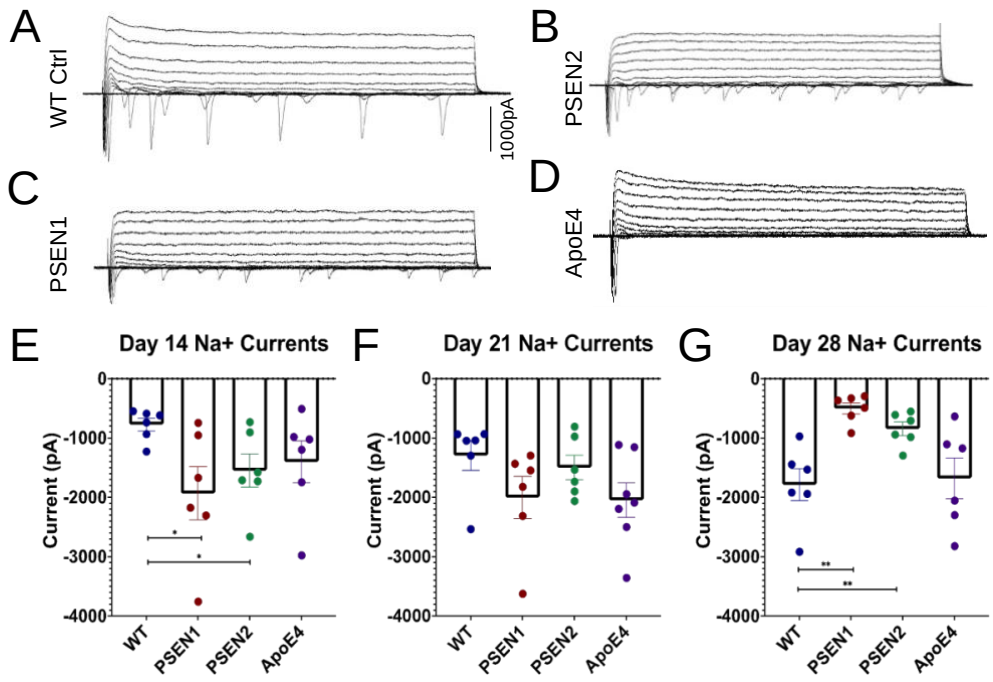

Figure 24: **Whole-Cell Patch Clamp Recordings of Sodium Currents Overtime.** Representative traces of neuronal currents at 28 DIV for **(A)** WT Control, **(B)** PSEN1, **(C)** PSEN2, and **(D)** ApoE4. Graphs detailing neuronal firing in patch clamp experiments on **(E)** 14 DIV, **(F)** 21 DIV, and **(G)** 28 DIV illustrating the hyperactivity present in the PSEN1 and PSEN2 cortical neurons at 14 DIV that exhibit a marked decrease at 28 DIV compared to the WT control cortical neurons. Statistical significance was determined via Student's t-test, * $p<0.05$, ** $p<0.01$, *** $p<0.001$.

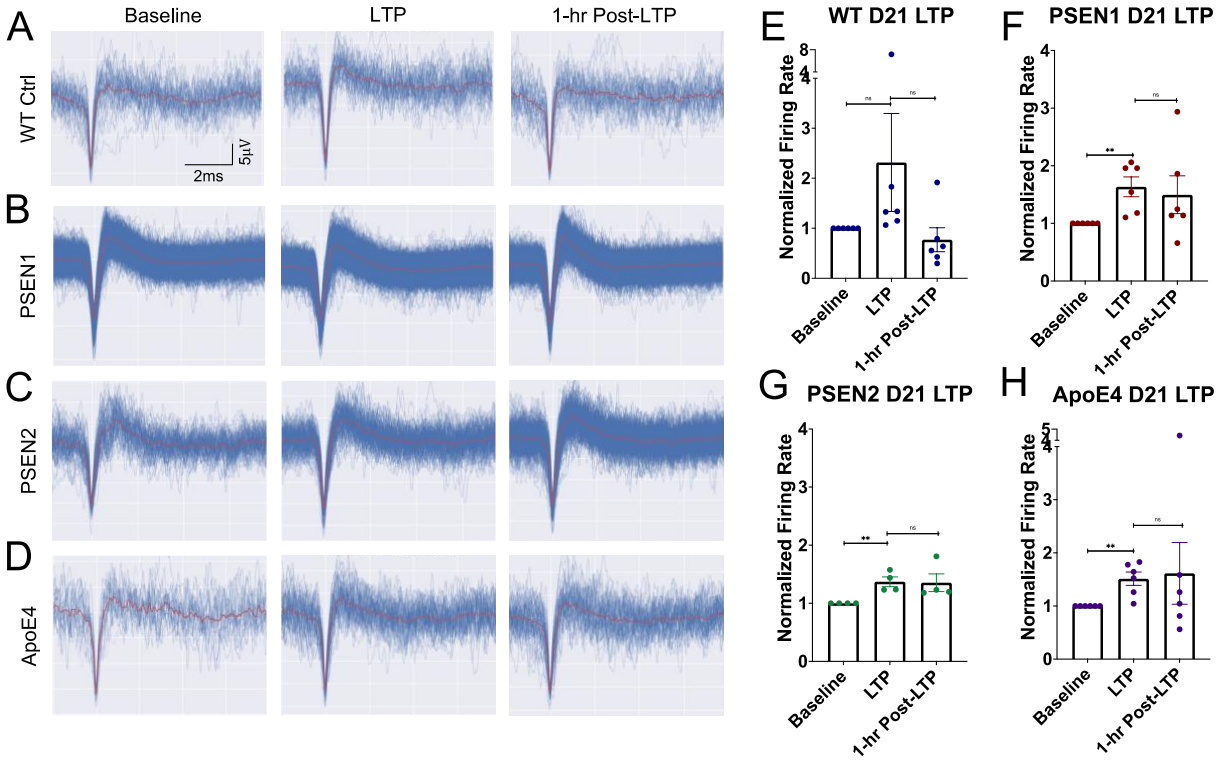

Figure 25: **Induction of Long-Term Potentiation in AD Lines at 21 DIV.** Representative traces of neuronal activity on MEAs at 21 DIV for baseline (left), immediate post-LTP stimulation (middle), and 1-hr post-LTP stimulation (right) for **(A)** WT control cortical neurons, **(B)** PSEN1 cortical neurons, **(C)** PSEN2 cortical neurons, and **(D)** ApoE4 cortical neurons. **(E-H)** Graphs quantifying LTP induction and maintenance normalized to baseline levels indicating that LTP could not be maintained in WT control cortical neurons, but LTP persistence at 1-hour was significant for the PSEN1 and PSEN2 cortical neurons. Statistical analysis was determined via One-Way ANOVA and Tukey's post-hoc analysis, * $p<0.05$, ** $p<0.01$, *** $p<0.001$.

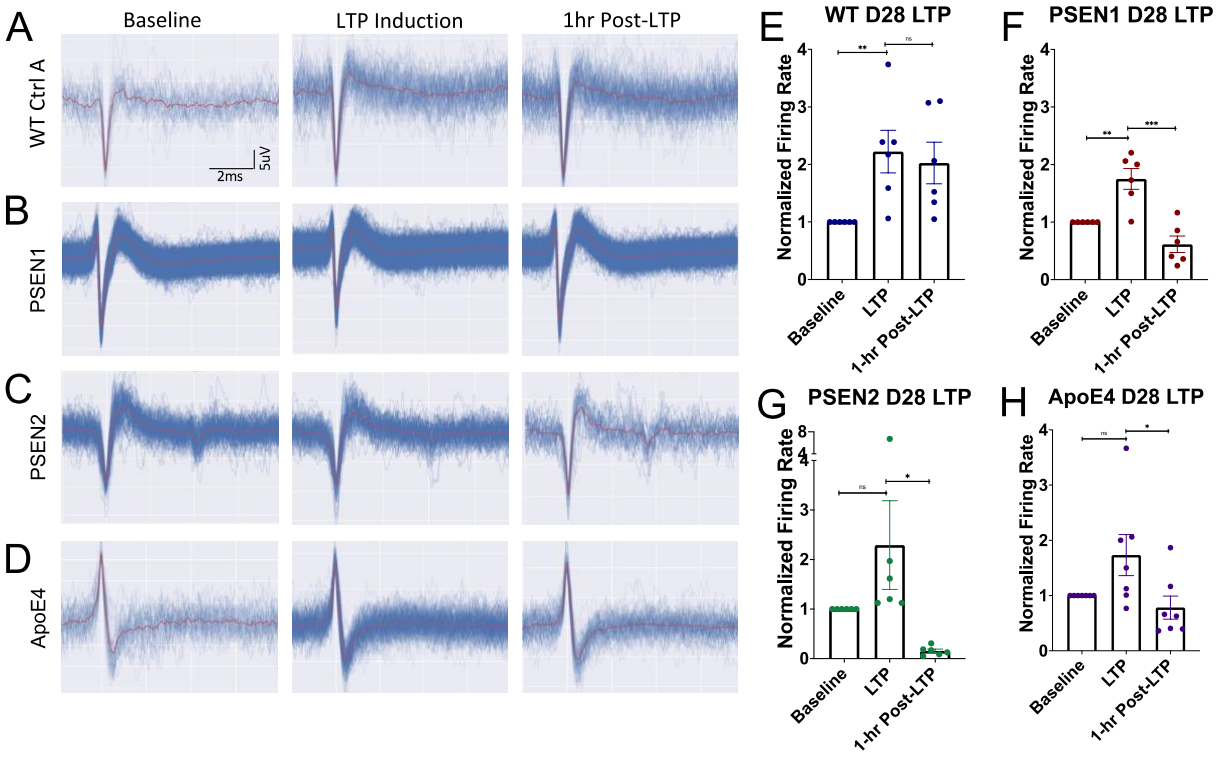

Figure 26: **Induction of Long-Term Potentiation in AD lines at 28 DIV.** Representative traces of neuronal activity on MEAs at 28 DIV for baseline (left), immediate post-LTP stimulation (middle), and 1-hr post-LTP stimulation (right) for **(A)** WT control cortical neurons, **(B)** PSEN1 cortical neurons, **(C)** PSEN2 cortical neurons, and **(D)** ApoE4 cortical neurons. **(E-H)** Graphs quantifying LTP induction and maintenance normalized to baseline levels, indicating that, while LTP persistence is present in WT control cortical neurons, LTP was not maintained at 1-hour for the PSEN1, PSEN2, and ApoE4 lines. Statistical analysis was determined via One-Way ANOVA and Tukey's post-hoc analysis, * $p<0.05$, ** $p<0.01$, *** $p<0.001$.

Table 1: Formulation of N2B Media

N2B Media			
Component	**Company**	**Catalog #**	**Concentration**
DMEM/F-12	Fisher	21041-025	
Human apo-transferrin	R&D	3188-AT-001G	1.25 μM
Insulin	Millipore	407709-50MG	4.3 μM
D-(+)-Glucose, Anhydrous	Sigma	G8270	8.65 mM
Progesterone	Sigma	P-8783	20 nM
Putriscine	Sigma	P-5780	100 μM
Na+ Selenite	Sigma	214485-5G	30 nM

Table 2: Formulation of Differentiation Media I

Differentiation Media I			
Component	**Company**	**Catalog #**	**Concentration**
N2B			-
SB431542	TOCRIS	1614	6 μM
LDN193189	TOCRIS	6053	0.1 μM
DMH-1	TOCRIS	4126	2 μM
DKK1	Fisher	5439-DK-010	10 ng/ml

Table 3: Formulation of Differentiation Media II

Differentiation Media II			
Component	**Company**	**Catalog #**	**Concentration**
N2B			-
SB431542	TOCRIS	1614	6 μM
LDN193189	TOCRIS	6053	0.1 μM
DMH-1	TOCRIS	4126	2 μM
Cyclopamine	Millipore	239803	5 μM

Table 4: Formulation of Differentiation Media III/Maintenance Media

Differentiation Media III/Maintenance Media			
Component	**Company**	**Catalog #**	**Concentration**
Neurobasal	Fisher	21103049	-
Glutamax	Fisher	35-050-061	1X
N2 supplement	Fisher	17502048	1X
B27 (w/o VitA)	Fisher	12587-010	1X
BDNF	Cell Sciences	CRB600D	20ng/ml
GDNF	Cell Sciences	CRG400E	20ng/ml
Ascorbic acid	StemCell	72132	200nM
cAMP	Sigma	A9501-1G	1 μM
Laminin	Sigma	L2020	1 μg/ml
Antibiotic-Antimycotic	Fisher	15240-062	1X

Table 5: Formulation of BrainPhys Media

BrainPhys Media			
Component	**Company**	**Catalog #**	**Concentration**
BrainPhys Base Media	StemCell	05793	-
N2-A Supplement	"	"	1X
SM1 Supplement	"	"	1X
BDNF	Cell Sciences	CRB600D	20ng/ml
GDNF	Cell Sciences	CRG400E	20ng/ml
Ascorbic acid	StemCell	72132	200nM
cAMP	Sigma	A9501-1G	1 μM
Laminin	Sigma	L2020	0.5 μg/ml
Antibiotic-Antimycotic	Fisher	15240-062	1X

Table 6: Line and Genotyping Details of AD iPSCs

Line	Line Details	Sex	Age	Mutation	ApoE Genotype
WT Control	ND41865	Male	64	N/A	E2/E3
PSEN1	CS40iFAD	Male	56	ALA246GLU	E3/E3
PSEN2	CS08iFAD	Female	81	ASN141ILE	E3/E3
ApoE4	BIONi010-C-4	Male	N/A	N/A	E4/E4

CHAPTER SIX: GENERAL DISCUSSION

Alzheimer's disease is described as a loss of cognition from the presence of Aβ42 plaques in the brain, generally characterized in models for AD assessment as a loss of neuronal function, both at the cellular and the synaptic level [252-256]. There are several notable mechanisms for the onset of AD, with the most well-known being the loss of synaptic networking through the agglomeration of senile Aβ42 [4], which also potentially onset Tau neurofibrillary tangles [257]. However, neurodegeneration in AD can also be exacerbated by neuroinflammation [6], Ca^{+2} dysfunction [258, 259], and the accrual of reactive oxygen species [36]. Due to limited neuronal cell sources for developing in vitro models of AD, human-derived iPSCs were utilized to develop a serum-free differentiation protocol, and the maturation of the neuronal culture was tracked to optimize the timepoint for evaluating LTP, the in vitro correlate for learning and memory [260]. Once validated, this system could be further employed to SAD and FAD models for assessing cognitive deficits.

An iPSC to cortical neuron differentiation protocol was first established and characterized for LTP proficiency [151]. Serum-free medium formulations were used to initiate cortical neuron differentiation starting with dual-SMAD inhibition [74], inducing cortical neuron character mimicking the development of neurons in vivo. Following differentiation, neurons were evaluated throughout maturation, where they were characterized for common neuronal and cortical neuron markers and assessed for neuronal function using whole-cell patch clamp (Figures 1-3). Once the successful differentiation of cortical neurons was confirmed, neuronal networks were cultured on MEAs to assess neural population dynamics and LTP (Figure 4-5). It was discovered that the neurons also simulated immature inhibitory character [89, 261]. It was established that neurons

did not exhibit fully glutamatergic character until 30-40 DIV, and therefore could not maintain persistent LTP for 1-hour until this timepoint in maturation, due to possession of GABAergic neuronal character, impeding LTP capabilities at earlier timepoints (Figure 6).

Once validated, this model could be utilized to evaluate drug efficacy in neuronal culture. This iPSC-cortical neuron culture was used to establish a model of sporadic AD (SAD), where the neuronal cultured was supplemented with Aβ42 oligomers to incite the AD phenotype, characterized in our culture as an impedance of LTP. Following the confirmation of all drug targets in the iPSC-cortical neuron culture (Figure 8), neurons were cultures on MEAs for the evaluation of the ability of each drug to block the neurotoxic effects of Aβ42 (Figure 9). Whole-cell patch clamp electrophysiology was used to accompany the assessment of network integrity on MEAs. Donepezil is an acetylcholinesterase inhibitor, which works to increase the availability of acetylcholine within the synaptic cleft to preserve neuronal function [50]. It was observed to rescue Na^+ currents and spontaneous firing (Figure 10). Saracatinib inhibits the Fyn kinase, which is directly responsible for the amplified formation of Aβ42 plaques, and can be exacerbated by the presence of Aβ42 dosed in the culture media [52, 185]. Consequently, the co-administration of Saracatinib with Aβ42 oligomers significantly aided Na^+ currents, neuronal firing frequencies, and action potential amplitudes (Figure 11). Memantine specifically targets the NMDA receptor to counteract excitotoxicity-induced synaptic decline [49], and was shown to rescue neuronal firing amplitudes (Figure 12). Lastly, Rolipram, which increases intracellular cAMP by inhibiting its breakdown [53], displayed significant preventative effects on neuronal firing amplitudes (Figure 13). Chiefly, all the evaluated drugs were shown to significantly maintain LTP, preventing the Aβ42 oligomer-induced loss of synaptic function, in our neuronal systems (Figures 10-13).

Neurodegeneration onset of AD is characterized by a notable loss of synapse integrity [188]. To further enhance the capability of our system to evaluate synaptically transmitted LTP deficits, a surface pattern was employed to the MEAs to initiate synaptic pairing of neuronal populations (Figures 14-16). It was observed that LTP could be induced within a neuronal population from performing high frequency stimulation on its synaptically paired population, which was not found to be significantly different than LTP induced through direct stimulation (Figures 17-18).

The establishment of an hiPSC-cortical neuron protocol could be further expanded to encompass several known AD genetic mutation and predispositions, the mechanisms of which have been widely theorized but minimally explored. The resulting differentiation of our PSEN1, PSEN2, and ApoE4 cortical neurons have exhibited phenotypes consistent with known hypotheses for this mutation and other literature results. Enhanced neurogenesis was present in the PSEN1 mutant cortical neurons alongside a proclivity for self-differentiation [217], and hyperexcitability was characteristic in both the whole-cell patch clamp and MEA results (Figures 20-26). This hyperexcitability phenotype fueled the excitotoxicity within the culture, as the PSEN1 and PSEN2 neuronal cultures declined more quickly than the WT, and could not sustain LTP at the timepoint in which the WT neurons were established as a mature culture. The ApoE4 phenotype was observed in a similar fashion. While the differences were not significantly different from the WT control, patch clamp recordings confirmed the accelerated maturation phenotype previously cited in literature. This trend was mimicked in LTP recordings, indicating synaptic decline, as persistent LTP was achievable at 21 DIV, but was not present at later timepoints.

This model aimed to provide a biologically relevant system for assessing drug efficacy at the preclinical stage by establishing a functional disease phenotype. In this study, it was shown that the co-administration of AD therapeutic treatments blocked the neurotoxic effects of Aβ42 oligomers, and the previously validated iPSC-cortical neuron differentiation protocol could be adapted for the development of patient-derived neuronal cultures. The use of microelectrode arrays enables the development of minimally invasive, patient-specific neural networks that can be assessed for synaptic communication. The establishment of a human-based, in vitro, iPSC-derived cortical neuron model provides an apparatus for preclinical drug evaluation of CNS diseases.

LIST OF REFERENCES

1. *2020 Alzheimer's disease facts and figures.* Alzheimer's & Dementia, 2020. **16**(3): p. 391-460.

2. *2021 Alzheimer's disease facts and figures.* Alzheimer's & Dementia, 2021. **17**(3): p. 327-406.

3. Marsh, J. and P. Alifragis, *Synaptic dysfunction in Alzheimer's disease: the effects of amyloid beta on synaptic vesicle dynamics as a novel target for therapeutic intervention.* Neural regeneration research, 2018. **13**(4): p. 616-623.

4. Murphy, M.P. and H. LeVine, 3rd, *Alzheimer's disease and the amyloid-beta peptide.* Journal of Alzheimer's disease : JAD, 2010. **19**(1): p. 311-323.

5. Šimić, G., et al., *Tau Protein Hyperphosphorylation and Aggregation in Alzheimer's Disease and Other Tauopathies, and Possible Neuroprotective Strategies.* Biomolecules, 2016. **6**(1): p. 6-6.

6. Heneka, M.T., et al., *Neuroinflammation in Alzheimer's disease.* The Lancet. Neurology, 2015. **14**(4): p. 388-405.

7. Leng, F. and P. Edison, *Neuroinflammation and microglial activation in Alzheimer disease: where do we go from here?* Nature Reviews Neurology, 2021. **17**(3): p. 157-172.

8. Huang, W.-J., X. Zhang, and W.-W. Chen, *Role of oxidative stress in Alzheimer's disease.* Biomedical reports, 2016. **4**(5): p. 519-522.

9. Gella, A. and N. Durany, *Oxidative stress in Alzheimer disease.* Cell adhesion & migration, 2009. **3**(1): p. 88-93.

10. Francis, P.T., et al., *The cholinergic hypothesis of Alzheimer’s disease: a review of progress.* Journal of Neurology, Neurosurgery & Psychiatry, 1999. **66**(2): p. 137.

11. Hampel, H., et al., *Revisiting the Cholinergic Hypothesis in Alzheimer's Disease: Emerging Evidence from Translational and Clinical Research.* J Prev Alzheimers Dis, 2019. **6**(1): p. 2-15.

12. Chakroborty, S. and G.E. Stutzmann, *Early calcium dysregulation in Alzheimer's disease: setting the stage for synaptic dysfunction.* Sci China Life Sci, 2011. **54**(8): p. 752-62.

13. Kinney, J.W., et al., *Inflammation as a central mechanism in Alzheimer's disease.* Alzheimer's & dementia (New York, N. Y.), 2018. **4**: p. 575-590.

14. Mandrekar-Colucci, S. and G.E. Landreth, *Microglia and inflammation in Alzheimer's disease.* CNS & neurological disorders drug targets, 2010. **9**(2): p. 156-167.

15. Shankar, G.M. and D.M. Walsh, *Alzheimer's disease: synaptic dysfunction and Aβ.* Molecular Neurodegeneration, 2009. **4**(1): p. 48.

16. O'Brien, R.J. and P.C. Wong, *Amyloid precursor protein processing and Alzheimer's disease.* Annual review of neuroscience, 2011. **34**: p. 185-204.

17. Chen, Y. and C. Dong, *Abeta40 promotes neuronal cell fate in neural progenitor cells.* Cell Death Differ, 2009. **16**(3): p. 386-94.

18. Babaei, P., *NMDA and AMPA receptors dysregulation in Alzheimer's disease.* Eur J Pharmacol, 2021. **908**: p. 174310.

19. Danysz, W. and C.G. Parsons, *Alzheimer's disease, β-amyloid, glutamate, NMDA receptors and memantine--searching for the connections.* British journal of pharmacology, 2012. **167**(2): p. 324-352.

20. Kulijewicz-Nawrot, M., et al., *Astrocytes and glutamate homoeostasis in Alzheimer's disease: a decrease in glutamine synthetase, but not in glutamate transporter-1, in the prefrontal cortex.* ASN neuro, 2013. **5**(4): p. 273-282.

21. Wang, W.-Y., et al., *Role of pro-inflammatory cytokines released from microglia in Alzheimer's disease.* Annals of Translational Medicine, 2015. **3**(10): p. 7.

22. Rodríguez-Martín, T., et al., *Tau phosphorylation affects its axonal transport and degradation.* Neurobiology of aging, 2013. **34**(9): p. 2146-2157.

23. Combs, B., et al., *Tau and Axonal Transport Misregulation in Tauopathies.* Advances in experimental medicine and biology, 2019. **1184**: p. 81-95.

24. Metcalfe, M.J. and M.E. Figueiredo-Pereira, *Relationship between tau pathology and neuroinflammation in Alzheimer's disease.* The Mount Sinai journal of medicine, New York, 2010. **77**(1): p. 50-58.

25. Nisbet, R.M., et al., *Tau aggregation and its interplay with amyloid-β.* Acta neuropathologica, 2015. **129**(2): p. 207-220.

26. Xiao, X., et al., *APP, PSEN1, and PSEN2 Variants in Alzheimer's Disease: Systematic Re-evaluation According to ACMG Guidelines.* Frontiers in Aging Neuroscience, 2021. **13**.

27. Cortini, F., C. Cantoni, and C. Villa, *Epileptic seizures in autosomal dominant forms of Alzheimer's disease.* Seizure, 2018. **61**: p. 4-7.

28. Larner, A.J., *Presenilin-1 mutation Alzheimer's disease: a genetic epilepsy syndrome?* Epilepsy Behav, 2011. **21**(1): p. 20-2.

29. Emrani, S., et al., *APOE4 is associated with cognitive and pathological heterogeneity in patients with Alzheimer's disease: a systematic review.* Alzheimer's Research & Therapy, 2020. **12**(1): p. 141.

30. Liu, C.-C., et al., *Apolipoprotein E and Alzheimer disease: risk, mechanisms and therapy.* Nature reviews. Neurology, 2013. **9**(2): p. 106-118.

31. Dumanis, S.B., et al., *ApoE4 decreases spine density and dendritic complexity in cortical neurons in vivo.* The Journal of neuroscience : the official journal of the Society for Neuroscience, 2009. **29**(48): p. 15317-15322.

32. Verghese, P.B., et al., *ApoE influences amyloid-β (Aβ) clearance despite minimal apoE/Aβ association in physiological conditions.* Proceedings of the National Academy of Sciences of the United States of America, 2013. **110**(19): p. E1807-E1816.

33. Majdi, A., et al., *Amyloid-β, tau, and the cholinergic system in Alzheimer's disease: seeking direction in a tangle of clues.* Reviews in the Neurosciences, 2020. **31**(4): p. 391-413.

34. O'Callaghan, J.P. and D.B. Miller, *Neuroinflammation disorders exacerbated by environmental stressors.* Metabolism: clinical and experimental, 2019. **100S**: p. 153951-153951.

35. Bhatt, S., L. Puli, and C.R. Patil, *Role of reactive oxygen species in the progression of Alzheimer's disease.* Drug Discovery Today, 2021. **26**(3): p. 794-803.

36. Manoharan, S., et al., *The Role of Reactive Oxygen Species in the Pathogenesis of Alzheimer's Disease, Parkinson's Disease, and Huntington's Disease: A Mini Review.* Oxidative medicine and cellular longevity, 2016. **2016**: p. 8590578-8590578.

37. Kumar, A., *Long-Term Potentiation at CA3–CA1 Hippocampal Synapses with Special Emphasis on Aging, Disease, and Stress.* Front Aging Neurosci, 2011. **3**: p. 7.

38. Kim, H.Y., et al., *Induction of long-term potentiation and long-term depression is cell-type specific in the spinal cord.* Pain, 2015. **156**(4): p. 618-625.

39. Odawara, A., et al., *Induction of long-term potentiation and depression phenomena in human induced pluripotent stem cell-derived cortical neurons.* Biochemical and Biophysical Research Communications, 2016. **469**(4): p. 856-862.

40. Bliss, T.V.P. and S.F. Cooke, *Long-term potentiation and long-term depression: a clinical perspective.* Clinics (Sao Paulo, Brazil), 2011. **66 Suppl 1**(Suppl 1): p. 3-17.

41. Bliss, T.V.P. and G.L. Collingridge, *Expression of NMDA receptor-dependent LTP in the hippocampus: bridging the divide.* Molecular Brain, 2013. **6**(1): p. 5.

42. Citri, A. and R.C. Malenka, *Synaptic Plasticity: Multiple Forms, Functions, and Mechanisms.* Neuropsychopharmacology, 2008. **33**(1): p. 18-41.

43. Dong, Z., et al., *Long-term potentiation decay and memory loss are mediated by AMPAR endocytosis.* The Journal of clinical investigation, 2015. **125**(1): p. 234-247.

44. Lüscher, C. and R.C. Malenka, *NMDA receptor-dependent long-term potentiation and long-term depression (LTP/LTD).* Cold Spring Harbor perspectives in biology, 2012. **4**(6): p. a005710.

45. Sumi, T. and K. Harada, *Mechanism underlying hippocampal long-term potentiation and depression based on competition between endocytosis and exocytosis of AMPA receptors.* Scientific Reports, 2020. **10**(1): p. 14711.

46. Volianskis, A., et al., *Long-term potentiation and the role of N-methyl-d-aspartate receptors.* Brain Research, 2015. **1621**: p. 5-16.

47. Povysheva, N.V. and J.W. Johnson, *Effects of memantine on the excitation-inhibition balance in prefrontal cortex.* Neurobiology of disease, 2016. **96**: p. 75-83.

48. Thomas, S.J. and G.T. Grossberg, *Memantine: a review of studies into its safety and efficacy in treating Alzheimer's disease and other dementias.* Clinical interventions in aging, 2009. **4**: p. 367-377.

49. Molinuevo, J.L., A. Lladó, and L. Rami, *Memantine: targeting glutamate excitotoxicity in Alzheimer's disease and other dementias.* Am J Alzheimers Dis Other Demen, 2005. **20**(2): p. 77-85.

50. Cacabelos, R., *Donepezil in Alzheimer's disease: From conventional trials to pharmacogenetics.* Neuropsychiatric disease and treatment, 2007. **3**(3): p. 303-333.

51. Cutuli, D., et al., *Neuroprotective effects of donepezil against cholinergic depletion.* Alzheimer's Research & Therapy, 2013. **5**(5): p. 50.

52. Gage, M., et al., *Saracatinib, a Src Tyrosine Kinase Inhibitor, as a Disease Modifier in the Rat DFP Model: Sex Differences, Neurobehavior, Gliosis, Neurodegeneration, and Nitro-Oxidative Stress.* Antioxidants (Basel), 2021. **11**(1).

53. Kumar, A. and N. Singh, *Inhibitor of Phosphodiestearse-4 improves memory deficits, oxidative stress, neuroinflammation and neuropathological alterations in mouse models of dementia of Alzheimer's Type.* Biomed Pharmacother, 2017. **88**: p. 698-707.

54. Gong, B., et al., *Persistent improvement in synaptic and cognitive functions in an Alzheimer mouse model after rolipram treatment*. J Clin Invest, 2004. **114**(11): p. 1624-34.

55. Moradi, S., et al., *Research and therapy with induced pluripotent stem cells (iPSCs): social, legal, and ethical considerations.* Stem Cell Research & Therapy, 2019. **10**(1): p. 341.

56. Takahashi, K. and S. Yamanaka, *Induction of pluripotent stem cells from mouse embryonic and adult fibroblast cultures by defined factors.* Cell, 2006. **126**(4): p. 663-76.

57. Abu-Dawud, R., et al., *Pluripotent stem cells: induction and self-renewal.* Philosophical transactions of the Royal Society of London. Series B, Biological sciences, 2018. **373**(1750): p. 20170213.

58. Scudellari, M., *How iPS cells changed the world.* Nature, 2016. **534**(7607): p. 310-312.

59. Russo, F.B., et al., *Induced pluripotent stem cells for modeling neurological disorders.* World journal of transplantation, 2015. **5**(4): p. 209-221.

60. Martínez-Morales, P.L. and I. Liste, *Stem Cells as In Vitro Model of Parkinson's Disease.* Stem Cells International, 2012. **2012**: p. 980941.

61. Carter, R.L. and A.W.S. Chan, *Pluripotent stem cells models for Huntington's disease: prospects and challenges.* Journal of genetics and genomics = Yi chuan xue bao, 2012. **39**(6): p. 253-259.

62. Caneus, J., et al., *A Human Induced Pluripotent Stem Cell-Derived Cortical Neuron Human-on-a chip System to Study Aβ42 and Tau-induced Pathophysiological Effects on Long-Term Potentiation.* Alzheimer's & Dementia: Translational Research & Clinical Interventions, 2020. **6**(1): p. e12029.

63. Engle, S.J., L. Blaha, and R.J. Kleiman, *Best Practices for Translational Disease Modeling Using Human iPSC-Derived Neurons.* Neuron, 2018. **100**(4): p. 783-797.

64. Espuny-Camacho, I., et al., *Pyramidal Neurons Derived from Human Pluripotent Stem Cells Integrate Efficiently into Mouse Brain Circuits In Vivo.* Neuron, 2013. **77**(3): p. 440-456.

65. Qi, Y., et al., *Combined small-molecule inhibition accelerates the derivation of functional, early-born, cortical neurons from human pluripotent stem cells.* Nature biotechnology, 2017. **35**(2): p. 154-163.

66. Cao, S.-Y., et al., *Enhanced derivation of human pluripotent stem cell-derived cortical glutamatergic neurons by a small molecule.* Scientific Reports, 2017. **7**(1): p. 3282.

67. Odawara, A., et al., *Induction of long-term potentiation and depression phenomena in human induced pluripotent stem cell-derived cortical neurons.* Biochem Biophys Res Commun, 2016. **469**: p. 856-862.

68. Odawara, A., et al., *Toxicological evaluation of convulsant and anticonvulsant drugs in human induced pluripotent stem cell-derived cortical neuronal networks using an MEA system.* Scientific Reports, 2018. **8**(1): p. 10416.

69. Abraham, W.C. and A. Huggett, *Induction and reversal of long-term potentiation by repeated high-frequency stimulation in rat hippocampal slices.* Hippocampus, 1997. **7**(2): p. 137-45.

70. Huh, S., et al., *The reemergence of long-term potentiation in aged Alzheimer's disease mouse model.* Scientific reports, 2016. **6**: p. 29152-29152.

71. Hwang, K.-D., et al., *Restoring synaptic plasticity and memory in mouse models of Alzheimer's disease by PKR inhibition.* Molecular Brain, 2017. **10**(1): p. 57.

72. Dragoi, G., K.D. Harris, and G. Buzsáki, *Place Representation within Hippocampal Networks Is Modified by Long-Term Potentiation.* Neuron, 2003. **39**(5): p. 843-853.

73. Frega, M., et al., *Rapid Neuronal Differentiation of Induced Pluripotent Stem Cells for Measuring Network Activity on Micro-electrode Arrays.* JoVE, 2017. **119**: p. 54900.

74. Chambers, S.M., et al., *Highly efficient neural conversion of human ES and iPS cells by dual inhibition of SMAD signaling.* Nat Biotech, 2009. **27**(3): p. 275-280.

75. Nicoleau, C., et al., *Embryonic stem cells neural differentiation qualifies the role of Wnt/β-Catenin signals in human telencephalic specification and regionalization.* STEM CELLS, 2013. **31**(9): p. 1763-1774.

76. Neely, M., et al., *DMH1, a Highly Selective Small Molecule BMP Inhibitor Promotes Neurogenesis of hiPSCs: Comparison of PAX6 and SOX1 Expression during Neural Induction.* ACS chemical neuroscience, 2012. **3**: p. 482-91.

77. Gorski, J.A., et al., *Brain-Derived Neurotrophic Factor Is Required for the Maintenance of Cortical Dendrites.* The Journal of Neuroscience, 2003. **23**(17): p. 6856-6865.

78. Bonafina, A., et al., *GDNF/GFRα1 Complex Abrogates Self-Renewing Activity of Cortical Neural Precursors Inducing Their Differentiation.* Stem cell reports, 2018. **10**(3): p. 1000-1015.

79. Radner, S., et al., *β2 and γ3 laminins are critical cortical basement membrane components: Ablation of Lamb2 and Lamc3 genes disrupts cortical lamination and produces dysplasia.* Developmental Neurobiology, 2013. **73**(3): p. 209-229.

80. Bardy, C., et al., *Neuronal medium that supports basic synaptic functions and activity of human neurons in vitro.* Proceedings of the National Academy of Sciences, 2015. **112**(20): p. E2725.

81. Gunhanlar, N., et al., *A simplified protocol for differentiation of electrophysiologically mature neuronal networks from human induced pluripotent stem cells.* Molecular psychiatry, 2018. **23**(5): p. 1336-1344.

82. Ahmed, A.I., et al., *Endogenous GFAP-positive neural stem/progenitor cells in the postnatal mouse cortex are activated following traumatic brain injury.* Journal of neurotrauma, 2012. **29**(5): p. 828-842.

83. Ghatak, S., et al., *Mechanisms of hyperexcitability in Alzheimer's disease hiPSC-derived neurons and cerebral organoids vs isogenic controls.* eLife, 2019. **8**: p. e50333.

84. Prè, D., et al., *A Time Course Analysis of the Electrophysiological Properties of Neurons Differentiated from Human Induced Pluripotent Stem Cells (iPSCs).* PLoS One, 2014. **9**(7): p. e103418.

85. Onizuka, S.M.D., et al., *Lidocaine Increases Intracellular Sodium Concentration through Voltage-dependent Sodium Channels in an Identified Lymnaea Neuron.* Anesthesiology: The Journal of the American Society of Anesthesiologists, 2004. **101**(1): p. 110-120.

86. Putrenko, I., Ph.D. and S.K.W. Schwarz, M.D., Ph.D., F.R.C.P.C., *Lidocaine Blocks the Hyperpolarization-activated Mixed Cation Current, I h, in Rat Thalamocortical Neurons.* Anesthesiology: The Journal of the American Society of Anesthesiologists, 2011. **115**(4): p. 822-835.

87. Libbey, J.E., et al., *NBQX, a highly selective competitive antagonist of AMPA and KA ionotropic glutamate receptors, increases seizures and mortality following picornavirus infection.* Experimental neurology, 2016. **280**: p. 89-96.

88. Maric, D., et al., *GABA expression dominates neuronal lineage progression in the embryonic rat neocortex and facilitates neurite outgrowth via GABA(A) autoreceptor/Cl- channels.* J Neurosci, 2001. **21**(7): p. 2343-60.

89. Wang, D.D. and A.R. Kriegstein, *Defining the role of GABA in cortical development.* The Journal of physiology, 2009. **587**(Pt 9): p. 1873-1879.

90. Le Magueresse, C. and H. Monyer, *GABAergic Interneurons Shape the Functional Maturation of the Cortex.* Neuron, 2013. **77**(3): p. 388-405.

91. Steele, P.M. and M.D. Mauk, *Inhibitory control of LTP and LTD: stability of synapse strength.* J Neurophysiol, 1999. **81**(4): p. 1559-66.

92. Nadadhur, A.G., et al., *Multi-level characterization of balanced inhibitory-excitatory cortical neuron network derived from human pluripotent stem cells.* PloS one, 2017. **12**(6): p. e0178533-e0178533.

93. Grainger, A.I., et al., *In vitro models for seizure-liability testing using induced pluripotent stem cells.* Front. Neurosci., 2018. **12**: p. 590-590.

94. Oleaga, C., et al., *A functional long-term serum-free human hepatic in vitro system for drug evaluation.* Biotechnol Prog, 2021. **37**(1): p. 33069.

95. Stancescu, M., et al., *A phenotypic in vitro model for the main determinants of human whole heart function.* Biomaterials, 2015. **60**: p. 20-30.

96. Das, M., et al., *Long-term culture of embyonic rat cardiomyocytes on an organosilane surface in a serum free medium.* Biomaterials, 2004. **25**(25): p. 5643-5647.

97. Guo, X.F., et al., *Characterization of a human fetal spinal cord stem cell line NSI-566RSC and its induction to functional motoneurons.* J Tissue Eng Regen Med, 2010. **4**: p. 181-193.

98. Badu-Mensah, A., et al., *Skeletal muscle model derived from familial ALS patient iPSCs recapitulates hallmarks of disease progression.* Sci Rep, 2020. **10**: p. 14302.

99. Oleaga, C., et al., *Long-Term Electrical and Mechanical Function Monitoring of a Human-on-a-Chip System.* Advanced Functional Materials, 2019. **29**: p. 1805792.

100. Nicoll, R.A., *A Brief History of Long-Term Potentiation.* Neuron, 2017. **93**(2): p. 281-290.

101. Hata, K., et al., *Multicoding in neural information transfer suggested by mathematical analysis of the frequency-dependent synaptic plasticity in vivo.* Scientific Reports, 2020. **10**: p. 13974.

102. Mango, D., et al., *Targeting Synaptic Plasticity in Experimental Models of Alzheimer's Disease.* Front Pharmacol, 2019. **10**: p. 778.

103. Park, K., et al., *Learning-induced synaptic potentiation in implanted neural precursor cell-derived neurons.* Scientific Reports, 2015. **5**(1): p. 17796.

104. Narayanan, R. and D. Johnston, *Long-term potentiation in rat hippocampal neurons is accompanied by spatially widespread changes in intrinsic oscillatory dynamics and excitability.* Neuron, 2007. **56**(6): p. 1061-1075.

105. Loscher, W., *Critical review of current animal models of seizures and epilepsy used in the discovery and development of new antiepileptic drugs.* Seizure, 2011. **20**: p. 359–368.

106. Odawara, A., et al., *Physiological maturation and drug responses of human induced pluripotent stem cell-derived cortical neuronal networks in long-term culture.* Sci Rep, 2016. **6**: p. 26181.

107. Koch, G., et al., *Impaired LTP- but not LTD-Like Cortical Plasticity in Alzheimer's Disease Patients.* Journal of Alzheimer's Disease, 2012. **31**: p. 593-599.

108. Zhou, J.-L., et al., *Impaired single cell firing and long-term potentiation parallels memory impairment following recurrent seizures.* European Journal of Neuroscience, 2007. **25**(12): p. 3667-3677.

109. Chung, L., A.L. Bey, and Y.-H. Jiang, *Synaptic plasticity in mouse models of autism spectrum disorders.* The Korean journal of physiology & pharmacology : official journal of the Korean Physiological Society and the Korean Society of Pharmacology, 2012. **16**(6): p. 369-378.

110. Reyes-Garcia, S.Z., et al., *Robust Network Inhibition and Decay of Early-Phase LTP in the Hippocampal CA1 Subfield of the Amazon Rodent Proechimys.* Frontiers in Neural Circuits, 2018. **12**(81).

111. Chapman, C.A., Y. Perez, and J.C. Lacaille, *Effects of GABA(A) inhibition on the expression of long-term potentiation in CA1 pyramidal cells are dependent on tetanization parameters.* Hippocampus, 1998. **8**(3): p. 289-98.

112. Vaaga, C.E., M. Borisovska, and G.L. Westbrook, *Dual-transmitter neurons: functional implications of co-release and co-transmission.* Current Opin Neurobiol, 2014. **29**: p. 25-32.

113. Xu, J.-C., et al., *Cultured networks of excitatory projection neurons and inhibitory interneurons for studying human cortical neurotoxicity.* Science Translational Medicine, 2016. **8**(333): p. 333ra48.

114. Lam, R.S., et al., *Functional Maturation of Human Stem Cell-Derived Neurons in Long-Term Cultures.* PloS one, 2017. **12**(1): p. e0169506-e0169506.

115. Kumamaru, E., et al., *Valproic acid selectively suppresses the formation of inhibitory synapses in cultured cortical neurons.* Neurosci Lett, 2014. **569**: p. 142-7.

116. Nowak, L.M., A.B. Young, and R.L. Macdonald, *GABA and bicuculline actions on mouse spinal cord and cortical neurons in cell culture.* Brain Res, 1982. **244**(1): p. 155-64.

117. Colombi, I., et al., *Effects of antiepileptic drugs on hippocampal neurons coupled to micro-electrode arrays.* Frontiers in neuroengineering, 2013. **6**: p. 10-10.

118. Sharma, A.K., et al., *Mesial Temporal Lobe Epilepsy: Pathogenesis, Induced Rodent Models and Lesions.* Toxicologic Pathology, 2007. **35**(7): p. 984-999.

119. Campos, G., et al., *In vitro and in vivo experimental models employed in the discovery and development of antiepileptic drugs for pharmacoresistant epilepsy.* Epilepsy Research, 2018. **146**: p. 63-86.

120. Johnston, G.A.R., *Advantages of an antagonist: bicuculline and other GABA antagonists.* British journal of pharmacology, 2013. **169**(2): p. 328-336.

121. Davies, J.A., *Mechanisms of action of antiepileptic drugs.* Seizure, 1995. **4**(4): p. 267-71.

122. Lunden, J.W., et al., *Cortical interneuron function in autism spectrum condition.* Pediatric Research, 2019. **85**(2): p. 146-154.

123. Lieberman, R., et al., *Pilot study of iPS-derived neural cells to examine biologic effects of alcohol on human neurons in vitro.* Alcoholism, clinical and experimental research, 2012. **36**(10): p. 1678-1687.

124. Gonzalez, M., et al., *Polarity Induced in Human Stem Cell Derived Motoneurons on Patterned Self-Assembled Monolayers.* ACS Chemical Neuroscience, 2019. **10**(6): p. 2756-2764.

125. Edwards, D., et al., *Two cell circuits of oriented adult hippocampal neurons on self-assembled monolayers for use in the study of neuronal communication in a defined system.* ACS chemical neuroscience, 2013. **4**(8): p. 1174-1182.

126. Patel, A., et al., *Myelination and Node of Ranvier Formation in a Human Motoneuron–Schwann Cell Serum-Free Coculture.* ACS Chemical Neuroscience, 2020. **11**(17): p. 2615-2623.

127. Varghese, K., et al., *A new target for amyloid beta toxicity validated by standard and high-throughput electrophysiology.* PLoS One, 2010. **5**(1): p. e8643.

128. Obien, M.E.J., et al., *Revealing neuronal function through microelectrode array recordings.* Front Neurosci, 2015. **8**: p. 1-30.

129. Van Norman, G.A., *Limitations of Animal Studies for Predicting Toxicity in Clinical Trials: Is it Time to Rethink Our Current Approach?* JACC Basic Transl Sci, 2019. **4**(7): p. 845-854.

130. Michael Hay, D.W.T., John L Craighead, Celia Economides & Jesse Rosenthal *Clinical development success rates for investigational drugs.* Nature Biotechnology, 2014(32): p. 40-51.

131. Wong, C.H., K.W. Siah, and A.W. Lo, *Estimation of clinical trial success rates and related parameters.* Biostatistics, 2019. **20**(2): p. 273-286.

132. Munro, H.D.J., *Nature Reviews Drug Discovery.* Nature, 2019(18): p. 495-496.

133. Clinicaltrials.gov, *Alzheimer's Disease.* NIH - US National Library of Medicine, 2021.

134. Johnique T. Atkins, G.C.G., Kenneth Hess, Kathrina L. Marcelo-Lewis, Ying Yuan, Gautam Borthakur, Sean Khozin, Patricia LoRusso & David S. Hong, *Pre-clinical animal models are poor predictors of human toxicities in phase 1 oncology clinical trials.* British Journal of Cancer, 2020(123): p. 1496–1501.

135. Dowden, H. and J. Munro, *Trends in clinical success rates and therapeutic focus.* Nat Rev Drug Discov, 2019. **18**(7): p. 495-496.

136. Huang, Y., et al., *Recent advancements of human iPSC derived cardiomyocytes in drug screening and tissue regeneration.* Microphysiological Systems, 2020. **4**.

137. Pound, P. and M. Ritskes-Hoitinga, *Is it possible to overcome issues of external validity in preclinical animal research? Why most animal models are bound to fail.* J Transl Med, 2018. **16**(1): p. 304.

138. Perel, P., et al., *Comparison of treatment effects between animal experiments and clinical trials: systematic review.* BMJ, 2007. **334**(7586): p. 197.

139. Geerts, H., *Of Mice and Men.* CNS Drugs, 2009(23): p. 915–926.

140. Cummings, J.L., et al., *Alzheimer's disease: etiologies, pathophysiology, cognitive reserve, and treatment opportunities.* Neurology, 1998. **51**(1 Suppl 1): p. S2-17; discussion S65-7.

141. Chen, X.Q. and W.C. Mobley, *Alzheimer Disease Pathogenesis: Insights From Molecular and Cellular Biology Studies of Oligomeric Abeta and Tau Species.* Front Neurosci, 2019. **13**: p. 659.

142. Dolmetsch, R. and D.H. Geschwind, *The human brain in a dish: the promise of iPSC-derived neurons.* Cell, 2011. **145**(6): p. 831-4.

143. Kumar, S., J. Blangero, and J.E. Curran, *Induced Pluripotent Stem Cells in Disease Modeling and Gene Identification.* Methods Mol Biol, 2018. **1706**: p. 17-38.

144. Rowe, R.G. and G.Q. Daley, *Induced pluripotent stem cells in disease modelling and drug discovery.* Nat Rev Genet, 2019. **20**(7): p. 377-388.

145. Sharma, A., et al., *Multi-lineage Human iPSC-Derived Platforms for Disease Modeling and Drug Discovery.* Cell Stem Cell, 2020. **26**(3): p. 309-329.

146. Lamotte, J.D., et al., *hiPSC-Derived Neurons Provide a Robust and Physiologically Relevant In Vitro Platform to Test Botulinum Neurotoxins.* Front Pharmacol, 2020. **11**: p. 617867.

147. Whitemarsh, R.C., et al., *Novel application of human neurons derived from induced pluripotent stem cells for highly sensitive botulinum neurotoxin detection.* Toxicol Sci, 2012. **126**(2): p. 426-35.

148. Wikswo, J.P., *The relevance and potential roles of microphysiological systems in biology and medicine.* Exp Biol Med (Maywood), 2014. **239**(9): p. 1061-72.

149. Watson, D.E., R. Hunziker, and J.P. Wikswo, *Fitting tissue chips and microphysiological systems into the grand scheme of medicine, biology, pharmacology, and toxicology.* Exp Biol Med (Maywood), 2017. **242**(16): p. 1559-1572.

150. Caneus, J., et al., *A human induced pluripotent stem cell-derived cortical neuron human-on-a chip system to study Abeta42 and tau-induced pathophysiological effects on long-term potentiation.* Alzheimers Dement (N Y), 2020. **6**(1): p. e12029.

151. Autar, K., et al., *A functional hiPSC-cortical neuron differentiation and maturation model and its application to neurological disorders.* Stem Cell Reports, 2022. **17**(1): p. 96-109.

152. Ferreira-Vieira, T.H., et al., *Alzheimer's disease: Targeting the Cholinergic System.* Curr Neuropharmacol, 2016. **14**(1): p. 101-15.

153. Hampel, H., et al., *The cholinergic system in the pathophysiology and treatment of Alzheimer's disease.* Brain, 2018. **141**(7): p. 1917-1933.

154. Tibbo, A.J. and G.S. Baillie, *Phosphodiesterase 4B: Master Regulator of Brain Signaling.* Cells, 2020. **9**(5): p. 1254.

155. Liu, X., et al., *PDE4 Inhibition Restores the Balance Between Excitation and Inhibition in VTA Dopamine Neurons Disrupted by Repeated In Vivo Cocaine Exposure.* Neuropsychopharmacology, 2017. **42**(10): p. 1991-1999.

156. Adams, C.P. and V.V. Brantner, *Estimating the cost of new drug development: is it really 802 million dollars?* Health Aff (Millwood), 2006. **25**(2): p. 420-8.

157. Dahlin, E., et al., *Success rates for product development strategies in new drug development.* J Clin Pharm Ther, 2016. **41**(2): p. 198-202.

158. Shih, H.P., X. Zhang, and A.M. Aronov, *Drug discovery effectiveness from the standpoint of therapeutic mechanisms and indications.* Nat Rev Drug Discov, 2018. **17**(1): p. 19-33.

159. Wouters, O.J., M. McKee, and J. Luyten, *Estimated Research and Development Investment Needed to Bring a New Medicine to Market, 2009-2018.* JAMA, 2020. **323**(9): p. 844-853.

160. DiMasi, J.A., H.G. Grabowski, and R.W. Hansen, *Innovation in the pharmaceutical industry: New estimates of R&D costs.* J Health Econ, 2016. **47**: p. 20-33.

161. Dierynck, B. and P. Joos, *Research and Development Costs of New Drugs.* JAMA, 2020. **324**(5): p. 516-517.

162. Waring, M.J., et al., *An analysis of the attrition of drug candidates from four major pharmaceutical companies.* Nat Rev Drug Discov, 2015. **14**(7): p. 475-86.

163. Cummings, J.L., T. Morstorf, and K. Zhong, *Alzheimer's disease drug-development pipeline: few candidates, frequent failures.* Alzheimers Res Ther, 2014. **6**(4): p. 37.

164. Clinicaltrials.gov, List of Alzheirmer related drugs in clinical trials.

165. ALZFORUM, *Therapeutics: Memantine.* https://www.alzforum.org/therapeutics/memantine.

166. Mullard, A., *Landmark Alzheimer's drug approval confounds research community.* Nature, 2021.

167. Knowles, J., *Donepezil in Alzheimer's disease: an evidence-based review of its impact on clinical and economic outcomes.* Core Evid, 2006. **1**(3): p. 195-219.

168. Barry Reisberg, M.D., Rachelle Doody, M.D., Ph.D., Albrecht Stöffler, M.D., Frederick Schmitt, Ph.D., Steven Ferris, Ph.D., and Hans Jörg Möbius, M.D., Ph.D., *Memantine in Moderate-to-Severe Alzheimer's Disease.* NEJM, 2003(348): p. 1333-1341.

169. Cummings, J., et al., *Alzheimer's disease drug development pipeline: 2020.* Alzheimers Dement (N Y), 2020. **6**(1): p. e12050.

170. Kevin Mullane, M.W., *Alzheimer's therapeutics: Continued clinical failures question the validity of the amyloid hypothesis—but what lies beyond?* ScienceDirect, 2013. **85**(3): p. 289-305.

171. Harrison, R.K., *Phase II and phase III failures: 2013–2015.* Nat Rev Drug Discov, 2016(15): p. 817–818.

172. Jonathan J.Sabbagh, J.W.K., Jeffrey L.Cummings, *Animal systems in the development of treatments for Alzheimer's disease: challenges, methods, and implications.* ELSEVIER, 2013. **34**(1): p. 169-183.

173. Mak, I.W., N. Evaniew, and M. Ghert, *Lost in translation: animal models and clinical trials in cancer treatment.* Am J Transl Res, 2014. **6**(2): p. 114-8.

174. Morgan, P., et al., *Impact of a five-dimensional framework on R&D productivity at AstraZeneca.* Nat Rev Drug Discov, 2018. **17**(3): p. 167-181.

175. Caneus, J., et al., *A human induced pluripotent stem cell-derived cortical neuron human-on-a chip system to study Aβ42 and tau-induced pathophysiological effects on long-term potentiation.* Alzheimer's & Dementia: Translational Research & Clinical Interventions, 2020. **6**(1): p. e12029.

176. Calhoun, A., et al., *An evaluation of memantine ER + donepezil for the treatment of Alzheimer's disease.* Expert Opin Pharmacother, 2018. **19**(15): p. 1711-1717.

177. Berry, B.J., et al., *Morphological and functional characterization of human induced pluripotent stem cell-derived neurons (iCell Neurons) in defined culture systems.* Biotechnol Prog, 2015. **31**(6): p. 1613-22.

178. Stine, W.B., Jr., et al., *In vitro characterization of conditions for amyloid-beta peptide oligomerization and fibrillogenesis.* J Biol Chem, 2003. **278**(13): p. 11612-22.

179. Kuns B, R.A., Varghese D., *Memantine.* In: StatPearls [Internet], 2021.

180. Dooley, M. and H.M. Lamb, *Donepezil: a review of its use in Alzheimer's disease.* Drugs Aging, 2000. **16**(3): p. 199-226.

181. Shigeta, M. and A. Homma, *Donepezil for Alzheimer's disease: pharmacodynamic, pharmacokinetic, and clinical profiles.* CNS Drug Rev, 2001. **7**(4): p. 353-68.

182. ALZFORUM, *THERAPEUTICS: Saracatinib.* ALZForum.

183. Tang, S.J., et al., *Fyn kinase inhibition reduces protein aggregation, increases synapse density and improves memory in transgenic and traumatic Tauopathy.* Acta Neuropathol Commun, 2020. **8**(1): p. 96.

184. Kaufman, A.C., et al., *Fyn inhibition rescues established memory and synapse loss in Alzheimer mice.* Ann Neurol, 2015. **77**(6): p. 953-71.

185. Nygaard, H.B., *Targeting Fyn Kinase in Alzheimer's Disease.* Biol Psychiatry, 2018. **83**(4): p. 369-376.

186. Garcia-Osta, A., et al., *Phosphodiesterases as therapeutic targets for Alzheimer's disease.* ACS Chem Neurosci, 2012. **3**(11): p. 832-44.

187. Edwards, D., et al., *Comparison of NMDA and AMPA Channel Expression and Function between Embryonic and Adult Neurons Utilizing Microelectrode Array Systems.* ACS Biomater Sci Eng, 2017. **3**(12): p. 3525-3533.

188. Kashyap, G., et al., *Synapse loss and progress of Alzheimer's disease -A network model.* Scientific Reports, 2019. **9**(1): p. 6555.

189. Seeley, W.W., *Selective functional, regional, and neuronal vulnerability in frontotemporal dementia.* Current opinion in neurology, 2008. **21**(6): p. 701-707.

190. Bellucci, A., et al., *Review: Parkinson's disease: from synaptic loss to connectome dysfunction.* Neuropathol Appl Neurobiol, 2016. **42**(1): p. 77-94.

191. Casillas-Espinosa, P.M., K.L. Powell, and T.J. O'Brien, *Regulators of synaptic transmission: Roles in the pathogenesis and treatment of epilepsy.* Epilepsia, 2012. **53**(s9): p. 41-58.

192. Stover, K.R., et al., *Early detection of cognitive deficits in the 3xTg-AD mouse model of Alzheimer's disease.* Behav Brain Res, 2015. **289**: p. 29-38.

193. Berkowitz, L.E., et al., *Progressive impairment of directional and spatially precise trajectories by TgF344-Alzheimer's disease rats in the Morris Water Task.* Scientific Reports, 2018. **8**(1): p. 16153.

194. Sasaguri, H., et al., *Generation of nonhuman primate models of Alzheimer's disease.* Alzheimer's & Dementia, 2020. **16**(S2): p. e042244.

195. Cho, S., A. Wood, and M.R. Bowlby, *Brain slices as models for neurodegenerative disease and screening platforms to identify novel therapeutics.* Current neuropharmacology, 2007. **5**(1): p. 19-33.

196. Negri, J., V. Menon, and T.L. Young-Pearse, *Assessment of Spontaneous Neuronal Activity In Vitro Using Multi-Well Multi-Electrode Arrays: Implications for Assay Development.* eneuro, 2020. **7**(1): p. ENEURO.0080-19.2019.

197. Bruno, G., et al., *Microfluidic Multielectrode Arrays for Spatially Localized Drug Delivery and Electrical Recordings of Primary Neuronal Cultures.* Frontiers in Bioengineering and Biotechnology, 2020. **8**.

198. Schulte, S., et al., *Using multielectrode arrays to investigate neurodegenerative effects of the amyloid-beta peptide.* Bioelectronic Medicine, 2021. **7**(1): p. 15.

199. Qi, G., et al., *Unveiling the Synaptic Function and Structure Using Paired Recordings From Synaptically Coupled Neurons.* Frontiers in Synaptic Neuroscience, 2020. **12**.

200. Penney, J., W.T. Ralvenius, and L.-H. Tsai, *Modeling Alzheimer's disease with iPSC-derived brain cells.* Molecular Psychiatry, 2020. **25**(1): p. 148-167.

201. Perez-Catalan, N.A., C.Q. Doe, and S.D. Ackerman, *The role of astrocyte-mediated plasticity in neural circuit development and function.* Neural Development, 2021. **16**(1): p. 1.

202. Lalo, U., A. Bogdanov, and Y. Pankratov, *Diversity of Astroglial Effects on Aging- and Experience-Related Cortical Metaplasticity.* Frontiers in Molecular Neuroscience, 2018. **11**(239).

203. Andersen, J.V., et al., *Glutamate metabolism and recycling at the excitatory synapse in health and neurodegeneration.* Neuropharmacology, 2021. **196**.

204. Shen, Y. and D.J. Linden, *Long-Term Potentiation of Neuronal Glutamate Transporters.* Neuron, 2005. **46**(5): p. 715-722.

205. Davis, S., S.P. Butcher, and R.G. Morris, *The NMDA receptor antagonist D-2-amino-5-phosphonopentanoate (D-AP5) impairs spatial learning and LTP in vivo at intracerebral concentrations comparable to those that block LTP in vitro.* J Neurosci, 1992. **12**(1): p. 21-34.

206. Lodge, D., et al., *The 1980s: d-AP5, LTP and a Decade of NMDA Receptor Discoveries.* Neurochemical Research, 2019. **44**(3): p. 516-530.

207. Natarajan, A., et al., *Temporal Characterization of Neuronal Migration Behavior on Chemically Patterned Neuronal Circuits in a Defined in Vitro Environment.* ACS biomaterials science & engineering, 2018. **4**(10): p. 3460-3470.

208. Tu, S., et al., *Oligomeric Aβ-induced synaptic dysfunction in Alzheimer's disease.* Molecular Neurodegeneration, 2014. **9**(1): p. 48.

209. Maina, M.B., et al., *The Involvement of Aβ42 and Tau in Nucleolar and Protein Synthesis Machinery Dysfunction.* Frontiers in Cellular Neuroscience, 2018. **12**.

210. Esposito, Z., et al., *Amyloid β, glutamate, excitotoxicity in Alzheimer's disease: are we on the right track?* CNS Neurosci Ther, 2013. **19**(8): p. 549-55.

211. Meraz-Ríos, M.A., et al., *Inflammatory process in Alzheimer's Disease.* Frontiers in integrative neuroscience, 2013. **7**: p. 59-59.

212. Zhang, X., et al., *The γ-secretase complex: from structure to function.* Frontiers in cellular neuroscience, 2014. **8**: p. 427-427.

213. Kwart, D., et al., *A Large Panel of Isogenic APP and PSEN1 Mutant Human iPSC Neurons Reveals Shared Endosomal Abnormalities Mediated by APP β-CTFs, Not Aβ.* Neuron, 2019. **104**(2): p. 256-270.e5.

214. Xia, D., et al., *Presenilin-1 knockin mice reveal loss-of-function mechanism for familial Alzheimer's disease.* Neuron, 2015. **85**(5): p. 967-981.

215. Sannerud, R., et al., *Restricted Location of PSEN2/γ-Secretase Determines Substrate Specificity and Generates an Intracellular Aβ Pool.* Cell, 2016. **166**(1): p. 193-208.

216. Kelleher, R.J., 3rd and J. Shen, *Presenilin-1 mutations and Alzheimer's disease.* Proceedings of the National Academy of Sciences of the United States of America, 2017. **114**(4): p. 629-631.

217. Arber, C., et al., *Familial Alzheimer's Disease Mutations in PSEN1 Lead to Premature Human Stem Cell Neurogenesis.* Cell Reports, 2021. **34**(2): p. 108615.

218. Yang, J., et al., *Early pathogenic event of Alzheimer's disease documented in iPSCs from patients with PSEN1 mutations.* Oncotarget, 2017. **8**(5): p. 7900-7913.

219. Deaton, C.A. and G.V.W. Johnson, *Presenilin 1 Regulates Membrane Homeostatic Pathways that are Dysregulated in Alzheimer's Disease.* Journal of Alzheimer's disease : JAD, 2020. **77**(3): p. 961-977.

220. Grilli, M., et al., *Presenilin-1 regulates the neuronal threshold to excitotoxicity both physiologically and pathologically.* Proc Natl Acad Sci U S A, 2000. **97**(23): p. 12822-7.

221. Toniolo, S., A. Sen, and M. Husain, *Modulation of Brain Hyperexcitability: Potential New Therapeutic Approaches in Alzheimer's Disease.* International journal of molecular sciences, 2020. **21**(23): p. 9318.

222. Wan, K., et al., *A Novel Probable Pathogenic PSEN2 Mutation p.Phe369Ser Associated With Early-Onset Alzheimer's Disease in a Chinese Han Family: A Case Report.* Frontiers in Aging Neuroscience, 2021. **13**.

223. Wong, E., G.R. Frost, and Y.-M. Li, *γ-Secretase Modulatory Proteins: The Guiding Hand Behind the Running Scissors.* Frontiers in Aging Neuroscience, 2020. **12**.

224. Moreno, C.L., et al., *iPSC-derived familial Alzheimer's PSEN2 N141I cholinergic neurons exhibit mutation-dependent molecular pathology corrected by insulin signaling.* Molecular Neurodegeneration, 2018. **13**(1): p. 33.

225. Wolozin, B., et al., *Participation of presenilin 2 in apoptosis: enhanced basal activity conferred by an Alzheimer mutation.* Science, 1996. **274**(5293): p. 1710-3.

226. Dai, M.-H., et al., *The genes associated with early-onset Alzheimer's disease.* Oncotarget, 2017. **9**(19): p. 15132-15143.

227. Fernandez, C.G., et al., *The Role of APOE4 in Disrupting the Homeostatic Functions of Astrocytes and Microglia in Aging and Alzheimer's Disease.* Frontiers in Aging Neuroscience, 2019. **11**.

228. Martins, I.J., et al., *Apolipoprotein E, cholesterol metabolism, diabetes, and the convergence of risk factors for Alzheimer's disease and cardiovascular disease.* Molecular Psychiatry, 2006. **11**(8): p. 721-736.

229. Wildsmith, K.R., et al., *Evidence for impaired amyloid β clearance in Alzheimer's disease.* Alzheimer's Research & Therapy, 2013. **5**(4): p. 33.

230. Kanekiyo, T., H. Xu, and G. Bu, *ApoE and Aβ in Alzheimer's disease: accidental encounters or partners?* Neuron, 2014. **81**(4): p. 740-754.

231. Huang, Y. and R.W. Mahley, *Apolipoprotein E: structure and function in lipid metabolism, neurobiology, and Alzheimer's diseases.* Neurobiol Dis, 2014. **72 Pt A**: p. 3-12.

232. Qi, G., et al., *ApoE4 Impairs Neuron-Astrocyte Coupling of Fatty Acid Metabolism.* Cell Rep, 2021. **34**(1): p. 108572.

233. Mattsson, N., et al., *Increased amyloidogenic APP processing in APOE ε4-negative individuals with cerebral β-amyloidosis.* Nature Communications, 2016. **7**(1): p. 10918.

234. Zhao, J., et al., *APOE4 exacerbates synapse loss and neurodegeneration in Alzheimer's disease patient iPSC-derived cerebral organoids.* Nature Communications, 2020. **11**(1): p. 5540.

235. Meyer, K., et al., *REST and Neural Gene Network Dysregulation in iPSC Models of Alzheimer's Disease.* Cell reports, 2019. **26**(5): p. 1112-1127.e9.

236. Dixit, S., J.P. Fessel, and F.E. Harrison, *Mitochondrial dysfunction in the APP/PSEN1 mouse model of Alzheimer's disease and a novel protective role for ascorbate.* Free Radic Biol Med, 2017. **112**: p. 515-523.

237. van Tijn, P., et al., *Presenilin mouse and zebrafish models for dementia: Focus on neurogenesis.* Progress in Neurobiology, 2011. **93**(2): p. 149-164.

238. Balu, D., et al., *The role of APOE in transgenic mouse models of AD.* Neurosci Lett, 2019. **707**: p. 134285.

239. Vazin, T., et al., *Efficient derivation of cortical glutamatergic neurons from human pluripotent stem cells: a model system to study neurotoxicity in Alzheimer's disease.* Neurobiology of disease, 2014. **62**: p. 62-72.

240. Parent, A.T. and G. Thinakaran, *Modeling Presenilin-Dependent Familial Alzheimer's Disease: Emphasis on Presenilin Substrate-Mediated Signaling and Synaptic Function.* International Journal of Alzheimer’s Disease, 2010. **2010**: p. 825918.

241. Barak, M., et al., *Human iPSC-Derived Neural Models for Studying Alzheimer's Disease: from Neural Stem Cells to Cerebral Organoids.* Stem Cell Reviews and Reports, 2022. **18**(2): p. 792-820.

242. Kazim, S.F., et al., *Neuronal Network Excitability in Alzheimer's Disease: The Puzzle of Similar versus Divergent Roles of Amyloid β and Tau.* eneuro, 2021. **8**(2): p. ENEURO.0418-20.2020.

243. Kelly, L., et al., *Identification of intraneuronal amyloid beta oligomers in locus coeruleus neurons of Alzheimer's patients and their potential impact on inhibitory neurotransmitter receptors and neuronal excitability.* Neuropathol Appl Neurobiol, 2021. **47**(4): p. 488-505.

244. Cai, Y., S.S.A. An, and S. Kim, *Mutations in presenilin 2 and its implications in Alzheimer's disease and other dementia-associated disorders.* Clinical interventions in aging, 2015. **10**: p. 1163-1172.

245. Wolfe, M.S. and B.A. Yankner, *Sorting Out Presenilins in Alzheimer's Disease.* Cell, 2016. **166**(1): p. 13-5.

246. Fedeli, C., et al., *PSEN2 (presenilin 2) mutants linked to familial Alzheimer disease impair autophagy by altering Ca(2+) homeostasis.* Autophagy, 2019. **15**(12): p. 2044-2062.

247. Safieh, M., A.D. Korczyn, and D.M. Michaelson, *ApoE4: an emerging therapeutic target for Alzheimer's disease.* BMC Medicine, 2019. **17**(1): p. 64.

248. Konings, S.C., et al., *Astrocytic and Neuronal Apolipoprotein E Isoforms Differentially Affect Neuronal Excitability.* Frontiers in Neuroscience, 2021. **15**.

249. Bilousova, T., et al., *Apolipoprotein E/Amyloid-β Complex Accumulates in Alzheimer Disease Cortical Synapses via Apolipoprotein E Receptors and Is Enhanced by APOE4.* Am J Pathol, 2019. **189**(8): p. 1621-1636.

250. Murugan, R., et al., *Biomaterial Surface patterning of self assembled monolayers for controlling neuronal cell behavior.* International journal of biomedical engineering and technology, 2009. **2**(2): p. 104-134.

251. Obien, M.E.J., et al., *Revealing neuronal function through microelectrode array recordings.* Frontiers in Neuroscience, 2015. **8**.

252. Shirwany, N.A., et al., *The amyloid beta ion channel hypothesis of Alzheimer's disease.* Neuropsychiatric disease and treatment, 2007. **3**(5): p. 597-612.

253. Kuperstein, I., et al., *Neurotoxicity of Alzheimer's disease Aβ peptides is induced by small changes in the Aβ42 to Aβ40 ratio.* Embo j, 2010. **29**(19): p. 3408-20.

254. Gavello, D., et al., *Early Alterations of Hippocampal Neuronal Firing Induced by Abeta42.* Cerebral Cortex, 2016. **28**(2): p. 433-446.

255. Parihar, M.S. and G.J. Brewer, *Amyloid-β as a modulator of synaptic plasticity.* Journal of Alzheimer's disease : JAD, 2010. **22**(3): p. 741-763.

256. Rajmohan, R. and P.H. Reddy, *Amyloid-Beta and Phosphorylated Tau Accumulations Cause Abnormalities at Synapses of Alzheimer's disease Neurons.* Journal of Alzheimer's disease : JAD, 2017. **57**(4): p. 975-999.

257. Kametani, F. and M. Hasegawa, *Reconsideration of Amyloid Hypothesis and Tau Hypothesis in Alzheimer's Disease.* Frontiers in Neuroscience, 2018. **12**.

258. Supnet, C. and I. Bezprozvanny, *Neuronal calcium signaling, mitochondrial dysfunction, and Alzheimer's disease.* J Alzheimers Dis, 2010. **20 Suppl 2**(Suppl 2): p. S487-98.

259. Wang, Y., Y. Shi, and H. Wei, *Calcium Dysregulation in Alzheimer's Disease: A Target for New Drug Development.* Journal of Alzheimer's disease & Parkinsonism, 2017. **7**(5): p. 374.

260. LYNCH, M.A., *Long-Term Potentiation and Memory.* Physiological Reviews, 2004. **84**(1): p. 87-136.

261. Wang, C.-Z., et al., *Early-generated interneurons regulate neuronal circuit formation during early postnatal development.* eLife, 2019. **8**: p. e44649.